

UNIVERSITY OF CALIFORNIA

Santa Barbara

Critical Behavior in Non-Equilibrium Systems

A Dissertation submitted in partial satisfaction  
of the requirements for the degree of

Doctor of Philosophy

in

Physics

by

Benjamin Philip Lee

Committee in charge:

Professor John L. Cardy, Chairman

Professor Jim Langer

Professor David S. Cannell

July 1994

The dissertation of  
Benjamin Philip Lee is approved:

---

---

---

Committee Chairman

July 1994

## ACKNOWLEDGMENTS

I am grateful to John Cardy for his patience and support, and for the many helpful discussions which were invaluable lessons in how to conduct research, and to Mike Lakey and Mike Kraff for introducing me to physics, and to Mike, John, Toby, Will, and Todd, for providing a great atmosphere for inquiry and, of course, a lot of fun, and to many others in Santa Barbara and Oxford who have helped to make my graduate studies a pleasure, including Jeff, Brian, Ingrid, Kristina, Rich, Youngchul, Shirley, and Random, and to my parents, and to Kathrin, for the sunshine.

# Curriculum Vitae

May 5, 1967	born in Osage, Iowa
1989	B.S. Physics, Texas A&M University
1989-92	Teaching Assistant, University of California, Santa Barbara
1991-93	Research Assistant, University of California, Santa Barbara
1993-94	Research Assistant, University of Oxford

## PUBLICATIONS

“Phase Ordering in One-Dimensional Systems with Long-Range Interactions,” with J. L. Cardy, Phys. Rev. E **48**, 2452 (1993).

“Renormalization Group Calculation for the Reaction  $kA \rightarrow \emptyset$ ,” J. Phys. A **27**, 2633 (1994).

# Abstract

Critical Behavior in Non-Equilibrium Systems

by

Benjamin Philip Lee

This thesis concerns itself with the critical behavior found in the late stages of relaxation towards equilibrium. The two examples considered here are phase ordering and reaction-diffusion processes.

We study the dynamics of phase ordering of a non-conserved, scalar order parameter in one dimension, with long-range interactions characterized by a power law  $r^{-d-\sigma}$ . It is found that, at least for  $\sigma > 1$ , the model exhibits evolution to a self-similar state characterized by a length scale which grows with time as  $t^{1/(1+\sigma)}$ , and that the late time dynamics is independent of the initial length scale. The insensitivity of the dynamics to the initial conditions is consistent with the scenario of an attractive, non-trivial renormalization group fixed point which governs the late time behavior. For  $\sigma \leq 1$  indications are found in both the simulations and an analytic method that this behavior may be system size dependent.

The  $kA \rightarrow \emptyset$  and  $A + B \rightarrow \emptyset$  reaction-diffusion systems are known to have upper critical dimensions  $d_c$ . We derive a field-theoretic description of the dynamics, in order to study via the renormalization group the effect of fluctuations for  $d < d_c$ . These field theories can be renormalized exactly. For the one-species reaction an expansion scheme is developed which allows explicit calculation of the density and correlation function, both of which are universal, in powers of  $\epsilon = d_c - d$ . The density exponent is exact to all orders in  $\epsilon$ , whereas the amplitude is calculated perturbatively to second order. The formalism is generalized to the reaction  $kA \rightarrow \ell A$ ,  $\ell < k$ .

The physics of the  $A + B \rightarrow \emptyset$  system is quite different, due to a conserved mode in the dynamics, and as a result there is no analogous  $\epsilon$  expansion. Nonetheless, for  $d > 2$  an effective field theory is developed, from which the density and correlation functions can be calculated exactly, although they are not universal. These calculations are generalized to the case where the two species have unequal diffusion constants. Also, the exact renormalization of the field theory, combined with scaling arguments, leads to new exponents characterizing the reaction zones, for both homogeneous and inhomogeneous initial conditions.

# Table of Contents

CHAPTER 1. Introduction . . . . .	1
1.1. The Renormalization Group and Non-Equilibrium Systems . . . . .	3
1.2. Phase Ordering . . . . .	5
1.3. Reaction-Diffusion Systems . . . . .	12
CHAPTER 2. Phase Ordering of One-Dimensional Systems with Long-Range Interactions . . . . .	20
2.1. The Model . . . . .	20
2.2. Scaling Arguments and Numerical Results . . . . .	25
2.3. Renormalization Group Approach . . . . .	33
2.4. Fugacity Expansion . . . . .	35
2.5. Truncation Scheme for the Two-Particle Distribution Function . . . . .	45
2.6. Simulations . . . . .	49
2.7. Discussion . . . . .	51
Appendix 2.A. $Q$ State Potts Model . . . . .	53
Appendix 2.B. 3-Body Problem for $\sigma = 1$ . . . . .	54
Appendix 2.C. $\sigma = 0$ Solution . . . . .	56
CHAPTER 3. Field Theory for Reaction-Diffusion Systems . . . . .	58
3.1. Master Equation and Second Quantized Representation . . . . .	60
3.2. Coherent State Representation . . . . .	64
3.3. Action for the One-Species Reaction . . . . .	69
3.4. Action for the Two-Species Reaction . . . . .	73
Appendix 3.A. Derivation of the Propagator . . . . .	75
CHAPTER 4. One-Species Reaction $kA \rightarrow \emptyset$ . . . . .	77
4.1. Renormalization Group Scheme . . . . .	80
4.2. Tree Diagrams . . . . .	85
4.3. Density Calculation . . . . .	87

4.4. Correlation Function Calculation . . . . .	94
4.5. Logarithmic Corrections for $d = d_c$ . . . . .	98
4.6. Generalization to the Reaction $kA \rightarrow \ell A$ . . . . .	99
Appendix 4.A. Symmetry Factors . . . . .	101
CHAPTER 5. Two-Species Reaction $A + B \rightarrow \emptyset$ . . . . .	103
5.1. Previous Analytical and Numerical Work . . . . .	105
5.2. Field Theory . . . . .	109
5.3. Effective Field Theory for $d > 2$ . . . . .	112
5.4. Density Calculation for $2 < d < 4$ . . . . .	117
5.5. Density for $d \geq 4$ . . . . .	121
5.6. Renormalization for $d \leq 2$ . . . . .	122
5.7. Reaction Zones . . . . .	125
5.8. Unequal Diffusion Constants, $D_A \neq D_B$ , for $d > 2$ . . . . .	131
5.9. Correlation Functions for $2 < d < 4$ . . . . .	139
REFERENCES . . . . .	144

# Chapter 1. Introduction

The behavior of equilibrium systems close to a second order critical point is now quite well understood. An explanation of the features which are generally observed in the critical region, specifically universality and scale invariance, has been found in the framework of the renormalization group. In contrast, there are relatively few well established results for non-equilibrium systems. Nonetheless, nature indicates that the features of scale invariance and universality can also arise from non-equilibrium dynamics in the late stages of evolution. This presents a challenge in theoretical physics to develop some fundamental of understanding these phenomena. Given the success of the renormalization group in describing the equilibrium critical behavior, it seems appropriate to seek to apply similar methods to non-equilibrium systems.

There are two main classes into which non-equilibrium systems can be divided: those which are driven, and so evolve to a steady state, but never approach equilibrium, and those which are relaxing to an equilibrium final state. There are many examples of the former class which exhibit critical behavior. These include all driven systems which can be tuned to a non-equilibrium phase transition, and also sandpiles and other models of self-organized criticality. However, the primary concern of this thesis is the latter class, those systems which are relaxing to equilibrium.



In general, relaxation to equilibrium occurs exponentially in time, with the rate determined by a characteristic scale of the equilibrium end state. However, in some cases the final state will have no characteristic scale. An example of this is critical dynamics, which is the dynamics of relaxation to a second order critical point. There it is found that the system relaxes as a power law in time, and also exhibits other critical features such as universality. We consider in this thesis two examples of systems which evolve toward an equilibrium end state with no length scale: phase ordering and reaction-diffusion. For these processes the final state is one where all the phase boundaries, in the case of phase ordering, or all the particles, in the case of reaction-diffusion, have left the system. While these scale-invariant end states are trivial, nonetheless they have the consequence that these systems exhibit power law-decay in time, as well as other features associated with critical behavior.

The general theme of this thesis is the application of renormalization group methods to the problems of phase ordering and reaction-diffusion processes. An introduction to these systems is presented later in this chapter. Chapter two is concerned with the phase ordering of a one-dimensional system with long-range interactions, a problem which, at the time the research was conducted, had not been previously studied. The results of this study are published in reference [1]. The remainder of the thesis involves reaction-diffusion systems, in which a field-theoretic approach is used. This is motivated by the fact that most successful analytic applications of the renormalization group are based on field theories. In chapter three is reviewed the derivation of the field theory for these models. In chapter four we consider the general one-species reaction  $kA \rightarrow \emptyset$  and present the first complete renormalization group calculation for this system. This work is published in reference [2]. Finally, in chapter five we study the two-species reaction  $A + B \rightarrow \emptyset$  with the field theory formalism, and present results which are to be published.

## 1.1. THE RENORMALIZATION GROUP AND NON-EQUILIBRIUM SYSTEMS

The relative underdevelopment of theoretical non-equilibrium physics is largely due to the absence of a formalism analogous to equilibrium statistical mechanics. Instead, one must start with some phenomenological model, and such models often involve nonlinearities, making progress difficult. In recent years the addition of simulations, which allow one to extract general features from a model even when a solution is not available, has contributed much to our understanding. It is found that a variety of simple phenomenological models contain the essential ingredients for demonstrating scale invariance at asymptotically late times. This is analogous to the situation in equilibrium critical phenomena, where it is known that the nearest neighbor Ising model captures the essence of the phase transition.

In the latter case this is now understood to be a consequence of universality, the concept that the behavior near a critical point depends only on a few general conditions. In equilibrium phase transitions it is found that one can group various critical systems by the universality classes to which they belong. For example, when the interactions of the degrees of freedom are sufficiently short-ranged, then the critical behavior depends only the dimension of space and the symmetries of the Hamiltonian. All other microscopic details of the system are irrelevant. One of the goals, then, in the study of the dynamics of non-equilibrium systems is to systematically determine the universality classes.

The universal quantities which characterize the behavior near a phase transition are the critical exponents and certain amplitude ratios. The critical exponents describe how various singular quantities, such as the order parameter and the specific heat, depend on the temperature  $|T - T_c|$ . An analogous control parameter in non-equilibrium critical behavior might be the time  $t$ , as it is found that observable quantities go as  $t$  to some power for large  $t$ . Then the critical “point” would be the limit  $t \rightarrow \infty$ .

To discuss how renormalization group ideas can be applied to non-equilibrium systems it is useful to build on the analogy with the equilibrium case. The basic idea of the

renormalization group (RG) is to remove systematically the short length scale degrees of freedom. This is done via a two-step transformation. First one integrates out the degrees of freedom for distances between  $a$ , the short distance cutoff manifest in the theory, and  $ba$ , where  $b$  is some arbitrary scale factor. This creates an effective theory with a cutoff  $ba$ . Next one rescales the system by the factor  $1/b$  so that the cutoff is restored to its original value. The net result is a transformation on the Hamiltonian of the system which is parameterized by the factor  $b$ . Usually this is expressed as a transformation of the coupling constants which couple the degrees of freedom to the Hamiltonian. There is a correspondence between a fixed point of the RG transformation to which the couplings flow for large  $b$  and a second order critical point, which can be understood by introducing the correlation length.

For  $T \neq T_c$  there is an intrinsic length in the system known as the correlation length  $\xi$ , which is defined to be the largest length to which the degrees of freedom are correlated. In general  $\xi$  is of the order of a few atomic spacings, but near a critical point it becomes quite large, and at the critical point it diverges as some negative power of  $|T - T_c|$ . This is viewed as the physical origin of the singular behavior near the critical point, since a diverging correlation length means that there are correlated fluctuations on all length scales. If  $\xi$  is infinite then one can iterate the RG an infinite number of times, and the result is that the couplings will flow to the fixed point of the transformation, if it exists. Since a wide range of initial values for a given coupling will flow to the same fixed point, then the behavior of the system will be universal. If the correlation length is finite, then after a finite number of transformations the cutoff will be of order  $\xi$ , and then it is no longer possible to integrate out the degrees of freedom. However, for large  $\xi$  the couplings of the theory will be very near the fixed point values, which has the result that universality is not observed just at the critical point, but in the vicinity of it as well.

This approach can be extended directly to dynamical systems. Instead of just integrating out the degrees of freedom between  $a$  and  $ba$ , one also evolves the system from

time  $t_0$  to  $b^z t_0$ , where  $z$  is some exponent which is to be determined. Then the system is rescaled by the factor  $1/b$ , restoring the time to  $t_0$ . If there is an attractive fixed point to this transformation, then it will describe the asymptotically late time evolution. Since non-equilibrium systems exhibit features associated with critical phenomena, then it seems plausible to conjecture that a renormalization group fixed point is describing the asymptotic evolution of the system.

There is usually associated with critical phenomena an upper critical dimension, above which one can neglect the effect of correlations. Typically the resultant mean-field theory is simple enough that it can be solved and the mean-field critical exponents found. In most cases these exponents are independent of the dimension of the system. From the renormalization group viewpoint, the fixed point which represents the complete, correlated system changes with dimension, and the critical dimension is where this fixed point joins that of the mean-field theory. Generally there is a critical coupling which has a non-zero value for  $d < d_c$ , and which flows to zero when  $d \geq d_c$ . Exactly at the critical dimension the coupling is marginally irrelevant and flows to zero slowly, which results in the system exhibiting mean-field exponents, but with logarithmic corrections.

## 1.2. PHASE ORDERING

Phase ordering refers to the dynamics of a system following a rapid temperature quench from an equilibrated state in the one-phase region of the phase diagram into the two-phase region. The subject has been the focus of much theoretical, numerical, and experimental work, and is reviewed in references [3–6]. A schematic representation of a quench is shown in fig. 1.1.<sup>1</sup> The temperature is plotted on the vertical axis and some scalar order parameter, taken here to be a concentration, is plotted on the horizontal axis.

---

<sup>1</sup> A temperature quench is used, for example, in binary alloys, where the associated rate constants are quite slow. However, for fluid systems one usually performs a pressure quench, which is much more effectively transmitted through the system.

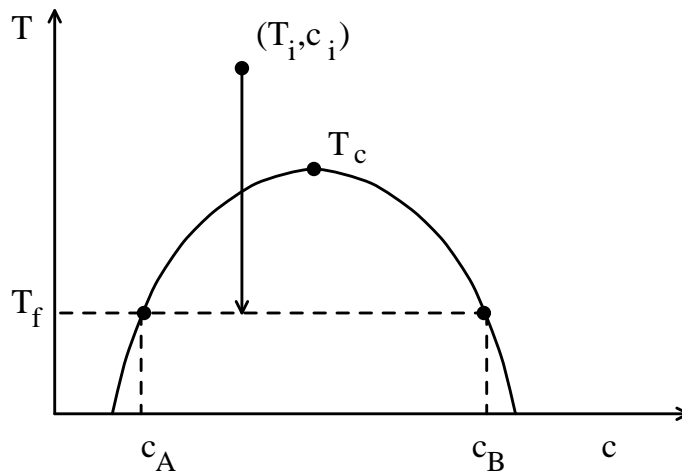


FIGURE 1.1. The schematic for a temperature quench into the two-phase region. The order parameter is a concentration of one of the species in a binary system. The equilibrium concentrations at the post quench temperature  $T_f$  are given by  $c_A$  and  $c_B$ .

There are a variety of experimental systems in which phase ordering is observed, including binary alloys [7], binary fluids, nematic liquid crystals [8,9].

The initial dynamics following the quench are generally non-universal, and roughly speaking fall into two categories. Spinodal decomposition refers to the dynamics which result from quenches deep into the coexistence region, where the system is then unstable to long wavelength perturbations. For quenches closer to the coexistence curve the system is metastable and evolves via the nucleation of droplets which are larger than some critical radius.

In the late stages phase ordering is characterized by large domains of equilibrated phase, regardless of whether the early time evolution for a given quench is described by spinodal decomposition or nucleation. The typical size of these domains increases with time, which is a process referred to as coarsening. The width of the interfaces separating the domains is determined by  $T_f$ , at least for systems with short-range interactions, and does not depend on time. At late times, then, the domain walls become sharp objects

separating regions of equilibrated phase, and one can recast the dynamics as the evolution of the domain walls themselves. This picture is more complicated with a vector order parameter, but in general the dynamics can be expressed in terms of the appropriate topological defects for the dimension of the order parameter and the dimension of space.

What is found is that asymptotically the domain wall morphology is characterized by a single length scale which grows with time. This self-similar evolution is usually expressed via the dynamic scaling hypothesis, which is the statement that the correlation function has the form  $C(\mathbf{r}, t) = f(r/L(t))$ , where  $L(t)$  is the characteristic length scale of the domains. Equivalently one has for the structure function  $S(\mathbf{k}, t)$ , the Fourier transform of the correlation function,

$$S(\mathbf{k}, t) = k^{-d} g(kL(t)). \quad (1.1)$$

The structure function is directly measurable via scattering experiments, and therefore the dynamic scaling hypothesis and the growth law for  $L(t)$  can be tested. It is found that this length scale has a power law dependence on time,  $L \sim t^{1/z}$ , and that the exponent  $z$  is universal.

The universality classes of phase ordering are fairly well established. It is believed that the exponent  $z$  depends on the presence or absence of conservation laws, the dimension of the order parameter, and the range of interactions. However, in contrast to equilibrium critical phenomena, the dimension of the system appears not to matter. Also irrelevant are the relative volume fractions of the equilibrated phases and the final temperature. The accepted values for short-range interactions are  $z = 2$  for a non-conserved order parameter,  $z = 3$  for a conserved, scalar order parameter, and  $z = 4$  for conserved, vector order parameters. The latter result is believed to hold for  $d > n$ , where  $n$  is the dimension of the  $O(n)$  symmetric order parameter. Although the value of the growth exponent does not depend on the dimension of space, it is believed that the critical behavior is not generally given by a mean-field theory, and that to describe accurately the system one must take into account correlated fluctuations.

The first solid result in the study of phase ordering was the theoretical work of Lifshitz and Slyozov [10], for the case of a conserved, scalar order parameter, which describes binary alloys and fluids. They consider a quench to a concentration which is very close to one of the equilibrium concentrations. In this case the minority phase will occupy a small fraction of the volume, and the dynamics are given by isolated droplets of the minority phase interacting with a mean-field background. With this approach they demonstrated that the system evolved via self-similar coarsening and with dynamic exponent  $z = 3$ . It is now generally agreed that the value  $z = 3$  applies for all quenches with a conserved, scalar order parameter, of which the Lifshitz-Slyozov theory is the small volume fraction limit. However, apart from this original result, no fundamental theoretical derivation of the dynamical scaling hypothesis and power law domain growth has been found.<sup>2</sup> The goals in applying the renormalization group to phase ordering, then, are to put the dynamic scaling hypothesis on a firm, theoretical footing, and also to determine systematically the universality classes and the corresponding value of the dynamic exponent  $z$ .

To begin one must select a phenomenological model of the system. The two most common types are continuum Langevin equations, in which the noise strength is determined by  $T_f$ , and kinetic Ising models, with either spin-flip (Glauber) or spin-exchange (Kawasaki) dynamics, depending on the conservation law for the order parameter. A relatively new approach is that of cell dynamical systems [11], which was developed as a means of improving the efficiency of simulations, but is also argued to be as fundamental as other phenomenological models. Once a model has been selected one can proceed to apply renormalization group methods. One approach is to use a Monte Carlo renormalization group scheme [12,13]. This has been moderately successful in calculating the dynamic exponent  $z$ , although it has proven to be difficult to reach the asymptotic regime. For example, in [12] it was found that  $z = 4$  for a conserved, scalar order parameter system

---

<sup>2</sup> The Lifshitz-Slyozov result can be viewed as the limit of the volume fraction of the minority species going to zero. As discussed in [6], it appears that a small volume fraction expansion about this solution is a singular perturbation.

rather than  $z = 3$ , although it is now agreed that the latter result will hold if the true asymptotic limit is reached. There have also been analytic approaches to applying the renormalization group, in which the idea is to renormalize the equations of motion. If a  $T = 0$  fixed point is assumed to exist, then one can renormalize the Langevin equations describing a conserved, scalar order parameter system by making the argument that integrating out the short distance modes cannot introduce any singular dependence on the long wavelength modes [14]. However, this approach is still less than fundamental, as it assumes the existence of a fixed point rather than explicitly demonstrating it. At present there has been no successful, systematic derivation of a renormalization group fixed point which gives rise to the late time self-similar evolution.

Often it is useful for difficult problems to study first a one-dimensional version of the model. In equilibrium critical phenomena it is known that onedimensional systems with short-range interactions have no ordered phase. However, with power law interactions given by  $V(r) \sim -r^{-1-\sigma}$  for  $0 < \sigma \leq 1$  these systems do have a non-trivial phase transition [15]. Furthermore, it was shown that a renormalization group scheme can be implemented in the case of  $\sigma = 1$  [16,17]. Since these models exhibit non-trivial phase transitions, then they contain a two-phase region of the phase diagram and are thus suitable for studying phase ordering. The defects, or domain walls, are point objects in one dimension, which allows for simpler analytical and numerical treatment.

In chapter two we consider such a one-dimensional model, with a non-conserved, scalar order parameter and long-range interactions, and apply analytic and numerical techniques. First, we show that for long-range interactions the kinetic Ising model with Glauber dynamics is equivalent to a Langevin equation without noise terms for the evolution of the domain walls. Next we demonstrate that the dynamics of the domain walls is given by that of charges on a line, moving via interactions with other charges, and annihilating on contact. While this model is only strictly valid for  $\sigma \leq 1$ , we consider larger values of  $\sigma$  as well, in order to gain some insight towards the asymptotic evolution. From the simulations we find that for  $\sigma = 1, 2$  the behavior is consistent with the existence of an attractive



renormalization group fixed point. In particular, the asymptotic density is independent of the initial value of the density, and the density decays with a power  $t^{-1/(1+\sigma)}$ . This latter result agrees with a study of long-range interacting systems in which the dynamic scaling hypothesis was assumed, and resulting growth laws derived [18].<sup>3</sup> However, for  $\sigma = 1/2$  the simulations exhibit no convincing scaling regime from which to extract a power law growth, and, surprisingly, the asymptotic density appears to depend on the system size.

There are also indications of anomalous behavior for  $\sigma \leq 1$  from an analytic approach. A fugacity expansion of the initial conditions is developed which allows one to calculate perturbatively the function  $f(x)$  defined by the scaling relation derived in §2.2

$$n(t) = n_0 f(n_0 t^{1/(1+\sigma)}). \quad (1.2)$$

Here  $n(t)$  refers to the density and  $n_0$  is the initial density. The first order term in the expansion comes from a two-body calculation and is found for all  $\sigma$ . The second order term involves a three-body calculation, and while it cannot be computed for arbitrary  $\sigma$ , it is calculable in the case  $\sigma = 1$ . It is found that the coefficient of the second order expansion term diverges as the logarithm of the system size,  $L$ . It is also shown that for general  $\sigma \leq 1$  this coefficient will diverge as  $L \rightarrow \infty$ . One possible interpretation of this result is that the coefficients are simply system size dependent, and that the bulk limit  $L \rightarrow \infty$  cannot be taken. Another possibility is that these terms are the consequence of a non-analyticity in the function  $f(x)$ , and that a sum to all orders might restore a finite limit for  $L \rightarrow \infty$ .

We also use the fugacity expansion to study the fixed point for  $\sigma > 1$ . In particular, by taking the large  $\sigma$  limit we can calculate to third order the expansion of the scaling function  $f(x)$ , with the result

$$f(x) = 1 - 2x + 3x^2 - \frac{34}{9}x^3 + O(x^4). \quad (1.3)$$

---

<sup>3</sup> In one dimension the density of the domain walls is just the inverse of the characteristic domain size  $L(t)$  studied in [18].

We introduce a Callan-Symanzik-type  $\beta$  function for the “coupling”  $g_R = \tau^{1/(1+\sigma)}n(\tau)$ , which describes the approach to the renormalization group fixed point, and show that from the result above that

$$\beta(g_R) = \sigma^{-1} \left[ g_R - 2g_R^2 - 2g_R^3 - \frac{10}{3}g_R^4 + O(g_R^5) \right]. \quad (1.4)$$

Truncating this expansion at order  $g_R^4$  gives a zero of the  $\beta$  function  $g_R^* \approx 0.33$ . The fixed point coupling is equivalent to the amplitude of the density decay, as can be seen by the definition above. It turns out that the exact value of the fixed point coupling for large  $\sigma$  is known [19], and is given by  $g_R^* = e^{-\gamma_E}/2 \approx 0.28$ . From the fugacity expansion approach one can argue that the expansion coefficients will exhibit only weak  $\sigma$  dependence for  $\sigma > 1$ , which is confirmed by the simulations for  $\sigma = 1, 2$  in which the amplitude is found to be  $A = 0.31$ . The shortcoming of this approach is that it lacks a small expansion parameter, the analog of the  $\epsilon$  expansion in equilibrium critical phenomena, which enables the calculation of the fixed point in a controlled way.

An alternate approach is also considered in chapter two, which is a truncation scheme that exhibits naturally the attractive fixed point which describes asymptotic regime. The small density, early time limit for the two-point distribution function  $n_2(r, t)$  can be calculated via the fugacity expansion. With a heuristic truncation scheme we find a form of the two-point distribution function which is exact for small  $r$  and for  $r \rightarrow \infty$ , and is of the form

$$n_2(r, t) = n(t)^2 r^\sigma g \left( (r^{1+\sigma} + t)^{1/(1+\sigma)} \right). \quad (1.5)$$

From the large  $r$  limit of (1.5) it follows that  $g(x) \sim x^{-\sigma}$  for large  $x$ , which then gives the large  $t$  limit also. The asymptotic form of the distribution function can be used to derive an equation for the density

$$\frac{dn}{dt} = -\frac{2}{1+\sigma} n^2 t^{-\sigma/(1+\sigma)}, \quad (1.6)$$

which is consistent with the scaling solution  $n \sim t^{-1/(1+\sigma)}$ . Furthermore, by assuming the truncation scheme is valid for all  $t$  the evolution of the density can be found in terms of the initial correlations. That is,

$$\frac{dn(\tau)}{d\tau^{1/(1+\sigma)}} = 2n_2(r = \tau^{1/(1+\sigma)}, t = 0). \quad (1.7)$$

This is tested numerically by considering an initial distribution which contains zeros in the distribution function  $n_2(r, 0)$ , with results in qualitative agreement with (1.7).

In §2.7 we discuss recent simulations of this model by Rutenberg and Bray, which have been conducted in the time since the work presented in chapter two.

### 1.3. REACTION-DIFFUSION SYSTEMS

A number of chemical processes are known to be diffusion-controlled reactions, which means that reaction is sufficiently short-ranged that the constituents rely on diffusion to be brought together. Some examples include radiolysis in liquids, which produces electrons and cations which then diffuse and recombine [20], solutions of fluorophores and quenchers in inert solvents [21], and a large variety of chemical reactions in gels [22]. These reactions exhibit in lower dimensions what is termed anomalous kinetics, where the time dependence of the reactant densities cannot be derived from simple rate equations. This is now understood to be the consequence of non-trivial fluctuations in the density. General reviews of these phenomena are given in [23,24].

Recently there has been interest in studying systems where the reactants are completely segregated initially. The subsequent reactions are confined to a reaction zone, which can be studied experimentally [25], and which has interesting scaling behavior with new exponents. These reaction fronts also provide a starting point for studying pattern forming systems. For example, it has been demonstrated in experiments that reaction-diffusion processes are capable of producing Turing structures, which are stationary patterns in the concentration fields [26,27]. Unlike hydrodynamic pattern forming systems,

such Rayleigh-Bénard convection cells and Taylor-Couette flows, these patterns have a characteristic wavelength which is not set by the geometry of the system.

The models for studying these systems are generally quite simple. The examples mentioned above are two-species reactions, which are modeled with two types of particles,  $A$  and  $B$ , moving via diffusion, and reacting upon contact to form an inert particle. There are a number of variations: particles in a continuum which react within a certain capture radius  $r_c$ , or particles on a lattice, with or without multiple occupancy allowed, which react when they meet on a single lattice site, and so on. One hopes to extract from these models features which are universal, and can therefore be related to real systems.

The simplest possible reaction-diffusion system is the reaction  $kA \rightarrow \emptyset$ . Here there is just one species of particle, and the reaction occurs whenever  $k$  particles meet. This model has less general applicability than the two-species reaction, although it can be related to other non-equilibrium systems. For example  $A + A \rightarrow \emptyset$  is equivalent to the phase ordering of a non-conserved scalar order parameter in one dimension, and  $kA \rightarrow \emptyset$  is related to one-dimensional models of monolayer  $k$ -mer deposition. For our purposes the one-species reaction provides a simplified starting point for developing the renormalization group techniques.

The  $A + B \rightarrow \emptyset$  and the  $kA \rightarrow \emptyset$  systems are similar in that for both there exists an upper critical dimension  $d_c$ . For  $d > d_c$  one can argue that the fluctuations in the density are irrelevant, in which case mean-field type rate equations are applicable. For  $d < d_c$  the fluctuations affect the decay rate of the density, producing slower dynamics than that predicted by the rate equation. However, apart from the common feature of an upper critical dimension, the one- and two-species reaction are quite different. For example, it is found from scaling arguments that the upper critical dimension of the  $kA \rightarrow \emptyset$  reaction is  $d_c = 2/(k - 1)$ . For  $d < d_c$  the asymptotic density goes as  $n \sim A_k t^{-d/2}$  with an amplitude which is independent of the details of the initial state. In contrast, scaling arguments for the  $A + B \rightarrow \emptyset$  reaction predict fluctuation dependence for  $d < d_c = 4$  (as opposed

to  $d_c = 2$  for  $A + A \rightarrow \emptyset$ ), with the density  $n \sim At^{-d/4}$ . In this case the amplitude is determined entirely by the fluctuations present in the initial conditions. The origin of the dissimilarity of these systems is the conserved mode present in the two-species reaction: the number difference  $n_A - n_B$  is unaffected by  $A + B \rightarrow \emptyset$ . As is usually the consequence of a conserved mode, the two-species reaction has slower dynamics.

To apply RG techniques to these systems it is useful to work with a field theoretic version of the problem. The dynamics are defined by a master equation, which can then be mapped to a field theory, as will be shown in chapter three. The mapping is a two-step process, where the master equation is first recast in terms of a second quantized representation, which is in turn mapped to a field theory by use of the coherent state representation. This procedure involves no coarse-graining, unlike more phenomenological approaches, and so the coupling constants of the field theory are directly related to the rate constants of the microscopic system defined by the master equation. There exists a general review article on this procedure [28], but we present a full derivation for completeness and to establish our notation.

### *One-Species Reaction*

In chapter four we study the problem of the one-species reaction with homogeneous random initial conditions. The first observation which can be made from the corresponding field theory is that there is no dressing of the propagator, and therefore no anomalous dimension. This is due to the property of the interaction vertices that the number of propagators never increases with time. The lack of anomalous dimension has the consequence that simple scaling arguments are probably sufficient for deriving the exponent of the density decay. Secondly, from power counting it is found that the coupling  $\lambda_0$ , which is directly related to the reaction rate constant in the master equation, is relevant for dimensions  $d < d_c = 2/(k - 1)$ . Furthermore, it is shown that the coupling can be

renormalized exactly to all orders and that it flows to an order  $\epsilon = d_c - d$  fixed point for large times.

From the field theory it is possible to calculate the density and other quantities as expansions in powers of the initial density  $n_0$ , and the coupling  $\lambda_0$ . Under renormalization group flows the coupling goes to an order  $\epsilon$  fixed point for  $d < d_c$ , but the initial density is a relevant parameter for all  $d$ , and flows to infinity for large  $t$ . Therefore a valid perturbation theory must include sums over all powers of  $n_0$ , grouped in such a way as to give a finite expansion in powers of  $\lambda_0$ . In chapter four we show how identify and to evaluate these groups of sums. The result is a formalism which enables us to calculate perturbatively the density and correlation functions of the system for general  $k$ . For example, we find that the density for  $d < d_c$  is given by  $n \sim A_k(Dt)^{-d/2}$  with

$$A_2 = \frac{1}{4\pi\epsilon} + \frac{2\ln 8\pi - 5}{16\pi} + O(\epsilon) \quad (1.8)$$

$$A_3 = \left( \frac{\sqrt{3}}{12\pi\epsilon} \right)^{1/2} + \frac{9\sqrt{2\pi}}{64} + O(\epsilon^{1/2}), \quad (1.9)$$

and for  $d = d_c$

$$n(t) \sim \left( \frac{(k-2)!}{4\pi k^{1/(k-1)}} \right)^{1/(k-1)} \left( \frac{\ln t}{Dt} \right)^{1/(k-1)}, \quad (1.10)$$

where  $D$  is the usual diffusion constant. We are also able to calculate various universal quantities for this system. These include the connected correlation function, the fluctuations in total particle number, and the fluctuations in particle number in a small volume  $v$ .

The density amplitude for  $k = 2$  can be compared to an exact solution for a particular model in  $d = 1$  of  $A_2 = (8\pi)^{-1/2} \approx 0.20$  [29]. Putting  $\epsilon = 1$  in our expansion yields  $A_2 = 0.08 + 0.03 + \dots$ . The agreement is less than satisfactory, indicating that the  $\epsilon$  expansion will not be quantitatively accurate to  $\epsilon = 1$ . However, the  $\epsilon$  expansion provides the only systematic derivation of universality and scaling.

### *Two-Species Reaction*

The field theory for the reaction  $A + B \rightarrow \emptyset$  is developed in chapter three. In chapter five we use this field theory to study the two-species system with an initial state of randomly distributed  $A$  and  $B$  particles with equal densities. As in the one-species case, we find that there is no anomalous dimension, and so the usual scaling arguments are likely to give the correct exponents.

By performing the same power counting as before, one finds the couplings are relevant for  $d < 2$ , which is the same critical dimension as the one-species reaction for  $k = 2$ . Furthermore, the coupling can still be renormalized exactly, differing from the previous case only by a factor of two. However, the two-species reaction exhibits anomalous kinetics for  $d < 4$ . This can be understood from the field theory to be the consequence of initial terms which are generated by the irrelevant bulk couplings. These initial terms are relevant for  $d < 4$ . Due to the irrelevance of the coupling, we can construct for  $2 < d < 4$  an effective field theory which is valid for large times, in which only the relevant bulk and surface terms remain. This effective field theory is equivalent to the classical equations of motion

$$\begin{aligned}\partial_t a &= \nabla^2 a - \lambda_{\text{eff}} ab \\ \partial_t b &= \nabla^2 b - \lambda_{\text{eff}} ab,\end{aligned}\tag{1.11}$$

where  $\lambda_{\text{eff}}$  is some effective coupling constant. These equations are often assumed, incorrectly, to be the continuum limit of the master equation for all values of the spatial dimension.

The densities  $\langle a \rangle = \langle b \rangle$  can be calculated exactly from the effective theory, with the result

$$\langle a \rangle = \frac{\Delta^{1/2}}{\pi^{1/2}(8\pi)^{d/4}}(Dt)^{-d/4}.\tag{1.12}$$

The parameter  $\Delta$  is a measure of the strength of the initial fluctuations in the field  $\psi$ , due to the randomness in the initial state. From central limit arguments one finds  $\Delta = n_0$ , the initial density of  $A, B$  particles. However, these arguments are based on the assumption

that the equations (1.11) apply from  $t = 0$ , rather than just at late times. Using the field theory for  $2 < d < 4$  we can show that there are corrections to this result, and that instead  $\Delta = n_0 + Cn_0^{d/2} + \text{higher order terms}$ . These correction terms could become quite large for an initial state of a nearly full lattice in which only single occupancy is allowed, as is often used in simulations. This would explain why a recent numerical study found that the amplitude was not proportional to  $\sqrt{n_0}$  [30], as they expected it would be. In other simulations, where it was attempted to keep to the low initial density limit, it was found that the amplitude was proportional to  $\sqrt{n_0}$  [31].

The result (1.12) was previously derived by Toussaint and Wilczek [31], with  $\Delta = n_0$ . However, in their calculation they made the assumption that the particles become completely segregated at late times. That is, they assume that asymptotically there will only be either  $A$  or  $B$  particles present in a given region. Rather than just assuming segregation, we are able to demonstrate that it occurs for  $d < 4$  by using the field theory approach. It should be noted, though, that these amplitudes are not universal. The strength of the initial fluctuations in  $\psi$  will depend, for example, on whether one considers a lattice model with single occupancy or multiple occupancy, and so on.

When  $d \leq 2$  the coupling flows to an order  $\epsilon$  fixed point, as was found for the one-species reaction. However, the field theory for  $A + B \rightarrow \emptyset$  is sufficiently more complicated that we are unable to derive a systematic expansion in powers of the coupling, as we could in the one-species case. We present an argument that the amplitude found for  $d > 2$  is the leading order term in an  $\epsilon$  expansion for  $d < 2$ .

Also studied in chapter five are the reaction zones formed in two-species reactions. The regions where the reactions occur, which are the interfaces between domains of  $A$  particles and  $B$  particles, have a finite width. This width  $w$  grows in time, but more slowly than do the domains themselves, which is consistent with the earlier statements about asymptotic segregation. What is found is that this width grows as a power law in time with a non-trivial exponent, that is, an exponent which is not determined by the



bulk-density,  $\langle a \rangle^{-1/d} \sim (\text{length}) \sim t^{1/4}$  for  $d < 4$ . Another non-trivial length scale in these reaction zones can be found from the characteristic nearest neighbor distance  $\ell_{rz}$ . This latter quantity can be measured directly in simulations, utilizing the fact that if a particle has as its nearest neighbor an unlike particle, then they are in the reaction zone.

When  $d > 2$  then the irrelevance of the coupling implies that the rate of reaction is proportional to the product of the densities  $ab$ , which is essentially the content of equations (1.11). From this result the exponents for  $w$  and  $\ell_{rz}$  can be derived, but when  $d \leq 2$  one can no longer use this method. For  $d \leq 2$  the renormalization of the coupling implies that these lengths cannot depend on  $\lambda_0$ , since it flows to an order  $\epsilon$  fixed point. This, it can be shown, is sufficient for determining the exponents. The results for the width are

$$w \sim \begin{cases} t^{(d+2)/4(d+1)} & d \leq 2 \\ t^{(d+2)/12} & 2 < d < 4 \end{cases} \quad (1.13)$$

and for the nearest neighbor distance

$$\ell_{rz} \sim \begin{cases} t^{(d+2)/4(d+1)} & d \leq 2 \\ t^{(d+2)/6d} & 2 < d < 4. \end{cases} \quad (1.14)$$

The exponents for  $\ell_{rz}$  are consistent with numerical results for  $d = 1, 2, 3$  [30,32].<sup>4</sup> The general technique for deriving these exponents is by comparison to the reaction zone formed in the steady state by currents of  $A$  and  $B$  particles directed towards each other. A similar analogy can be constructed for a system with a single reaction zone, created by inhomogeneous initial conditions. That is, if in some direction  $x$  only  $A$  particles are present for  $x < 0$  and only  $B$  for  $x > 0$ , then a time-dependent reaction zone is established. The same quantities  $w$  and  $\ell_{rz}$  can be studied, with the results

$$w \sim \begin{cases} t^{1/2(d+1)} & d \leq 2 \\ t^{1/6} & d > 2 \end{cases} \quad \ell_{rz} \sim \begin{cases} t^{1/2(d+1)} & d \leq 2 \\ t^{2/3d} & d > 2. \end{cases} \quad (1.15)$$

The exponents for  $d \leq 2$  are in reasonable agreement with numerical studies [33].

---

<sup>4</sup> We disagree with the analysis of the  $d = 3$  case in these references.

It is usually assumed, for two-species reactions, that the diffusion constants for  $A$  and  $B$  particles are the same. This has the result, as can be seen in equations (1.11), that the field  $a - b$  satisfies the diffusion equation. When  $D_A \neq D_B$  then this is no longer true, which complicates the analysis. We consider the case of unequal diffusion constants, and find from the field theory that for  $2 < d < 4$  the density is given by

$$\langle a \rangle = \frac{\sqrt{\Delta Q(d, \delta)}}{\pi^{1/2} (8\pi)^{d/4}} (\bar{D}t)^{-d/4}, \quad (1.16)$$

where  $\bar{D} = (D_A + D_B)/2$  and  $\delta = (D_A - D_B)/(D_A + D_B)$ . The function  $Q(d, \delta)$  has the form

$$Q(d, \delta) = 4 \frac{(1 + \delta)^{2-d/2} + (1 - \delta)^{2-d/2} - 2}{\delta^2 (d - 2)(d - 4)}, \quad (1.17)$$

and is finite for all  $-1 \leq \delta \leq 1$ ,  $d < 4$ . As argued before, it is plausible that the answer for  $d > 2$  gives the leading order term for an  $\epsilon$  expansion when  $d \leq 2$ . However, this amplitude, just as in the equal diffusion constant case, is not universal.

## Chapter 2. Phase Ordering of One-Dimensional Systems with Long-Range Interactions

In this chapter we consider the dynamics of phase ordering for a one-dimensional system with power law interactions  $V(r) \sim r^{-1-\sigma}$ . Recently interest has been directed towards the problem of long-range interactions in phase ordering [18,19,34]. By assuming the dynamic scaling hypothesis and using energy dissipation arguments, Bray and Rutenberg find the growth law exponent to depend on the value of  $\sigma$  [18,19]. In particular, they argue that, in the case of a non-conserved scalar order parameter system, the dynamic exponent  $z = 1 + \sigma$  for  $\sigma < 1$ , and that  $z = 2$  with logarithmic corrections for  $\sigma = 1$ . For  $\sigma > 1$  they recover the traditionally accepted exponent  $z = 2$  for systems with short-range interactions [35–37]. We begin our treatment of the problem by a discussion of the phenomenological model for the system.

### 2.1. THE MODEL

In the following section we present a low-temperature mapping from the long-ranged Ising Hamiltonian with spin degrees of freedom to a Hamiltonian with domain wall degrees of freedom. The dynamics are introduced to the system via Langevin equations without a

noise term. This is shown to be equivalent to Glauber dynamics when  $\sigma \leq 1$ . Finally, we discuss related models which are motivated by the simplifications they offer.

Consider the one-dimensional Ising Hamiltonian

$$H = -J \sum_{i < j} s_i s_j V(x_i - x_j) \quad (2.1)$$

where

$$V(x_i - x_j) = |x_i - x_j|^{-(1+\sigma)}. \quad (2.2)$$

and the lattice spacing  $a = 1$ . It is known [15] that this system has a phase transition with some non-zero  $T_c$  when  $0 < \sigma \leq 1$ , and so there is a two-phase equilibrium region for  $T < T_c$ . Since we are interested in the dynamics of the domain walls, which are points objects in this one-dimensional case, it is convenient to map this Hamiltonian with spin degrees of freedom to one with domain wall degrees of freedom via a lattice equivalent of integration by parts. The resultant Hamiltonian is (apart from surface terms)

$$H = J \sum_{i < j} s'_i s'_j U(x_i - x_j) \quad (2.3)$$

where the lattice derivatives are defined as  $s'_i = s_{i+1} - s_i$ , and the function  $U(x_i - x_j)$ , the lattice equivalent of the second anti-derivative of  $V(x_i - x_j)$ , is defined by

$$V(r) = U(r+1) - 2U(r) + U(r-1). \quad (2.4)$$

The boundary conditions are chosen so that  $U(r)$  contains no constant or linear pieces, with the solution for  $r \gg 1$

$$U(r) = \begin{cases} \frac{|r|^{1-\sigma}}{\sigma(1-\sigma)} + O(1/r) & \sigma \neq 1 \\ -\log|r| + O(1/r) & \sigma = 1. \end{cases} \quad (2.5)$$

Since the limit of zero lattice spacing is well-behaved, and the important contributions from the long-ranged interactions should be arising at large  $r$ , the late time dynamics of the theory should be unaffected by taking the continuum limit.

The  $s'_i$  are zero everywhere neighboring spins are aligned, and equal to  $\pm 2$  at the domain boundaries. Therefore the sum over spins can be replaced by a sum over the positions of the domain walls. The sign, or charge, of the domain walls will be alternating, with the consequence that nearest neighbors will attract, next-nearest neighbors will repel, and so on. Absorbing the coupling constant  $J$  into a rescaling of the spin results in the Hamiltonian

$$H = \sum_{i < j} (-1)^{i+j} U(x_i - x_j). \quad (2.6)$$

To add dynamics to this Hamiltonian we use Langevin-type equations of motion, introducing a kinetic coefficient  $\Gamma$ .

$$\frac{dx_i}{dt} = -\Gamma \frac{\partial H}{\partial x_i}. \quad (2.7)$$

We neglect any possible noise term, for reasons which are explained below. There is an additional rule to the dynamics. When two charges meet each other they annihilate, and are both removed from the system. In the original spin picture this corresponds to an island of up spins shrinking to zero in a background of down spins, or vice versa.

These equations of motion for the domain walls are equivalent, for  $\sigma \leq 1$  and low temperatures, to using Glauber dynamics for the spins [38]. To see this, consider a Glauber dynamical Ising model with temperature  $\beta$ , lattice spacing  $a$ , and characteristic free spin flip rate  $\alpha$ . The flip rates for interacting spins are found via detailed balance:

$$\frac{w(+)}{w(-)} = \exp(-\beta \Delta E) \quad (2.8)$$

where  $w(-)$  and  $w(+)$  are the rates for flips down and up, respectively, and  $\Delta E = E_+ - E_-$  is the energy difference of the spin positions. The parameter range of interest is where  $w(-)$  and  $w(+)$  are nearly equal to  $\alpha$ , or  $\beta \Delta E$  is small.

Consider an isolated pair of domain walls separated by distance  $\ell$  as shown in fig. 2.1. The domain wall on the left can move through either a spin A flip up or spin B flip down. If it is assumed that the  $w(+)$  in the neighborhood of the domain wall are equal to  $w(A+)$ ,

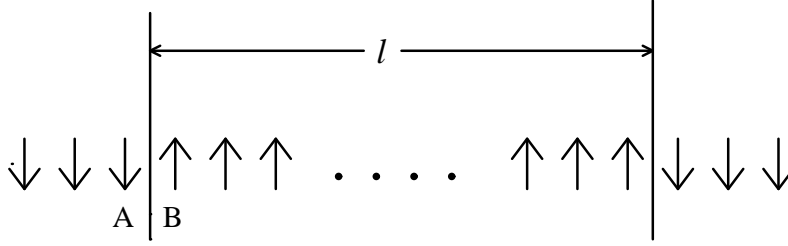


FIGURE 2.1. An isolated pair of domain walls separated by a distance  $\ell$ . The domain wall on the left can move via a flip of spin A or spin B. The difference in the up and down flip rates gives rise to a drift velocity.

and the  $w(-)$  are equal to  $w(B-)$ , then the motion of the wall will be a random walk superimposed over a slight drift with velocity

$$\begin{aligned}
 v_d &= a [w(-) - w(+)] \\
 &= aw(-) [1 - e^{-\beta\Delta E}] \\
 &= a\alpha\beta\Delta E + O((\beta\Delta E)^2).
 \end{aligned} \tag{2.9}$$

The energy difference  $\Delta E = J[U(\ell + a) - U(\ell)] \simeq aJ(dU/d\ell)$  if  $\ell \gg a$ . If the domain wall position is labeled by  $x$  (so  $d\ell/dx = -1$ ), then the drift velocity equation is

$$\frac{dx}{dt} = -a^2\alpha\beta J \frac{\partial U}{\partial x}. \tag{2.10}$$

This can be generalized to systems of multiple domain walls by considering  $U(x - y)$  to be a pairwise interaction energy which carries with it the appropriate sign for attractive and repulsive interactions. By comparison to the original Langevin equations one can identify the kinetic coefficient  $\Gamma = a^2\alpha\beta J$ .

Thus far the possibility of domain wall pair creation has been neglected. The energy for pair creation at distances of order  $a$  is small, and even at low temperatures will occur frequently. However, the energy required to create a pair separated at a macroscopic distance  $\ell'$  is quite large relative to the energy required to move a domain wall a distance

$a$  in the presence of another domain wall at  $\ell$ . That is, for large  $\beta$  it is possible to satisfy simultaneously  $\beta JU(\ell') \gg 1$  and  $a\beta J(dU/d\ell) \ll 1$  for finite  $U, dU/d\ell$ . The next question to address is which process, the random walk or the deterministic drift, dominates the dynamics at late times.

The characteristic length of a random walk at time  $t$  is

$$\begin{aligned}\ell_{rw} &= (\text{number of steps} \times a)^{\frac{1}{2}} \\ &= (a\alpha t)^{\frac{1}{2}}.\end{aligned}\tag{2.11}$$

Since  $\alpha \propto \Gamma T$  then

$$\ell_{rw} \sim T^{\frac{1}{2}} t^{\frac{1}{2}}.\tag{2.12}$$

There is also a length scale determined by the drift velocity which grows with time as

$$\ell_d \sim t^{1/(1+\sigma)},\tag{2.13}$$

which is found from the equations of motion (see §2.2). The time dependence of these length scales determines which process controls the dynamics. When  $\sigma > 1$  then  $\ell_{rw} > \ell_d$  for large  $t$ , so a pair of charges can escape annihilation via a random walk. This is the dynamical picture of the disordered phase, as was found in the nearest neighbor Ising model [39]. When  $\sigma = 1$  and  $T < T_c$  then  $\ell_d > \ell_{rw}$ , which means that a pair of charges can no longer escape annihilation. For  $\sigma < 1$  also the drift dominates the dynamics at low temperatures. While this argument for  $\sigma < 1$  would suggest that the drift dominates for all  $T$ , it ignores higher order screening effects which renormalize  $J$ , causing the random walk effects to dominate above the critical point. When the drift does dominate, the presence of the random walk should cause at most a finite renormalization of the kinetic coefficient  $\Gamma$ . To summarize, the Glauber model of dynamics is equivalent to the Langevin equations without noise for  $\sigma \leq 1$  and  $T < T_c$ , and otherwise is equivalent to domain walls undergoing random walks.

## *Related Models*

While  $\sigma \leq 1$  is the physically interesting range, the model, without noise, can be extended to values of  $\sigma > 1$ . If the late time dynamics is described by some renormalization group fixed point, then this fixed point might be qualitatively similar for all  $\sigma$ . For example, we find in simulations that, to within our accuracy, the length scale given by the density grows with power law  $t^{1/(1+\sigma)}$  for both  $\sigma = 1$  and  $\sigma = 2$ . In §2.4 we show that the dynamical equations simplify in the large  $\sigma$  limit of this model. From this limit one can then work back to study the behavior of models with smaller values of  $\sigma$ .

A similar but more simple system than the Ising model is the  $Q$ -state Potts model in the limit of  $Q \rightarrow \infty$ . This model can be mapped to an interacting defect Hamiltonian which has the same power law interactions as the Ising model, but only between nearest neighbors. All other pairs are non-interacting, which makes this system much easier to simulate on the computer. The annihilation rules are modified as well, in that a pair of defects annihilate to leave behind a single defect. A derivation of the properties of this model is given in appendix 2.A.

## 2.2. SCALING ARGUMENTS AND NUMERICAL RESULTS

The initial conditions for the dynamical system are drawn from some distribution. Measurements of the system, such as the density  $n(t)$ , or the two-particle distribution function  $n_2(r, t)$ , are defined to be averaged over this distribution. One could use a thermal distribution corresponding to  $T_0$ , the pre-quench temperature of the system. Instead we use an initial distribution where charges are placed randomly with some initial density  $n_0$ , which for  $n_0 = (2a)^{-1}$  corresponds to the system being prepared at  $T = \infty$  prior to quenching. For values of  $n_0 < (2a)^{-1}$  the random distribution is no longer representative of a thermal distribution, but this approach enables us to explore the sensitivity to initial conditions without the complication of initial correlations.



To write scaling functions for the quantities such as the density  $n(t)$ , we consider all the dimensionful parameters in the model. The initial density  $n_0$  gives a length scale, as does the system size  $L$  for finite systems. The lattice spacing has been taken to zero. There is one other length scale, given by time. One way to define this length is by the range over which an isolated pair of charges will annihilate in time  $t$ . For a pair of charges separated by some distance  $\ell$  the equations of motion can be written as a single differential equation

$$\frac{d\ell}{dt} = -2\Gamma\ell^{-\sigma} \quad (2.14)$$

which has the solution

$$\ell(t)^{1+\sigma} = \ell(0)^{1+\sigma} - 2(1+\sigma)\Gamma t. \quad (2.15)$$

By setting  $\ell(t) = 0$  one finds the time to annihilation as a function of the initial distance  $\ell$  is

$$t = \frac{1}{2(1+\sigma)\Gamma} \ell^{1+\sigma}. \quad (2.16)$$

We rescale the time

$$2(1+\sigma)\Gamma t \rightarrow t \quad (2.17)$$

so that the length scale associated with time is

$$\ell_t = t^\zeta \quad (2.18)$$

where

$$\zeta = \frac{1}{1+\sigma} \quad (2.19)$$

is introduced for notational convenience. This length scale given by  $t^\zeta$ , as well as those of  $L$  and  $n_0^{-1}$  are the only dimensionful quantities in the system. Therefore

$$n(t) = n_0 \Phi(n_0 t^\zeta, L t^{-\zeta}). \quad (2.20)$$

Generally it is assumed that the density does not depend on the system size, in which case we get the stronger scaling law

$$n(t) = n_0 f(n_0 t^\zeta). \quad (2.21)$$

### *Simulations for $\sigma \geq 1$*

To determine which of these scaling functions apply, we first turn to numerical simulations (for details, see §2.6). By varying the initial number of charges  $N_0$  and system size  $L$  such that the initial density  $n_0$  is unchanged, the system size dependence of the model can be directly probed. For  $\sigma = 2$  these plots superpose, shown in fig. 2.2, implying no system size dependence. For  $\sigma = 1$  we find a slight system size dependence (fig. 2.3) wherein the smaller systems drop below the scaling curve at late  $t$ .

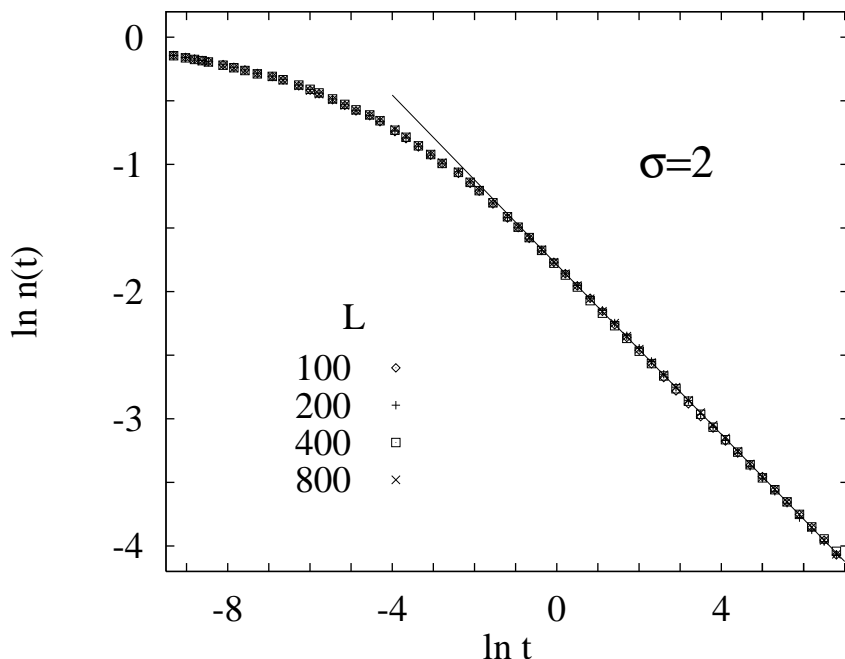


FIGURE 2.2. Simulations for  $\sigma = 2$ , shown on a log-log plot. The system sizes used are  $L = 100, 200, 400$ , and  $800$ , and the initial density is fixed at  $n_0 = 1$ . The data shows no system size dependence. The power law  $n \sim t^{-1/3}$  is plotted as a visual reference, and is in good agreement with the data. The error bars for the data are smaller than the points plotted.

We also measure the time dependence of the density for  $\sigma = 2$ , and find that it is consistent with the  $\sigma < 1$  prediction of  $n(t) \sim t^{-\zeta}$  for large  $t$  [18]. This result and the

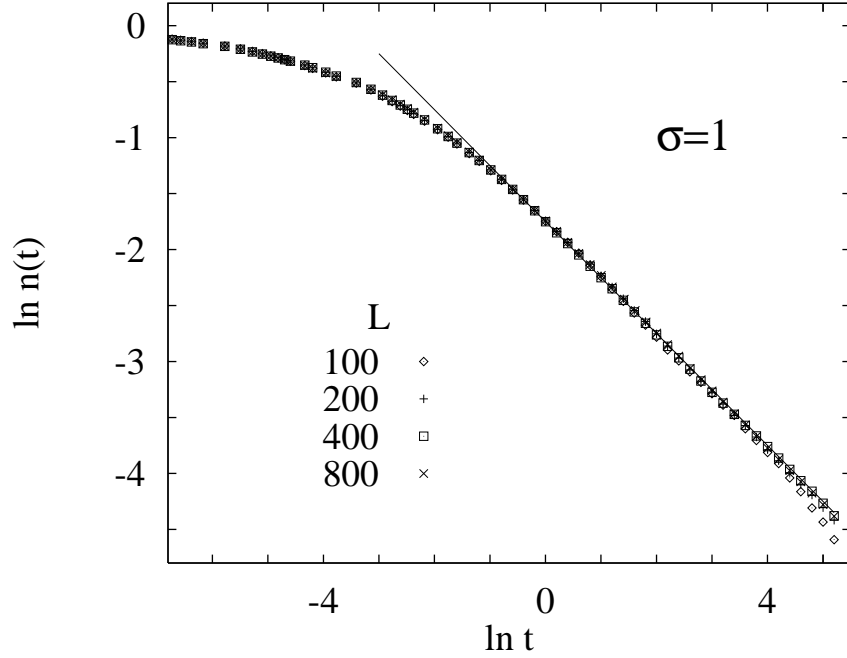


FIGURE 2.3. Simulations for  $\sigma = 1$ . The same range of system sizes are used as in fig. 2.2. The data for smaller  $L$  values exhibits slight system size dependence. The power law  $n \sim t^{-1/2}$  is plotted as a visual reference. The statistical error bars are smaller than the points plotted.

scaling form of the density (2.21) have the corollary that  $n(t)$  is independent of  $n_0$ . That is, since  $f(x) = Ax^{-1}$  for large  $x$ , then

$$n(t) \sim n_0 \frac{A}{n_0 t^\zeta} = At^{-\zeta}. \quad (2.22)$$

We can plot the same data shown in fig. 2.2, but rescaled so all the runs have the same system size, but different initial densities. In fig. 2.4 we see that the plots converge to the same function asymptotically. We propose that the lack of dependence on the initial length scale may be a general feature of the late time dynamics. This is suggestive of  $T_0$  independence for initial conditions corresponding to thermal distributions.

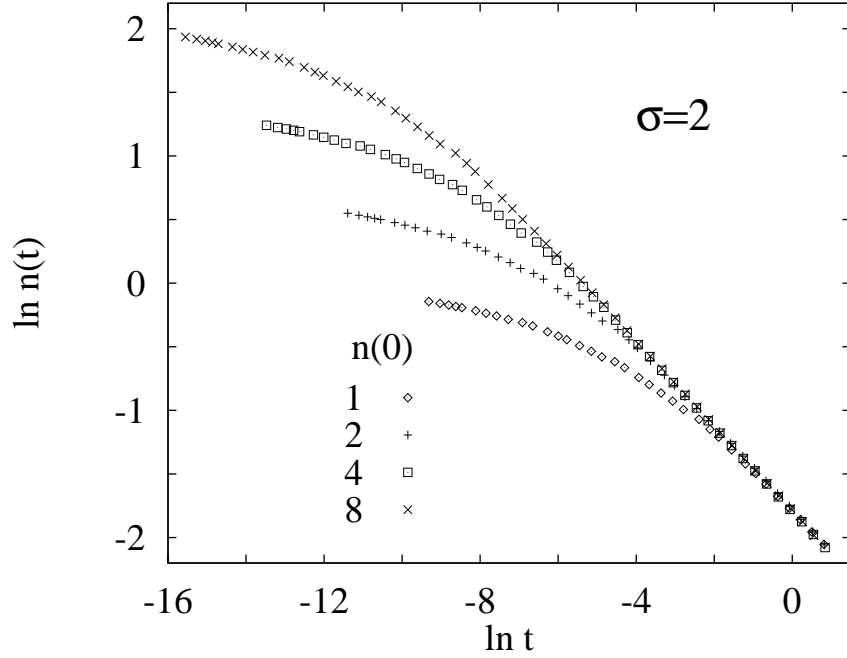


FIGURE 2.4. The same data for  $\sigma = 2$  as shown in fig. 2.2, but rescaled so that  $L = 100$  and the initial density  $n_0 = 1, 2, 4$ , and  $8$ . The curves collapse to a single function, implying the system is independent of the initial density at late times.

#### *Anomalous Behavior for $\sigma = 1/2$*

For the case of  $\sigma = 1/2$  we find that the expected power law behavior of  $n(t) \sim t^{-\zeta}$  is not observed. The simulations, shown in fig. 2.5, exhibit less than convincing power law behavior, and the density decays with an exponent of at least  $-1/z = -0.75$ . From the scaling forms (2.20) and (2.21) it follows that this implies either a dependence on  $n_0$  at late times, or dependence the system size  $L$ , or both. The data indicates a fairly strong  $L$  dependence.

These simulations are quite difficult. We attempted to reproduce periodic boundary conditions by including interactions wrapped around the system, up to some long range cutoff. For  $\sigma = 1/2$  the system is more sensitive to the cutoff than in the previous cases, and requires inclusion of many more replicas to simulate periodic boundary conditions (for

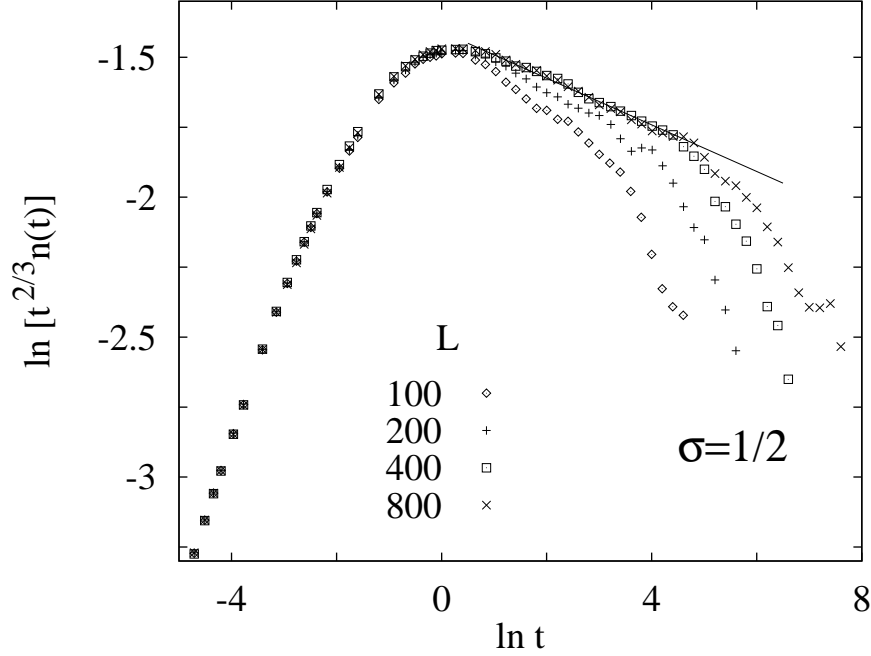


FIGURE 2.5. Simulations for  $\sigma = 1/2$ . The initial density is fixed at  $n_0 = 1$ , and the system size varies from  $L = 100$  to  $800$ . On the vertical axis is plotted  $\ln t^{2/3}n$ , which should be a constant in the scaling regime. The data shows strong system size dependence, and no range over which the density has the expected  $t^{-2/3}$  power law dependence. The line drawn represents  $n \sim t^{-0.75}$ . The error bars for the  $L = 800$  data are smaller than the size of the points plotted up to  $\ln t = 4$ .

a discussion of our methods see §2.6). We were unable to average over as many realizations of the system, and as a consequence the statistical error bars in the numerical results are appreciable toward the later times. The data is too imprecise to determine whether the system is independent of the initial density, as was shown for  $\sigma = 2$  in fig. 2.2.

#### $Q \rightarrow \infty$ Potts Model

We have also simulated the  $Q \rightarrow \infty$  Potts model for values of  $\sigma = 1/2$  and  $2$ , and found that the naive result  $n \sim t^{-\zeta}$  is consistent with the data for both values of  $\sigma$ . The data is

shown in fig. 2.6. One might expect to see different behavior from the Ising system, since in the Potts case there is no need to include multiple wrappings in the interactions. For periodic boundary conditions the only requirement is to include the interaction between the first and last charge.

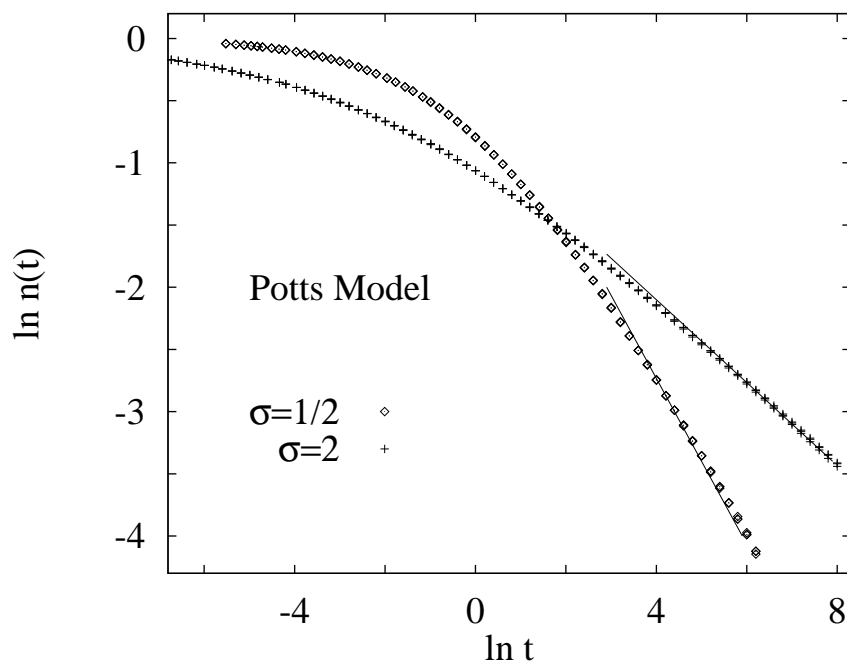


FIGURE 2.6. Simulations of the  $Q \rightarrow \infty$  Potts model for  $\sigma = 1/2$  and  $\sigma = 2$ . The lines for both data sets correspond to the  $n \sim t^{-\zeta}$  curves. For both values of  $\sigma$  the initial density  $n_0 = 1$  and the system sizes  $L = 100, 300$ , and  $1000$  are used. The data superposes very well for the different system sizes.

### *Heuristic Argument for Asymptotic Density*

We now present a heuristic argument for the lack of dependence on the initial density, which holds even when the system shows  $L$  dependence. Consider a system which has

evolved some very short time  $\delta t$ . Then

$$\begin{aligned} n(\delta t) &= n_0 \Phi(n_0 \delta t^\zeta, \delta t^\zeta / L) \\ &= n_0 - 2n_0^2 \delta t^\zeta + O(\delta t^{2\zeta}) \end{aligned} \tag{2.23}$$

where  $x = n_0 t^\zeta$ ,  $y = t^\zeta / L$ , and the coefficient of the  $\delta t^\zeta$  term,  $\partial \Phi(0, 0) / \partial x = 2$ , is found in §2.4. Also in §2.4 we show that there can be no  $L$  dependence until at least order  $n_0^3$ , so  $\partial \Phi(0, 0) / \partial y$  is zero. In this short time  $\delta t$  the system will build up correlations, but primarily at short distances. This short distance information is quickly leaving the system via annihilation. We assume that although there are long-distance correlations building up, they, nevertheless, depend on only one length scale, given by  $n(t)$ . This assumption is expressed in terms of (2.20) by taking  $n_0 \rightarrow n(\delta t)$  and  $t \rightarrow t - \delta t$ , so that

$$n_0 \Phi(n_0 t^\zeta, t^\zeta / L) = n(\delta t) \Phi(n(\delta t)(t - \delta t)^\zeta, (t - \delta t)^\zeta / L). \tag{2.24}$$

If we expand the right hand side of the equation to order  $\delta t^\zeta$  ( $\zeta < 1$ ) then

$$n(t) = n_0 \Phi - 2\delta t^\zeta n_0^2 \Phi - 2\delta t^\zeta n_0^2 x \frac{\partial \Phi}{\partial x}. \tag{2.25}$$

Setting the  $O(\delta t^\zeta)$  term to zero gives the differential equation

$$x \frac{\partial \Phi}{\partial x} = -\Phi \tag{2.26}$$

which has the solution

$$\Phi(x, y) \sim g(y) x^{-1}. \tag{2.27}$$

This argument predicts that the late time behavior will exhibit lack of dependence on  $n_0$ , even though it may depend on  $L$  through  $g(y)$ . The form of the function  $g(y)$  is unspecified, and may play a direct role in the asymptotic time dependence.

The original argument which led to equation (2.24) is difficult to make rigorous. The result of the calculation can only be true for asymptotically late times. The short distance correlations take some time to leave the system before the long-distance correlations dominate the dynamics.

### 2.3. RENORMALIZATION GROUP APPROACH

The dynamics of the system, for  $\sigma = 2$  at least, appears to be scale invariant at late times. That is, evolving the system from time  $t_1$  to  $t_2$ , where both times are chosen from the late time regime, is the same as rescaling the system at  $t_1$  by a factor of

$$b = \left(\frac{t_2}{t_1}\right)^\zeta. \quad (2.28)$$

Stated another way, the time dependent domain wall probability distribution is invariant under a rescaling of the system that includes the length scale of time (but not the initial length scale). The numerical data for the density is consistent with this presumed scale invariance, since  $n(t) = At^{-\zeta}$  is preserved under rescaling  $n \rightarrow n/b$  and  $t \rightarrow tb^{1/\zeta}$ .

This scale invariance motivates an analogy to a second order critical point in equilibrium statistical mechanics, as discussed in chapter one, where renormalization group methods are applicable [40]. To describe the flow of the theory to its fixed point we define a Callan-Symanzik  $\beta$  function [41]. First we define the renormalized coupling as the density at an arbitrary but fixed late time  $\tau$ . This is the analog of the normalization point. The dimensionless coupling constant, which will be invariant under rescaling, is then

$$g_R = (\Gamma_R \tau)^\zeta n(\tau). \quad (2.29)$$

We have restored the time constant  $\Gamma$  in the problem, since it is possible that renormalization effects may cause an effective time dependence in  $\Gamma_R$ . This will be discussed at the end of §2.4. For the purposes of the present argument we will assume that  $\Gamma$  is a constant and can be absorbed into a rescaling of time. A late time correlation function of the system can be expressed either in terms of the random initial state evolved in time, or from the normalization point where the initial state information has been lost. That is, for some correlation function  $G(r, t)$  we have

$$G(r, t, n_0) = G_R(r, t, g_R, \tau). \quad (2.30)$$



The value of  $G$  is independent of the normalization scale, so

$$\tau \frac{\partial}{\partial \tau} G \Big|_{r,t,n_0} = 0 \quad (2.31)$$

which implies a Callan-Symanzik equation

$$\left[ \tau \frac{\partial}{\partial \tau} + \beta(g_R) \frac{\partial}{\partial g_R} \right]_{r,t,n_0} G_R = 0 \quad (2.32)$$

where

$$\beta(g_R) = \tau \frac{\partial g_R}{\partial \tau} \Big|_{r,t,n_0}. \quad (2.33)$$

If  $G_R$  has dimensions  $(\text{length})^n$ , then dimensional analysis gives

$$\left[ -n + \frac{\tau}{\zeta} \frac{\partial}{\partial \tau} + \frac{t}{\zeta} \frac{\partial}{\partial t} + r \frac{\partial}{\partial r} \right]_{g_R} G_R(r, t, g_R, \tau) = 0. \quad (2.34)$$

Combining (2.32) and (2.34) to eliminate the explicit  $\tau$  dependence gives

$$\left[ n - \frac{t}{\zeta} \frac{\partial}{\partial t} - r \frac{\partial}{\partial r} + \beta(g) \frac{\partial}{\partial g} \right] G_R = 0. \quad (2.35)$$

If  $\beta(g_R^*) = 0$  for some value of the dimensionless coupling  $g_R^*$ , then

$$G_R = r^n h(rt^{-\zeta}) \quad (2.36)$$

which is the self-similar fixed point. Also, for  $g_R(\tau) = g_R^*$  we find

$$n(t) = g_R^* t^{-\zeta}, \quad (2.37)$$

the asymptotic form of the density predicted in the energy dissipation arguments. The flow into this fixed point for a given set of initial conditions is determined by the  $\beta$  function. We stress that in this formalism the assumption of a zero of  $\beta$  is mathematically completely equivalent to the statement that  $n(t)t^\zeta \rightarrow \text{constant}$ , but it gives a conceptually different approach to the problem, and from an approximation standpoint, a method for extrapolating from the early to the late time regime. In §2.4 we will discuss a method for finding the  $\beta$  function in the large  $\sigma$  limit.

## 2.4. FUGACITY EXPANSION

A technique for calculating the density  $n(t)$  and other correlation functions as expansions in powers of the initial density  $n_0$  is developed in this section. This result is used to calculate the  $\beta$  function defined in §2.3 to order  $g_R^4$ , from which we estimate the fixed point coupling  $g_R^*$ .

### *Machinery*

We can use the ideas of equilibrium statistical mechanics to calculate quantities which are averages over the distribution of initial conditions. In doing so it is necessary to use finite systems, although at the end of the calculation the  $L \rightarrow \infty$  limit may be taken, if it exists. The canonical ensemble, with a fixed initial density, is too difficult to work with, so instead we use the fixed fugacity or grand canonical ensemble. One can check afterwards that the fluctuations in the grand canonical ensemble are of order  $1/\sqrt{L}$ . The average of some quantity is calculated by expanding in powers of the fugacity  $y$ . The coefficient of the  $y^k$  term is given by the integral of this quantity over all the initial conditions for the  $k$ -body system. To normalize these averages we use the analog of the grand canonical partition function

$$\Xi = \sum_k y^k V_k \quad (2.38)$$

where  $V_k$  is just the volume of configuration space for the  $k$ -body system. We will work with ordered charges, so this volume is  $V_k = L^k/k!$ . From this it follows that

$$\Xi = e^{yL}. \quad (2.39)$$

The initial number of charges can be found in terms of the fugacity, since the value of  $N_0$  for a  $k$ -body system is just  $k$ .

$$\begin{aligned} N(0) &= \Xi^{-1} \sum_k y^k k \frac{L^k}{k!} \\ &= yL e^{-yL} \sum_k \frac{(yL)^{k-1}}{(k-1)!} \\ &= yL \end{aligned} \quad (2.40)$$

Therefore the fugacity is equal to the initial density  $n_0$ .

The calculations are actually simpler for a non-periodic system. It is then important to comment on the boundary conditions, that is the values of the spins at  $x = 0$  and  $x = L$ . The spin degeneracy factor of two can be ignored, leaving as the possible boundary conditions either the spins at each end being equal, or being opposite. These correspond respectively to there being an even or odd number of charges in the system. For convenience, we sum over both cases, corresponding to free boundary conditions on the Ising spins.

We can use the fugacity expansion to calculate the time-dependent number of charges  $N(t)$ . First we define  $N_k(x_1, \dots, x_k, t)$  to be the number of charges that remain at time  $t$ , given  $k$  charges at  $t = 0$  with initial positions  $x_1, x_2, \dots, x_k$ . For regions of the configuration space of initial conditions where no annihilation has occurred by time  $t$ ,  $N_k(t) = k$ . For regions where exactly one annihilation has occurred by time  $t$ ,  $N_k(t) = k - 2$ . This continues down to regions where  $N_k(t) = 0$  or  $1$ , after which no more annihilation is possible. Integrating  $N_k(t)$  over the distribution of initial conditions gives the coefficient of the  $y^k$  term in the fugacity expansion, which we define to be  $Q_k(t)$ . That is

$$Q_k(t) = \int_{0 < x_1 < \dots < x_k < L} \prod_{i=1}^k dx_i N_k(x_1, \dots, x_k, t). \quad (2.41)$$

Calculating  $Q_k(t)$  for the random distribution is then a process of partitioning the volume in configuration space by the number of charges at time  $t$ , and then summing these regions weighted by their respective charge numbers.

In general the division of configuration space at time  $t$  into regions of  $k$ ,  $k - 2$ , etc. charges requires solving the  $k$ -body problem given by our equations of motion. The two-body problem can be solved for all  $\sigma$ , and was found in §2.2 and used to rescale time  $t$ . We can use this result to calculate  $Q_2(t)$  for general  $\sigma$  (note that  $Q_1(t) = L$  for all  $t$ ). As defined

$$Q_2(t) = \int_{0 < x_1 < x_2 < L} dx_1 dx_2 2 \theta(x_2 - x_1 - t^\zeta), \quad (2.42)$$

that is, there is a contribution of two from regions of the integral where  $x_2(0) - x_1(0)$  is greater than the annihilation distance given by  $t$ , and a contribution of zero from the rest. The integration variables are the *initial* positions of the particles. The time dependence is explicit in the integrand. Integrating gives

$$Q_2(t) = L^2 - 2Lt^\zeta + t^{2\zeta}. \quad (2.43)$$

This allows us to calculate  $n(t)$  to order  $y^2$ . Expanding  $\Xi^{-1} = e^{-yL}$  to order  $y$  gives

$$\begin{aligned} N(t) &= (1 - yL)(0 + yL + y^2L^2 - 2y^2Lt^\zeta + y^2t^{2\zeta}) + O(y^3) \\ &= Ly(1 - 2yt^\zeta) + O(L^0, y^3). \end{aligned} \quad (2.44)$$

Dividing both sides by  $L$  and taking the  $L \rightarrow \infty$  limit (or just considering  $L \gg t^\zeta$ ) gives

$$n(t) = n_0 [1 - 2n_0t^\zeta] + O(n_0^3t^{2\zeta}) \quad (2.45)$$

or, from (2.21),

$$f(x) = 1 - 2x + O(x^2). \quad (2.46)$$

### *Large $\sigma$ Calculation*

The higher order terms become quite difficult. We can solve the three-body system for  $\sigma = 1$  (see appendix 2.B), but in general some simplification is needed to proceed. By taking the large  $\sigma$  limit the equations of motion effectively decouple, and we can solve for the higher order terms. As stated earlier, this limit merits consideration since the value of  $\sigma$  seems to play only a minor role in the nature of the fixed point which characterizes the late times, at least for  $\sigma > 1$ . For the three body case the equations of motion can be reduced to two equations by introducing the variables  $r_i = x_{i+1} - x_i$ . In terms of  $r_1, r_2$  the equations of motion are

$$\begin{aligned} 2(1 + \sigma)\dot{r}_1 &= -2r_1^{-\sigma} + r_2^{-\sigma} + (r_1 + r_2)^{-\sigma} \\ 2(1 + \sigma)\dot{r}_2 &= -2r_2^{-\sigma} + r_1^{-\sigma} + (r_1 + r_2)^{-\sigma}. \end{aligned} \quad (2.47)$$

Now suppose  $r_1 < r_2$ . In the large  $\sigma$  limit the equation of motion for  $r_1$  becomes

$$2(1 + \sigma)\dot{r}_1 = -2r_1^{-\sigma} \quad (2.48)$$

and the charges have decoupled. More exactly, the closest pair moves together and annihilates in a time that is infinitely smaller than the time scales of the rest of the charges. With these simplified dynamics we are able to calculate higher order terms.

For the  $k = 3$  case we divide our configuration space into two regions corresponding to the order in which the charges annihilate:  $r_1 < r_2$  so  $x_1, x_2$  annihilates first, or  $r_1 > r_2$  so  $x_2, x_3$  annihilates first. The equations of motion are symmetric with respect to  $r_1$  and  $r_2$ , so we can consider just one of these conditions, say  $r_2 > r_1$ , and double the resulting calculation. We have

$$Q_3(t) = 2 \int_{0 < x_1 < x_2 < x_3 < L} d^3x \theta(r_2 - r_1) [3\theta(x_2 - x_1 - t^\zeta) + \theta(t^\zeta - x_2 + x_1)]. \quad (2.49)$$

We can rewrite the square bracket piece as  $3 - 2\theta(t^\zeta - x_2 + x_1)$ . To evaluate this integral it is convenient to take the derivative with respect to  $t^\zeta$ , which turns the  $\theta$ -function into a  $\delta$ -function.

$$\begin{aligned} \frac{\partial Q_3(t)}{\partial t^\zeta} &= 2 \int_0^L dx_3 \int_0^{x_3} dx_2 \int_0^{x_2} dx_1 \theta(x_3 - 2x_2 + x_1)(-2) \\ &\quad \times \delta(t^\zeta - x_2 - x_1) \\ &= -2L^2 + 8Lt^\zeta - 8t^{2\zeta} \end{aligned} \quad (2.50)$$

Integrating this we get

$$Q_3(t) = \frac{L^3}{2} - 2L^2 t^\zeta + 4L t^{2\zeta} - \frac{8}{3} t^{3\zeta} \quad (2.51)$$

where the constant of integration is given by the  $t = 0$  value,  $Q_k = kL^k/k!$ .

To calculate the  $k = 4$  integral we divide the configuration space into three regions, distinguishable by which pair annihilates first:  $(1, 2)$ ,  $(2, 3)$ , or  $(3, 4)$ . By symmetry the first

and last cases give identical contributions to the integral. The next step in evaluating the integral is to take the derivative  $\partial Q_4/\partial L$ . The  $L$  dependence of the integral is contained in the  $\theta(L - x_k)$  term implicit in the limits of integration. The  $L$  derivative replaces this  $\theta$ -function with a  $\delta(L - x_k)$ , against which we can integrate  $x_k$ . The remaining  $k - 1$  integrals over the  $x_i$  are changed to integrals over  $r_i$  with the constraints  $\sum_{i=1}^{k-1} r_i < L$  and  $r_i > 0$ . Then

$$\begin{aligned} \frac{\partial Q_4(t)}{\partial L} = & \int_{r_1+r_2+r_3 < L} d^3r \left[ 2\theta(r_3 - r_1)\theta(r_2 - r_1)\{2\theta(r_1 - t^\zeta) + 2\theta(r_3 - t^\zeta)\} \right. \\ & \left. + \theta(r_3 - r_2)\theta(r_1 - r_2)\{2\theta(r_2 - t^\zeta) + 2\theta(r_1 + r_2 + r_3 - t^\zeta)\} \right]. \end{aligned} \quad (2.52)$$

By taking the  $t^\zeta$  derivative as before, the integral can be done fairly straightforwardly, with the result

$$\frac{\partial^2 Q_4(t)}{\partial t^\zeta \partial L} = -3L^2 + 14Lt^\zeta - \frac{58}{3}t^{2\zeta}. \quad (2.53)$$

Integrating this we get

$$Q_4(t) = \frac{L^4}{6} - L^3t^\zeta + \frac{7}{2}L^2t^{2\zeta} - \frac{58}{9}Lt^{3\zeta} + \text{const. } t^{4\zeta} \quad (2.54)$$

where again the initial value of  $Q_4$  is used to find the constant of integration. The unknown function of  $t$  is proportional to  $t^{4\zeta}$ , with a proportionality constant which could be calculated by evaluating the integral without the  $L$  derivative.

On the basis of the scaling relation (2.21) one might think that the only piece of the  $y^k$  integral that is of interest is the  $t^{(k-1)\zeta}$  term. In this case we could take  $k - 1$  derivatives with respect to  $t^\zeta$  and then evaluate the remaining integral for  $t = 0$ , a considerable simplification. However, it turns out that all the pieces from lower order terms, and not just the  $t^{(k-1)\zeta}$  piece, feed back into the calculation of higher order terms. This is a consequence of boundary effects introduced by working with a non-periodic system. Writing a more careful scaling form for  $N(t)$  where both  $t$  and  $L$  are finite we get

$$N(t) = Lyf(yt^\zeta) + g(yt^\zeta) \quad (2.55)$$

where  $f$  is the original scaling function, and  $g$  some function which corresponds to our choice of boundary conditions. Writing  $f(x) = \sum_i f_i x^i$  and  $g(x) = \sum_i g_i x^i$ , we find

$$\begin{aligned} \sum_k y^k Q_k(t) &= N(t) e^{yL} \\ &= Ly(1 + f_1 y t^\zeta + f_2 y^2 t^{2\zeta} + f_3 y^3 t^{3\zeta}) e^{yL} + \left( g_0 + g_1 y t^\zeta \right. \\ &\quad \left. + g_2 y^2 t^{2\zeta} + g_3 y^3 t^{3\zeta} + g_4 y^4 t^{4\zeta} \right) e^{yL} + O(y^5 t^{4\zeta}). \end{aligned} \quad (2.56)$$

The coefficients for  $f$  and  $g$  can be determined by comparing powers of  $y$  on each side of the equation. In general, extracting the coefficient  $f_k$  from the  $k+1$ -body integral requires knowing all the  $g_i$  for  $i \leq k$ . To order  $y^4$  we find that  $g(x) = x^2 - (8/3)x^3 + O(x^4)$  and

$$f(x) = 1 - 2x + 3x^2 - \frac{34}{9}x^3 + O(x^4). \quad (2.57)$$

This density expansion is the main result of this calculation.

With a systematic expansion for the scaling function (2.21) we have equivalently an expansion for the  $\beta$  function defined by (2.29) and (2.33) in powers of  $g_R$ . Since  $g_R(x) = x f(x)$ ,

$$\begin{aligned} \sigma\beta &= x \frac{d}{dx} g_R(x) \\ &= x - 4x^2 + 9x^3 - \frac{136}{9}x^4 + O(x^5). \end{aligned} \quad (2.58)$$

To find  $\beta(g_R)$  we invert the series  $g_R(x)$ , which gives

$$\sigma\beta(g_R) = g_R - 2g_R^2 - 2g_R^3 - \frac{10}{3}g_R^4 + O(g_R^5). \quad (2.59)$$

The fixed point value of  $g_R$  if  $\beta$  is truncated at the fourth order is  $g_R^* = 0.33$ . Truncating to third order would give  $g_R^* = 0.37$ , a ten percent difference. The value of  $g_R^*$  is the amplitude  $A$  in the asymptotic form of the density

$$n(t) \sim A t^{-\zeta}. \quad (2.60)$$

This number should be universal in that all systems with the same value of  $\sigma$  (but different  $n_0$ ) will have the same amplitude. We suspect only a weak  $\sigma$  dependence of this number

for values of  $\sigma > 1$ . The amplitude found from the numerical data for both  $\sigma = 1$  and  $\sigma = 2$  is  $A = 0.31$ .

Recently it has been pointed out by Rutenberg and Bray [19] that the fixed point  $g_R^*$  can be found exactly in the  $\sigma \rightarrow \infty$  limit, using a method developed by Kawasaki [42]. The idea is basically that at all times the nearest neighbor distances remain uncorrelated. That is, the intervals between nearest neighbors start out uncorrelated, and their distribution evolves by the rule that the shortest interval is removed, and half of its length is added to two randomly selected intervals. The asymptotic form of the distribution of nearest neighbor distances can be found exactly, and consequently the coupling also, with

$$g_R^* = e^{-\gamma_E}/2 \approx 0.28 \quad (2.61)$$

where  $\gamma_E$  is Euler's constant. This value is reasonably close to that obtained by the expansion of the  $\beta$  function to order  $g_R^4$ .

### $\sigma \leq 1$ *Calculation*

While this approach of calculating the large  $\sigma$  terms may give a description of the fixed point, our real goal is to work with values of  $\sigma$  which lie in the range of physical interest. The two-body solution is known for all values of  $\sigma$ . For the three-body term the relevant calculation is the time to the first annihilation,  $T(r_1, r_2)$ . In the large  $\sigma$  limit this was just given by  $T = \min(r_1, r_2)^{1+\sigma}$ . For finite  $\sigma$  the presence of the third charge will affect the annihilation of the first and second charges, and always in the direction of slowing down the process. This slowing down will be a maximum when  $r_1$  and  $r_2$  are approximately equal. In fig. 2.7 curves of constant  $T$  are plotted in the plane of initial conditions  $r_1, r_2$ . The curve for the large  $\sigma$  limit is given by vertical and horizontal lines, while the  $\sigma = 1$ , constant  $T$  curve lies to the left and below. For any value of  $\sigma$  the area



bounded by the corresponding constant  $T$  curve is proportional to  $\partial Q_3(t)/\partial L$ , as can be seen by writing out the integral

$$\frac{\partial Q_3(t)}{\partial L} = -2 \int_{r_1+r_2 < L} dr_1 dr_2 \theta(t - T(r_1, r_2)). \quad (2.62)$$

Finding  $Q_3(t)$  for  $\sigma = 1$  is then a matter of finding the area between the  $T(r_1, r_2) = t$  curves for the large  $\sigma$  limit and  $\sigma = 1$ .

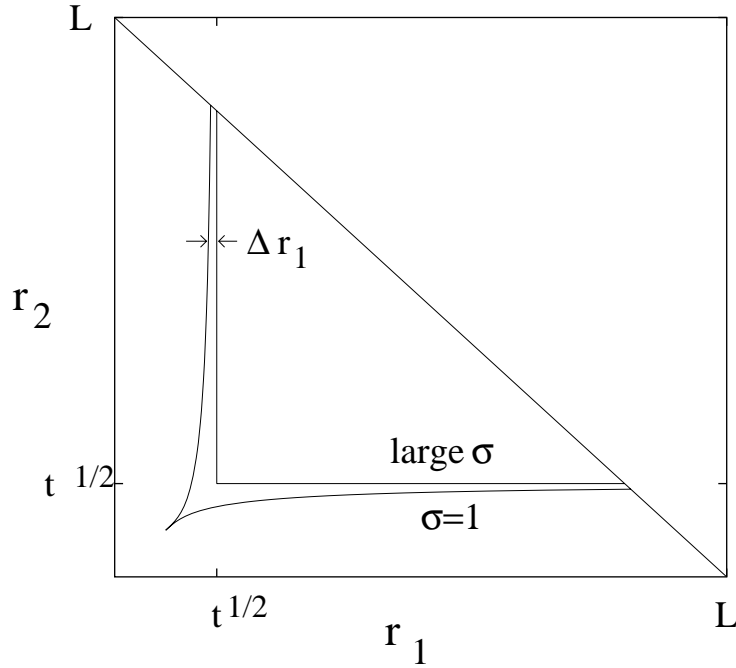


FIGURE 2.7. Curves of constant time to annihilation,  $T(r_1, r_2) = t$ , in the  $r_1, r_2$  plane for  $\sigma = 1$  and the large  $\sigma$  limit. The area bounded by these curves, the axes, and the line  $r_1 + r_2 = L$  gives  $\partial Q_3(t)/\partial L$ , as shown in the text. The contribution to the area between the  $\sigma = 1$  and large  $\sigma$  curves from the asymptotic region is divergent as  $L \rightarrow \infty$ . This can be shown by integrating  $\Delta r_1(r_2, t)$  out to  $r_2 = L$ .

For  $\sigma = 1$  an exact solution for  $T(r_1, r_2)$  can be found, the details of which are given in appendix 2.B. The result, however, gives an area between the two curves which diverges as  $L \rightarrow \infty$ . This is a general feature which occurs for all  $\sigma \leq 1$ , which can be understood

by examining the equations of motion. Consider a three charge configuration where one separation distance, say  $r_2$ , is much larger than the other. The equation of motion for the closer pair is then

$$2(1 + \sigma)\dot{r}_1 = -2r_1^{-\sigma} \left[ 1 - \frac{r_1^\sigma}{r_2^\sigma} + O\left(\frac{r_1^{2\sigma}}{r_2^{2\sigma}}\right) \right] \quad (2.63)$$

where the factor multiplying the left hand side is a consequence of our rescaling of time in (2.17). We treat  $r_2$  as a constant in the equation, and integrate the dynamical variable  $r_1$  from its initial value to zero

$$-\frac{1}{(1 + \sigma)} \int_0^T dt = \int_{r_1}^0 dr \left[ r^\sigma + \frac{r^{2\sigma}}{r_2^\sigma} + O\left(\frac{r^{3\sigma}}{r_2^{2\sigma}}\right) \right]. \quad (2.64)$$

This gives  $T(r_1, r_2)$  in the asymptotic region described. Performing the integral and inverting to find  $r_1(T, r_2)$  gives

$$r_1(T, r_2) = T^\zeta - \frac{T}{(1 + 2\sigma)r_2^\sigma} + O\left(\frac{T^{\zeta(1+2\sigma)}}{r_2^{2\sigma}}\right). \quad (2.65)$$

The first term is just the large  $\sigma$  solution, so the second term gives the leading contribution to  $\Delta r_1 = r_1^{(\infty)} - r_1^{(\sigma)}$ . Integrating  $\Delta r_1(r_2)$  out to  $r_2 = L$  gives the area contained in the asymptotic approach to the constant  $T$  line of the large  $\sigma$  limit. For  $\sigma = 1$  this piece gives  $\log L$ , and for smaller values of  $\sigma$  it gives an  $L^{1-\sigma}$  term. The significance of the divergences is that they will not cancel when the fugacity expansion is summed, as all the other  $L$  dependent terms do. For  $\sigma > 1$  the area remains finite as  $L \rightarrow \infty$ , and so the calculation for  $\sigma > 1$  should result in the same terms as in the case of the large  $\sigma$  limit, but with modified coefficients.

It is possible that there may be an infinite set of logarithms (for  $\sigma = 1$ ) which can be summed to restore the intensive behavior of the density. Such a summation may then be used, as in conventional critical dynamics [43], to renormalize the kinetic coefficient  $\Gamma$ , effectively making  $\Gamma_R$  a time dependent quantity. While this would imply no system size dependence and the density scaling form (2.21), the time dependence of  $\Gamma_R$  would give rise to anomalous time dependence for the density, as can be seen by (2.29). This

anomalous time dependence carries with it the implication that late time dynamics will exhibit dependence on the initial density.

An alternate possibility is that these divergent terms are indicating that the asymptotic dynamics truly has system size dependence. If the system were still independent of the initial density, as suggested by our heuristic argument in §2.2, then this system size dependence would give rise to anomalous time dependence, as can be seen by the scaling function (2.20). It is worth noting that if there is system size dependence, we can no longer expect our calculations, which are performed with free boundaries, to correspond directly to simulations with periodic boundary conditions.

It is possible that both of these effects, system size dependence and a time dependent  $\Gamma_R$ , occur. The simulations for  $\sigma = 1/2$ , as discussed in §2.2, are not decisive on this issue, although they do seem to indicate at least the former.

By studying a related model we might hope to find more clues for the significance of the divergences in the fugacity expansion. The  $Q \rightarrow \infty$  Potts model provides a contrast which further confuses the problem. In the Ising case the divergences were caused by a three body effect where the annihilation of a close pair, say  $(x_1, x_2)$ , is slowed by a distant charge,  $x_3$ . In the Potts case the distant charge is still interacting with the nearest neighbor,  $x_2$ , but not with the charge at  $x_1$ . This will give exactly half of the divergent effect seen in the Ising case. However, the simulations show no system size dependence, to within our accuracy.

There is a difference between the two models in the higher order divergent terms. Presumably the four body term in the Ising case will have divergent pieces when one of the end charges, say  $x_4$ , is distant, and is affecting both of the possible annihilations:  $(x_1, x_2)$  and  $(x_2, x_3)$ . In the  $Q \rightarrow \infty$  Potts case, the distant charge can only affect the annihilation of the pair which contains the nearest neighbor of the distant charge, in this case  $(x_2, x_3)$ . However, a quantitative analysis of this effect at higher orders is difficult.

## 2.5. TRUNCATION SCHEME FOR THE TWO-PARTICLE DISTRIBUTION FUNCTION

The fugacity expansion provides an exact scheme for calculating time dependent quantities in the system via the deterministic equations of motion. A simpler scheme can be developed which gives a qualitative description of the scaling regime, and of other features of the model. In this section we will present this method, and discuss the applicability for some different initial conditions.

The two-particle distribution function for the system,  $n_2(r, t)$ , can be used to find a dynamical equation for  $n(t)$ . Integrating the distribution function from  $r = 0$  to  $r = \delta r$  gives the density of charge pairs which are within  $\delta r$  of each other. For very small separations the charge pairs will become isolated from the rest of the system, and annihilate in a time  $\delta t = \delta r^{1/\zeta}$ . Therefore the rate of change of the density is given exactly by

$$\frac{dn}{dt} = \lim_{\delta t \rightarrow 0} -\frac{2}{\delta t} \int_0^{\delta t^\zeta} n_2(r, t) dr. \quad (2.66)$$

The distribution function can be calculated by the fugacity expansion described in the last section. The leading order term is the two-body term, which can be written

$$n_2(r, t) \propto y^2 \int_{r(0) < L} dr(0) \delta(r(t) - r). \quad (2.67)$$

A change of integration variables from  $r(0)$  to  $r(t)$  will introduce the Jacobian

$$J(r, t) = \left. \frac{dr(0)}{dr(t)} \right|_{r(t)=r} = \frac{r^\sigma}{(r^{1+\sigma} + t)^{\sigma/(1+\sigma)}} \quad (2.68)$$

which has the limit  $J = 1$  for  $r \rightarrow \infty$  or  $t = 0$ . Therefore the distribution function is

$$n_2(r, t) = n_0^2 J(r, t) + O(n_0^3). \quad (2.69)$$

Notice that the dynamics produces a ‘hole’ in the two-particle distribution function at short distances.

This expansion is only useful for low densities or early times. However, we can extend the range via a heuristic argument similar to that of §2.2. For an isolated pair of charges separated by a distance  $r$  at time  $t + \delta t$ , the separation at time  $t$  is given by  $(r^{1+\sigma} + \delta t)^\zeta$ . Therefore, for small  $r$  we expect the two-particle distribution functions of the arguments above to be related. The relation should also include the Jacobian, for the same reason it enters into the  $t = 0$  calculation. Therefore

$$n_2(r, t + \delta t) = J(r, \delta t) n_2((r^{1+\sigma} + \delta t)^\zeta, t) + \text{higher order terms.} \quad (2.70)$$

This equation should be exact in the small  $r$  limit, and the higher order terms are corrections for large  $r$ . The contributions from the higher order terms can be approximated by replacing  $n_2(r, t)$  with  $\bar{n}_2(r, t) = n_2(r, t)/n(t)^2$ , so that  $\bar{n}_2(r \rightarrow \infty, t) = 1$ . This results in a truncation scheme for  $\bar{n}_2$  which is correct both for small  $r$  and in the  $r \rightarrow \infty$  limit. Making this substitution and equating the order  $\delta t$  terms in (2.70) gives the differential equation

$$\frac{\partial \bar{n}_2}{\partial t} = - \left( \frac{\sigma}{1 + \sigma} \right) \frac{\bar{n}_2}{r^{1+\sigma}} + \left( \frac{1}{1 + \sigma} \right) \frac{1}{r^\sigma} \frac{\partial \bar{n}_2}{\partial r} \quad (2.71)$$

whose general solution is

$$\bar{n}_2(r, t) = r^\sigma g((r^{1+\sigma} + t)^\zeta). \quad (2.72)$$

For large  $x$ , we must have  $g(x) \sim x^{-\sigma}$  as determined by the  $r \rightarrow \infty$  limit of  $\bar{n}_2$ , corresponding to a scaling solution for the distribution function

$$\bar{n}_2(r, t) \sim J(r, t). \quad (2.73)$$

From (2.72) we see that this scaling form of  $\bar{n}_2(r, t)$  will also be the solution for large  $t$ . This is consistent with the RG picture of an attractive fixed point which describes the asymptotically late time dynamics for all initial distributions.

The solution for  $\bar{n}_2$  and equation (2.66) give two relations between the density and the distribution function. Using the small  $r$  limit of the distribution function,  $\bar{n}_2(r, t) = r^\sigma t^{-\zeta}$ , we get the equation

$$\frac{dn}{dt} = -2\zeta n^2 t^{\zeta-1}, \quad (2.74)$$

which is consistent with the scaling solution  $n \sim t^{-\zeta}$ . The amplitude is not correct, but the argument captures the qualitative features at least. Note that no system size dependence can appear in this approximation. For uncorrelated initial conditions the scaling solution for  $\bar{n}_2$  is valid at  $t = 0$ . Further qualitatively correct results may be obtained if we assume (2.73) holds for all  $t$ . Then the solution to (2.74) is

$$n(t) = \frac{n_0}{1 + 2n_0 t^\zeta}, \quad (2.75)$$

which exhibits the asymptotic time dependence, and also the lack of  $n_0$  dependence, we see in the simulations for  $\sigma \geq 1$ . In fact, under the same assumptions we can find  $g(x)$  for all values of  $x$  for correlated initial conditions. Setting  $t = 0$  in (2.72) gives

$$g(x) = x^{-\sigma} \bar{n}_2(x, 0) \quad (2.76)$$

from which it follows that

$$\bar{n}_2(r, t) = J(r, t) \bar{n}_2((r^{1+\sigma} + t)^\zeta, 0). \quad (2.77)$$

Combining this with (2.66) gives

$$\frac{dn}{dt} = -2\zeta n^2 t^{\zeta-1} \bar{n}_2(t^\zeta, 0) \quad (2.78)$$

which can be rewritten as

$$\frac{dn^{-1}}{dt^\zeta} = 2\bar{n}_2(t^\zeta, 0). \quad (2.79)$$

Thus the late time behavior of the density is completely determined by the initial two-particle distribution function in this approximation. We can test (2.79) by introducing correlations into the initial conditions. In particular, if we generate a system via the nearest neighbor distribution

$$P(x) = \begin{cases} \frac{1}{2n_0\Delta} & n_0^{-1}(1 - \Delta) < x < n_0^{-1}(1 + \Delta) \\ 0 & \text{otherwise} \end{cases} \quad (2.80)$$

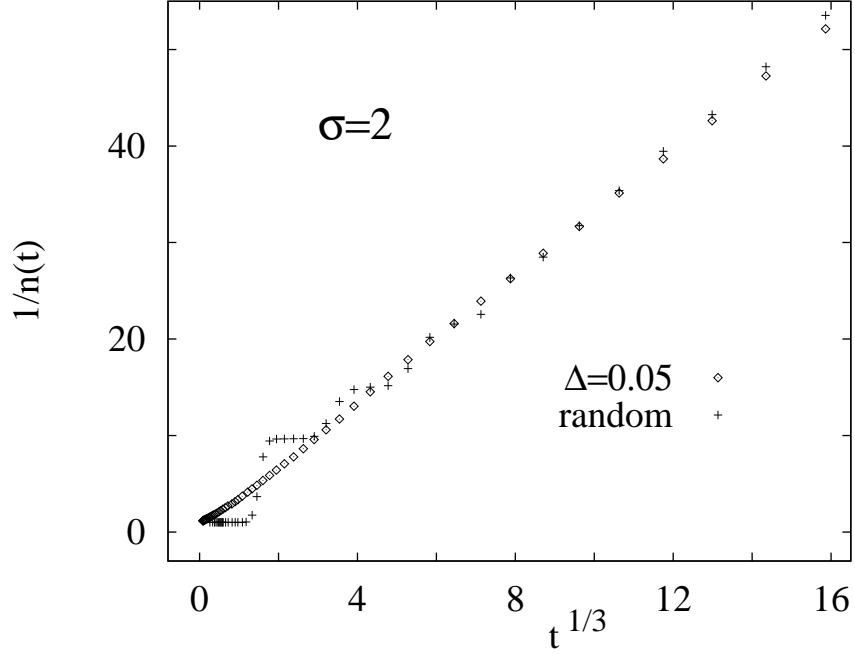


FIGURE 2.8. Simulations for the correlated initial conditions discussed in the text, for  $\sigma = 2$ ,  $\Delta = 0.05$ , and  $N_0 = 100$ . The data is plotted as  $n^{-1}$  versus  $t^{1/3}$ , which should give a staircase pattern as discussed in the text. The first three zeros of the slope are clearly visible. The data for the random initial conditions is plotted for reference.

then  $\bar{n}_2(r, 0)$  will be sharply peaked around  $r = n_0^{-1}$ , less sharply peaked around  $r = 2n_0^{-1}$ , and so on out to infinity where it is equal to 1. The first  $k = (1 + \Delta)/(2\Delta)$  peaks will have zeroes between them, which implies  $dn^{-1}/dt^\zeta = 0$ . Therefore we expect a plot of  $n^{-1}$  versus  $t^\zeta$  to have flat areas separated by sharp jumps, like a staircase, with the jumps smoothing to a straight line at late times.

The simulation results for these initial conditions (shown in fig. 2.8) verify the staircase pattern. Both the truncation method developed here and the property of lack of dependence on initial conditions are reinforced by this result.

## 2.6. SIMULATIONS

To simulate these systems we simply directly integrated the equations of motion

$$\dot{x}_i = \sum_{j \neq i} (-1)^{i+j} |x_j - x_i|^{-\sigma} \text{sgn}(x_i - x_j). \quad (2.81)$$

Whenever two charges pass each other they were removed from the system. We began with some number of charges  $N_0$  distributed randomly along a length  $L$ . To reproduce periodic boundary conditions exact replicas of the charge configuration were made, and added to the left and the right of the original system. Then the forces were calculated on the original charges, the positions updated, and the replicas replaced with updated copies. While this emulates a periodic system, it also adds a long-range cutoff to the interactions. It is important to separate the effect of the cutoff from possible system size dependence effects.

We parameterized the cutoff in the following way. If  $k$  replicas are added to the left and to the right of the original system, there are  $N_e = (2k+1)N(t)$  effective charges in the system. We imposed a minimum number of effective charges  $N_{\min}$ , and then determined the number of replicas needed so that  $N_e \geq N_{\min}$ . By comparing simulations with different values of  $N_{\min}$ , we could determine at what point the results are independent of the cutoff to our desired accuracy. We chose this method of introducing a cutoff, rather than a more obvious choice of including interactions out to a certain length, because otherwise small number effects entered into the simulations at late times. By keeping the effective number of charges at some minimum level we hoped to model more accurately the truly periodic system. The values we used for  $N_{\min}$  are given in the table 2.1.

The numbers for  $N_{\min}$  are large enough, particularly for  $\sigma = 1/2$ , to significantly slow the simulations. Some speed can be regained by exploiting the insensitivity of the system to the time step. For  $\sigma = 1/2$  and  $n_0 = 1$  we used an initial time step of  $\Delta t = 10^{-3}$ , which we stepped up to  $\Delta t = 1$  over the time interval  $t = (0, 20)$  (for other values of  $\sigma$  see table 1). Although these values for the time step seem large, the results of the simulation are



	$N_r$	$N_{\min}$	$\Delta t$	$t_0$
$\sigma = 1/2$	300	400	1	20
$\sigma = 1$	1000	30	.1	2
$\sigma = 2$	1000	20	.03	.6

TABLE 2.1. Values of the simulation parameters used. For all simulations  $n_0 = 1$  and  $N_0 = 100, 200, 400, 800$ . The time step is ramped from  $10^{-3}\Delta t$  to  $\Delta t$  in the range  $0 < t < t_0$ , and is equal to  $\Delta t$  for  $t > t_0$ .

quite insensitive to the size. Simulations performed with ten times this step size showed no appreciable change. This is somewhat expected, since the primary consequence of a large time step is to cause the annihilating pairs to stay around longer, but the force exerted on the system by a very close pair of charges is nearly zero. It is probable that an even larger time step than the one used here would be adequate.

We used the second order Runge-Kutta integration technique, which involves initially taking a half-step, reevaluating the forces at this midpoint, then going back and taking a full step with the modified forces. To use this method it is necessary to check for annihilation at the midpoint, or else the forces calculated at the midpoint for a pair which has just passed each other will be quite inaccurate. It seems likely that using the Euler integration method instead of Runge-Kutta would give the same results.

The third parameter in the simulations is the number of runs over which the quantities are averaged. That is, since the quantities are supposed to be averaged over the distribution of initial conditions, we average over multiple runs. To determine the number of runs  $N_r$  over which to average, we calculated the standard deviation of  $n(t)$  via the central limit theorem. For  $\sigma = 1/2$  we used  $N_r = 300$ , for which the one-sigma error bars were smaller than the point size of the plots for much of the scaling regime.

These simulations were performed on a DECstation 5000. Our goal was to use as simple an algorithm as possible, and to keep simulations at the level of a workstation problem. There are ways in which our techniques could be expanded or improved upon, for example by using a controlled time step which maximally exploits the insensitivity of the system, or of course, by using faster computers. It would be preferable to push the  $\sigma = 1/2$  system to larger values of  $N_0$ , but this was where we were reaching our limits.

## 2.7. DISCUSSION

The first of the principal results of this chapter is the appearance of system size dependence in simulations for  $\sigma = 1/2$ . We believe that this result also holds for all  $0 < \sigma \leq 1$  on the basis of our fugacity expansion, which demonstrates anomalous  $L$  dependence in the expansion coefficients for this range. The data for  $\sigma = 1$  exhibits only slight  $L$  dependence. However, the effect may be very small at the marginal value.

The other principal result is the possibly more general dynamical feature of lack of dependence on the initial length scale. From a renormalization group perspective this is an intuitive result: once the system has reached the fixed point, and is thus evolving in time via a rescaling of the domain length only, then the information about the path to the fixed point is lost. For the distributions we used, the information lost is the initial density and correlations. A variety of distributions may flow to this same fixed point, which can then be interpreted as a loss of information about the initial distribution itself, and not just its length scale. This is suggestive of a dynamical feature of lack of dependence on pre-quench temperature, if thermal distributions flow to the same fixed point. The RG picture is complicated by the presence of system size dependence, since the notion of a scale invariant fixed point will need modification. In the simulations we find a convincing lack of  $n_0$  dependence for  $\sigma = 1, 2$ , and a possible lack of  $n_0$  dependence for  $\sigma = 1/2$ . We also find, via an heuristic argument (2.24), that the presence of  $L$  dependence should not affect the lack of dependence on the initial length scale.

Our theoretical approaches include the fugacity expansion and the truncation method of §2.5. The latter approach is useful in providing a qualitative description of the dynamics, and includes quite naturally the dynamics at late times. In the former case, the original intent was to find results for the infinite system while calculating with finite  $L$ . We can find all the expansion coefficients for  $\sigma = 0$ , and thus the exact answer for  $n(t)$  (see appendix 2.C), but we find that the density decays exponentially. This indicates that  $\sigma = 0$  is singular in some sense, and that trying to expand about this solution is not likely to be fruitful. We can calculate the expansion coefficients to order  $y^4$  by taking the large  $\sigma$  limit. This calculation can be carried to higher orders, the problem becoming an exercise in bookkeeping. When we attempt to extrapolate the large  $\sigma$  result to lower values of  $\sigma$  we find divergences appearing in our expansion coefficients. This is a general feature for  $\sigma \leq 1$ , the physical range of interest. These divergences are of the form of  $L$  dependent expansion coefficients, whose presence may just be indicating system size dependence in the density  $n(t)$ .

Motivated by the results of this work, Bray and Rutenberg have recently performed simulations on substantially larger sized systems [19]. They conclude that no system size dependence is apparent. However, for most of their simulations they considered open rather than periodic boundary conditions. This introduces a cutoff in the range of interactions, given by the system size, which will cause boundary effects to enter into the asymptotic regime much earlier. These are distinguished from finite size effects, in that the latter would describe the system size dependence for a perfectly periodic system. Boundary effects, on the other hand, are the results of having a surface in the system. In our simulations it was found that the asymptotic regime was highly sensitive to boundary effects. It appears that the issue of whether or not these systems exhibit system size dependence for  $s \leq 1$  is still unsettled, particularly in view of the singularities encountered in the fugacity expansion for  $\sigma < 1$ .

Our expression for the density in the large  $\sigma$  limit can be used to calculate a Callan-Symanzik  $\beta$  function to order  $g_R^4$ . To this order the  $\beta$  function has a zero with the value

$g_R^* = 0.33$  which compares well with the exact value for  $\sigma \rightarrow \infty$  of  $g_R^* = 0.28$ . Unfortunately, we have not been able to find any analog of the  $\epsilon$  expansion of the equilibrium critical behavior, which would allow a systematic truncation of the series for the  $\beta$  function.

The one-dimensional system with long-ranged interactions appears to have complicated behavior for  $\sigma \leq 1$ . These interactions appear to be relevant in higher dimensional systems as well [18], suggesting that system size dependence may be a more general feature of long-ranged interacting systems. Simulations of these systems in higher dimensions, although difficult, could yield interesting results. More can be done with the one-dimensional simulations in the way of measuring correlation functions as well. A theoretical approach which treats the system size dependence in a controlled way, perhaps some modification of our density expansion, would be a possible next step in trying to understand these systems.

## APPENDIX 2.A. $Q$ STATE POTTS MODEL

We can generalize the Ising model Hamiltonian (2.1), which is the  $Q = 2$  Potts model, to the case of general  $Q$ . At each lattice site there is a variable  $s_i$ , which can be in one of  $Q$  states. The Hamiltonian is defined by

$$H = - \sum_{i < j} V(x_i - x_j) J(s_i, s_j) \quad (2.A.1)$$

where  $V(r)$  is the same as before, and

$$J(s_i, s_j) = 1 - \delta_{s_i s_j} \quad (2.A.2)$$

We can rewrite the Hamiltonian as

$$H = \sum_{i < j} U(x_i - x_j) [J(s_{i+1}, s_{j+1}) + J(s_i, s_j) - J(s_{i+1}, s_j) - J(s_i, s_{j+1})] + \text{surface terms.} \quad (2.A.3)$$

where the function  $U(r)$  is defined by (2.4) [17]. Notice the expression in the square brackets is zero for  $s_i = s_{i+1}$  or  $s_j = s_{j+1}$ . Therefore this term only contributes to the

energy when  $x_i$  and  $x_j$  are both locations of defects. A defect can be labeled by  $(\alpha, \beta)$ , meaning it is the boundary between a region of state  $\alpha$  and a region of state  $\beta$ . The interaction for a pair of defects of type  $(\alpha, \beta)$  and  $(\gamma, \delta)$  separated by a distance  $r$  is then

$$H_{\text{pair}} = U(r) [\delta_{\alpha\gamma} + \delta_{\beta\delta} - \delta_{\alpha\delta} - \delta_{\beta\gamma}]. \quad (2.A.4)$$

Consider a nearest neighbor pair of defects. This implies  $\beta = \gamma$ , and we assume  $\alpha \neq \delta$ . The interaction energy is then

$$H_{\text{pair}} = -U(r). \quad (2.A.5)$$

Also note that if all four states  $\alpha, \beta, \gamma, \delta$  are distinct then there is no interaction between the defects. Now we take the  $Q \rightarrow \infty$  limit of this model. Every domain in the system will find a unique state, and so all defect pairs will have  $\alpha, \beta, \gamma, \delta$  not equal, with the exception of nearest neighbors. These rules allow us to drop the designation of the states, and simply consider the model to be one where only nearest neighbors interact. The defect Hamiltonian can be written as

$$H = - \sum_i U(x_i - x_{i+1}). \quad (2.A.6)$$

We introduce the same equations of motion as before, with the consequence that now only the nearest neighbor on either side is included in calculating the force. There is another modification to the dynamics. When a nearest neighbor pair annihilate, a single defect remains. That is,

$$(\alpha, \beta) + (\beta, \gamma) \rightarrow (\alpha, \gamma). \quad (2.A.7)$$

## APPENDIX 2.B. 3-BODY PROBLEM FOR $\sigma = 1$

We start by taking the  $L$  derivative of  $Q_3(t)$ , leading to the calculation in the  $r_1, r_2$  plane as shown in fig. 2.7. We want to solve for the function which gives the time to first annihilation,  $T(r_1, r_2)$ . From this we can find  $Q_3(t)$  via

$$\frac{\partial Q_3(t)}{\partial L} = -2 \int_{r_1+r_2 < L} dr_1 dr_2 \theta(t - T(r_1, r_2)). \quad (2.B.1)$$

The time to annihilation has the scaling form

$$T(r_1, r_2) = r_2^2 f\left(\frac{r_1}{r_2}\right). \quad (2.B.2)$$

If  $r_1$  and  $r_2$  are evolved by a time  $\delta t$ , then  $T$  will change by  $-\delta t$ . That is, for  $r = r_1/r_2$

$$T - \delta t = (r_2 + \dot{r}_2 \delta t)^2 f(r + \dot{r} \delta t), \quad (2.B.3)$$

so to order  $\delta t$  we get the equation

$$2r_2 \dot{r}_2 f(r) + r_2^2 \dot{r} f'(r) = -1. \quad (2.B.4)$$

The three-charge equations of motion given by (2.47) and the rescaling of time (2.17) give

$$\begin{aligned} \frac{1}{4} r_2 \dot{r}_2 &= -2 + \frac{r_2}{r_1} + \frac{r_2}{r_1 + r_2} \\ &= -2 + \frac{1}{r} + \frac{1}{r+1} \end{aligned} \quad (2.B.5)$$

and

$$\begin{aligned} \frac{1}{4} r_2^2 \dot{r} &= r_2 \dot{r}_1 - r_1 \dot{r}_2 \\ &= -\frac{2}{r} + 2r + \frac{1}{r+1} - \frac{r}{r+1}. \end{aligned} \quad (2.B.6)$$

Therefore  $r_2$  can be eliminated from equation (2.B.4), giving the differential equation for  $f(r)$

$$\frac{2(1-2r^2)}{(r-1)(2r^2+3r+2)} f(r) + f'(r) = \frac{-4r(r+1)}{(r-1)(2r^2+3r+2)}. \quad (2.B.7)$$

Notice that the coefficients are singular at  $r = 1$ .

This equation can be integrated in closed form, which is somewhat surprising, with the result

$$f(r) = \frac{4}{3}(1+r+r^2) + C(r-1)^{2/7}(2r^2+3r+2)^{6/7} \quad (2.B.8)$$

where  $C$  is a constant of integration. To determine  $C$  we consider the large  $r$  limit of  $f(r)$ .

If  $r_1 \gg r_2$  then the time to annihilation is given by the separation  $r_2$  only, and is  $T = r_2^2$ .

This implies for large  $r$ ,  $f(r) = 1$ . If we choose as our integration constant  $C = -2^{8/7}/3$ , then the  $r^2$  and  $r$  parts of  $f(r)$  have coefficients of zero. Therefore, the exact solution is

$$f(r) = \frac{4}{3}(1 + r + r^2) - \frac{2^{8/7}}{3}(r - 1)^{2/7}(2r^2 + 3r + 2)^{6/7}. \quad (2.B.9)$$

When we plot  $T(r_1, r_2)$  on the  $r_1, r_2$  plane (see fig. 2.7) we see a cusp at  $r_1 = r_2$ . The appearance of the exponent  $1/7$  is curious. When we use this solution to calculate the area between the  $\sigma = 1$  and the large  $\sigma$  curves, we find this area is divergent, as mentioned in the text.

## APPENDIX 2.C. $\sigma = 0$ SOLUTION

For the  $\sigma \rightarrow 0$  limit of the model we have the equations of motion

$$\begin{aligned} \dot{x}_i &= -\frac{\partial}{\partial x_i} \sum_{j < k} (-1)^{j+k} |x_j - x_k| \\ &= \sum_{k \neq i} (-1)^k \text{sign}(i - k) \end{aligned} \quad (2.C.1)$$

The force on a given charge does not depend on the position of its neighbors, only on the global excess of charge on either side. It is necessary to consider only systems with even numbers of charges, since a system with an odd number of charges will have all forces equal to zero. For an even charge system the charges will be attracted in isolated pairs. That is, the leftmost charge, call it positive, will see a net negative charge to the right. The second charge from the left will be negative and see only a net positive charge to the left. This pair will then move toward each other and annihilate independent of the rest of the system.

The time dependent density in this model is entirely determined by the probability distribution for the location of the nearest neighbors. For the random initial conditions we used, this is a Poisson distribution

$$P(x)dx = n_0 e^{-n_0 x} dx \quad (2.C.2)$$

where  $P(x)dx$  is the probability of the nearest neighbor being located between  $x$  and  $x+dx$ . At a given time  $t$  all the paired charges which are located within a range  $\Delta x(t)$  will have annihilated. For the rescaled time given by (2.17)

$$\Delta x(t) = t. \quad (2.C.3)$$

The fraction of initial charges which remain at time  $t$  is then

$$\begin{aligned} \frac{n(t)}{n_0} &= 1 - \int_0^t dx n_0 e^{n_0 x} \\ &= e^{-n_0 t} \end{aligned} \quad (2.C.4)$$

so the density scaling function (2.21) is

$$f(x) = e^{-x}. \quad (2.C.5)$$

This result can be found also by using the fugacity expansion for  $\sigma = 0$ .



## Chapter 3. Field Theory for Reaction-Diffusion Systems

We are interested in describing the asymptotic regime of reaction-diffusion systems via the renormalization group. Most successful analytic applications of RG have as their basis field theory, and so it is useful to derive a field theory formulation the problem. The starting point of our analysis is a microscopic theory of reaction-diffusion, given by a probability master equation which describes the evolution of classical particles. This can be mapped to a field theory by a quite general two-step procedure. First, the master equation is recast in terms of second quantized operators in a procedure developed by Doi [44]. Second, this second quantized formulation is mapped to a field theory via the coherent state representation (see Schulman [45]). A comprehensive review of these techniques can be found in [28], although the methods presented there differ from ours. It should be noted that the result of this mapping is a quantum field theory, even though the original microscopic system consists of classical particles. This is a consequence of the stochastic processes inherent in the classical system.

There are various models used to describe reaction-diffusion. The model which we consider is one of particles on a lattice which undergo continuous time random walks. Whenever the appropriate particles necessary for a reaction are together on a single lattice

site, then the reaction occurs at some given rate. For example, in the one-species reaction  $kA \rightarrow \emptyset$  the particles can annihilate whenever  $k$  of them meet on a lattice site. For the two-species reaction  $A + B \rightarrow \emptyset$  the reaction occurs whenever one of each species is present, and the particles annihilate. These can be generalized to systems with arbitrary number of species and with different possible end products, *i.e.* the reaction  $(k_1 A_1 + k_2 A_2 + \dots) \rightarrow (\ell_1 A_1 + \ell_2 A_2 + \dots)$ . Multiple occupancy of all particle types on a lattice site is allowed. The particles are taken to be initially randomly distributed, with a Poisson distribution of occupation numbers at each lattice site.

It is worth mentioning two variations of this model. In the analysis of Bramson and Lebowitz [46,47] they consider a model in which the reaction occurs immediately whenever the appropriate particles meet on a lattice site. This has two results. First, it eliminates from the model a rate constant associated with the strength of the reaction, at which point one can no longer test the dependence of the system on such a parameter. Second, it has the effect in two-species reactions (or higher numbers) of not allowing multiple occupancy. That is, for the reaction  $A + B \rightarrow \emptyset$  one will never have  $A$  and  $B$  particles on the same lattice site. A second variation which is common in numerical simulations is to assume the instantaneous reaction and also to forbid any type of multiple occupancy. This allows for more efficient algorithms, which are necessary because of the large amounts of memory required by these simulations.

When constructing these models one hopes that the physical quantities, such as the density and the correlation function, are universal. Then the model can be expected to describe accurately real physical processes. One advantage of the renormalization group is that it is possible to determine whether or not a particular quantity is universal. The analysis of chapter four will show that for the one-species reaction the density and correlation functions are universal, and therefore all the various models above will yield the same results. However, in chapter five it is demonstrated that the amplitudes in the two-species reaction are non-universal, and can vary from one model to the next.

### 3.1. MASTER EQUATION AND SECOND QUANTIZED REPRESENTATION

Consider first the one-species reaction, with the particles on a hypercubic lattice of size  $a$ . The probability of particle configuration  $\{n\}$  occurring at time  $t$  is denoted by  $P(\{n\}, t)$ . Here  $\{n\} = (n_1, n_2, n_3, \dots)$ , where  $n_i$  is the occupation number of the  $i$ th lattice site. The appropriate master equation is

$$\begin{aligned} \frac{\partial}{\partial t} P(\{n\}, t) = & \frac{D}{a^2} \sum_{i,e} \left\{ (n_e + 1) P(\dots, n_i - 1, n_e + 1, \dots, t) - n_i P(\{n\}, t) \right\} \\ & + \lambda \sum_i \left\{ (n_i + k)(n_i + k - 1) \dots (n_i + 1) P(\dots, n_i + k, \dots, t) \right. \\ & \left. - n_i(n_i - 1) \dots (n_i - k + 1) P(\{n\}, t) \right\}, \end{aligned} \quad (3.1)$$

where  $i$  is summed over lattice sites, and  $e$  is summed over nearest neighbors of  $i$ . The first curly brackets piece describes diffusion with a diffusion constant  $D$ . This includes two terms, the first of which represents the flow of the probability of occupation number  $n_i - 1$  into that of occupation number  $n_i$  on a given lattice site, due to a particle hopping onto site  $i$  from a nearest neighbor. The second term gives the decrease of the probability of occupation number  $n_i$  due to a particle hopping away from site  $i$ . The second curly brackets piece corresponds to the annihilation process, with rate constant  $\lambda$ . Again there are two terms, with the first describing the increase in probability of there being  $n_i$  particles at a given site as a result of a reaction with  $n_i + k$  particles. The second describes the decrease in probability of  $n_i$  particles (when  $n_i \geq k$ ) due to a reaction occurring.

The initial values  $P(\{n\}, 0)$  are given by a Poisson distribution for random initial conditions with average occupation number  $\bar{n}_0$ . That is, for a single lattice site  $P_1(n) \propto \bar{n}_0^n / n!$ , so

$$P(\{n\}, 0) = C \prod_i \frac{\bar{n}_0^{n_i}}{n_i!} \quad (3.2)$$

where  $C$  is a normalization constant which depends on the total number of lattice sites, but not on the  $\{n\}$ .

These dynamics can be rewritten in terms of quantum mechanical operators by making a correspondence between the lattice site occupation number  $n_i$  and a quantum harmonic oscillator eigenstate, as shown by Doi [44]. Creation and annihilation operators are introduced for each lattice site, and are defined to obey the bosonic commutation relations

$$[a_i, a_j^\dagger] = \delta_{ij} \quad [a_i, a_j] = [a_i^\dagger, a_j^\dagger] = 0. \quad (3.3)$$

The vacuum ket  $|0\rangle$  is defined by the equations  $a_i|0\rangle = 0$  for all  $i$ . These operators act as raising and lower operators with respect to the state defined by  $|n_i\rangle \equiv (a_i^\dagger)^{n_i}|0\rangle$ , that is

$$a_i|n_i\rangle = n_i|n_i - 1\rangle \quad a_i^\dagger|n_i\rangle = |n_i + 1\rangle. \quad (3.4)$$

In terms of these quantities, the definition of the state of the system at time  $t$  is

$$|\phi(t)\rangle = \sum_{\{n\}} P(\{n\}, t) \prod_i (a_i^\dagger)^{n_i} |0\rangle. \quad (3.5)$$

As a result, the master equation becomes

$$-\frac{\partial}{\partial t}|\phi(t)\rangle = \hat{H}|\phi(t)\rangle \quad (3.6)$$

with the non-Hermitian time evolution operator

$$\hat{H} = -\frac{D}{a^2} \sum_i \sum_e a_i^\dagger (a_e - a_i) - \lambda \sum_i \left(1 - (a_i^\dagger)^k\right) a_i^k. \quad (3.7)$$

The equations of motion for the  $P(\{n\}, t)$  in this representation are identical to those of the master equation. For example, the  $a_i^\dagger a_e$  term in the diffusive part of the “Hamiltonian”  $\hat{H}$  corresponds to the probability of a particle hopping from lattice site  $e$  to  $i$ , just as the first term in (3.1) does. The  $a_i^\dagger a_i$  component of the diffusion is just the probability of a particle hopping away from site  $i$ , which is proportional to  $n_i$ , and so on.

Equation (3.6) has the formal solution  $|\phi(t)\rangle = \exp(-\hat{H}t)|\phi(0)\rangle$ . From the definition of  $|\phi(t)\rangle$  (3.5) and the initial conditions for  $P$  (3.2) we find

$$\begin{aligned} |\phi(0)\rangle &= C \sum_{\{n\}} \prod_i \frac{\bar{n}_0^{n_i} (a_i^\dagger)^{n_i}}{n_i!} |0\rangle \\ &= C \prod_i \sum_{n_i=0}^{\infty} \frac{\bar{n}_0^{n_i} (a_i^\dagger)^{n_i}}{n_i!} |0\rangle \\ &= C \prod_i e^{\bar{n}_0 a_i^\dagger} |0\rangle. \end{aligned} \tag{3.8}$$

The average of some observable is given in terms of the classical microscopic theory by

$$\langle\langle A(t) \rangle\rangle \equiv \sum_{\{n\}} A(\{n\}) P(\{n\}, t). \tag{3.9}$$

Notice that this averaging is linear in  $P$ . The state  $|\phi(t)\rangle$  of the second quantized representation is also linear in  $P$ , and so it is not possible to reconstruct the usual quantum mechanical expectation value, which goes as the square of  $|\phi\rangle$ . Instead one uses the *projection state*

$$\langle | \equiv \langle 0 | \prod_i e^{a_i}. \tag{3.10}$$

In terms of this state the average defined by (3.9) becomes

$$\langle\langle A(t) \rangle\rangle = \langle | \hat{A} |\phi(t)\rangle, \tag{3.11}$$

where  $\hat{A}$  is the second quantized operator analog of  $A(\{n\})$ . Note that the projection state has the property  $\langle | a_i^\dagger = \langle |$ .

The operator  $\hat{A}$  is found from the Taylor expansion of the function  $A(\{n\})$  with respect to all the variables  $n_i$ . That is,  $\hat{A}$  can be defined to be given by the same expansion, but with each classical variable  $n_i$  replaced by the operator  $\hat{n}_i = a_i^\dagger a_i$ . This procedure yields exactly the same expectation values as are found from the classical master equation. Also, since  $\langle | a_i^\dagger = \langle |$ , then any operator  $\hat{A}$  corresponding to an observable can be expressed entirely in terms of annihilation operators  $a_i$  by commuting to the left all the creation

operators  $a_i^\dagger$ . Then the  $a_i^\dagger$  act to the left, and are replaced with their eigenvalue of one. This results in a new operator, but one which yields the same expectation value. For example, the total density operator is found from the prescription above to be  $\hat{n} = V^{-1} \sum_i a_i^\dagger a_i$ , but it can also be written as

$$\hat{n} = V^{-1} \sum_i a_i. \quad (3.12)$$

The connected correlation function is given by the expectation value of the operator  $\hat{C}(r) = V^{-1} \sum_i a_{i+r}^\dagger a_{i+r} a_i^\dagger a_i$ , or equivalently,

$$\hat{C}(r) = V^{-1} \sum_i (a_{i+r} + \delta_{r,0}) a_i. \quad (3.13)$$

The significance of the  $\delta$  function term will be demonstrated in chapter four. It will be convenient in the derivation of the field theory to consider all observables as given by operators in this normal ordered form, with the  $a_i^\dagger$  then formally set equal to one.

Since the master equation must conserve probability, then

$$\sum_{\{n\}} P(\{n\}, t) = \langle |1| \phi(t) \rangle = 1, \quad (3.14)$$

or equivalently,

$$\frac{\partial}{\partial t} \langle |1| \phi(t) \rangle = \frac{\partial}{\partial t} \langle |e^{-\hat{H}t}| \phi(0) \rangle = -\langle |\hat{H}| \phi(t) \rangle = 0. \quad (3.15)$$

In order for the last equality to be satisfied for a general state  $|\phi(t)\rangle$ , then it follows that

$$\langle |\hat{H} = 0. \quad (3.16)$$

Therefore the equivalence of probability conservation in the second quantized representation is the property that the “Hamiltonian” acting to the left destroys the projection state. One consequence of this property is that an observable measured at time  $t$  is independent of the time  $t_f$  of the projection state, as long as  $t_f \geq t$ . That is, from equations (3.11) and (3.16) it follows that

$$\langle\langle A(t) \rangle\rangle = \langle |\hat{A} e^{-\hat{H}t}| \phi(0) \rangle = \langle |e^{-\hat{H}(t_f-t)} \hat{A} e^{-\hat{H}t}| \phi(0) \rangle. \quad (3.17)$$

This property will be discussed below in the context of the field theory.

An analogous formalism with Pauli spin matrices is often used, instead of the bosonic operators considered here. This corresponds to a master equation in which only single occupancy is allowed per lattice site. These techniques can be useful in one-dimension, where the resulting second quantized representation is a quantum spin-chain system, which is often integrable. However, our primary motive in introducing the second quantized representation is to map the problem to a field theory, and for this purpose the bosonic formalism developed above is more suitable.

### 3.2. COHERENT STATE REPRESENTATION

From the second quantized representation one can develop a field theory through the same path integral techniques as were developed for ordinary quantum mechanics. A thorough discussion of these methods is given by Schulman [45]. We begin with the expression for some observable

$$\langle\langle A(t) \rangle\rangle = \langle |\hat{A}e^{-\hat{H}t}|\phi(0)\rangle. \quad (3.18)$$

The basic idea is to divide the evolution of the system from time  $t = 0$  to  $t$  into a large number of slices  $N$ . Then for  $\Delta t = t/N$  we can use the Trotter formula

$$\exp(-\hat{H}t) = \lim_{\Delta t \rightarrow 0} (1 - \hat{H}\Delta t)^{t/\Delta t}. \quad (3.19)$$

Next a complete set of states is inserted at each time slice, before taking the limit  $N \rightarrow \infty$  or  $\Delta t \rightarrow 0$ . By finding the appropriate representation for the complete set of states, one then derives the path integral.

Associated with quantum harmonic oscillators are the coherent states, which are a continuous set of eigenstates of the annihilation operator  $a$ . It is possible to construct from these states a useful form of the identity operator. Consider first a single harmonic

oscillator. A particular coherent state is denoted by the complex number  $z$ , and is given by

$$|z\rangle = N(z) \exp(za^\dagger)|0\rangle \quad (3.20)$$

where  $N(z)$  is a normalization factor. Setting  $\langle z|z\rangle = 1$  gives  $N(z) = \exp(-|z|^2/2)$ . From (3.20) it follows that

$$a|z\rangle = z|z\rangle, \quad (3.21)$$

that is,  $z$  is the eigenvalue of the coherent state.

For the harmonic oscillator energy eigenstates, defined by  $|n\rangle = (a^\dagger)^n|0\rangle$ , the properly weighted complete set of states is

$$\mathbf{1} = \sum_i \frac{1}{n!} |n\rangle \langle n| = \sum_{m,n} \frac{1}{n!} |n\rangle \langle m| \delta_{mn}. \quad (3.22)$$

Using the relation

$$\delta_{mn} = \frac{1}{\pi m!} \int d^2 z e^{-|z|^2} z^{*m} z^n, \quad (3.23)$$

where  $d^2 z = d(\text{Re } z)d(\text{Im } z)$ , gives

$$\begin{aligned} \mathbf{1} &= \int \frac{d^2 z}{\pi} \sum_{m,n} \left( \frac{e^{-|z|^2/2} z^n}{n!} |n\rangle \right) \left( \langle m| \frac{e^{-|z|^2/2} z^{*m}}{m!} \right) \\ &= \int \frac{d^2 z}{\pi} |z\rangle \langle z|. \end{aligned} \quad (3.24)$$

The state  $|z\rangle$  is constructed from the operators at a single lattice site. This representation of the identity can be generalized by taking the vector product of these states for each lattice site. For notational convenience we denote the vector product by

$$|\{\phi\}\rangle = |\phi_1\rangle \otimes |\phi_2\rangle \otimes |\phi_3\rangle \otimes \dots \quad (3.25)$$

where  $\{\phi\} = (\phi_1, \phi_2, \dots)$ . The generalization of (3.24) is then

$$\mathbf{1} = \int \prod_i \left( \frac{d^2 \phi_i}{\pi} \right) |\{\phi\}\rangle \langle \{\phi\}| \quad (3.26)$$



The Trotter formula (3.19) is used to divide  $\exp(-\hat{H}t)$  into  $N = t/\Delta t$  slices, with the limit  $N \rightarrow \infty$  taken at the end of the calculation. Each time slice is labeled by the index  $j$ , so that  $t_j = j\Delta t$ . Inserting  $N + 1$  identity operators into the equation for observables (3.18), and then taking the limit  $N \rightarrow \infty$  gives

$$\begin{aligned} \langle\langle A(t) \rangle\rangle &= \mathcal{N}^{-1} \lim_{N \rightarrow \infty} \int \prod_{j=1}^N \left[ \left( \prod_i d^2 \phi_{i,j} \right) \langle \{\phi\}_j | 1 - \hat{H} \Delta t | \{\phi\}_{j-1} \rangle \right] \\ &\times \left( \prod_i d^2 \phi_{i,j=0} \right) \langle \hat{A} | \{\phi\}_{j=N} \rangle \langle \{\phi\}_{j=0} | \prod_i e^{\bar{n}_0 a_i^\dagger} | 0 \rangle \end{aligned} \quad (3.27)$$

The initial state is equivalent to a coherent state for each lattice site with  $z = \bar{n}_0$ , apart from the normalization. Henceforth we will denote the initial state by the coherent state  $|\bar{n}_0\rangle$ . The normalization factor and all the  $\pi$ 's are absorbed in the normalization constant  $\mathcal{N}$ . At the end of the calculation  $\mathcal{N}$  can be determined by the value of  $\langle\langle 1 \rangle\rangle^{-1}$ .

We define  $\hat{A}$  by its expansion in terms of the  $a_i$ , that is, all the  $a_i^\dagger$  are commuted to the left and set equal to one. Then the coherent states are eigenstates of  $\hat{A}$ , which implies that

$$\langle \hat{A} | \{\phi\}_N \rangle = \langle \{\phi\}_N | A(\{\phi\}_N) \rangle \quad (3.28)$$

where the function  $A(\{x\})$  is found from  $\hat{A}$  by taking  $a_i \rightarrow x_i$ . With this result and the definition

$$H(\{\phi\}_j, \{\phi\}_{j-1}) \equiv \frac{\langle \{\phi\}_j | \hat{H} | \{\phi\}_{j-1} \rangle}{\langle \{\phi\}_j | \{\phi\}_{j-1} \rangle} \quad (3.29)$$

we can rewrite (3.27) as

$$\begin{aligned} \langle\langle A(t) \rangle\rangle &= \mathcal{N}^{-1} \lim_{N \rightarrow \infty} \int \prod_{j=1}^N \left[ \left( \prod_i d^2 \phi_{i,j} \right) \langle \{\phi\}_j | \{\phi\}_{j-1} \rangle \right. \\ &\times \left( 1 - H(\{\phi\}_j, \{\phi\}_{j-1}) \Delta t \right) \Big] \\ &\times \left( \prod_i d^2 \phi_{i,0} \right) A(\{\phi\}_N) \langle \{\phi\}_N | \langle \{\phi\}_0 | \bar{n}_0 \rangle. \end{aligned} \quad (3.30)$$

Next we compute the overlap between the time slices. The coherent states at different lattice sites are orthogonal, and so the overlap is given by

$$\langle \{\phi\}_j | \{\phi\}_{j-1} \rangle = \prod_i \langle \phi_{i,j} | \phi_{i,j-1} \rangle. \quad (3.31)$$

Therefore product in the integral of (3.30) can be written

$$\lim_{N \rightarrow \infty} \prod_{j=1}^N \langle \{\phi\}_j | \{\phi\}_{j-1} \rangle = \prod_i \lim_{N \rightarrow \infty} \prod_{j=1}^N \langle \phi_{i,j} | \phi_{i,j-1} \rangle \quad (3.32)$$

Consider a single lattice site. For the next few steps we suppress the index  $i$  of the lattice sites. From the definition (3.20) of the coherent state  $|z\rangle$  it follows that

$$\langle \phi_j | \phi_{j-1} \rangle = \exp \left( -\frac{|\phi_j|^2}{2} - \frac{|\phi_{j-1}|^2}{2} + \phi_j^* \phi_{j-1} \right), \quad (3.33)$$

or equivalently,

$$e^{-\frac{1}{2}|\phi_j|^2} \langle \phi_j | \phi_{j-1} \rangle e^{\frac{1}{2}|\phi_{j-1}|^2} = \exp \left( -\phi_j^* (\phi_j - \phi_{j-1}) \right). \quad (3.34)$$

The difference term in (3.34) can be replaced by a derivative,

$$\phi_j - \phi_{j-1} = \frac{d\phi_j}{dt} \Delta t + O(\Delta t^2), \quad (3.35)$$

since only terms to order  $\Delta t$  are important in the Trotter formula. Apart from normalization, the projection state is a coherent state with  $z = 1$ , which implies<sup>5</sup>

$$\langle |\phi_N\rangle \propto \exp \left( -\frac{|\phi_N|^2}{2} + \phi_N \right). \quad (3.36)$$

Similarly, the overlap with the initial state is given by

$$\langle \{\phi\}_0 | \bar{n}_0 \rangle \propto \exp \left( -\frac{|\phi_0|^2}{2} + \bar{n}_0 \phi_0^* \right). \quad (3.37)$$

Combining the last four equations gives

$$\begin{aligned} & \lim_{N \rightarrow \infty} \langle |\phi_N\rangle \langle \phi_0 | \bar{n}_0 \rangle \prod_{j=1}^N \langle \phi_j | \phi_{j-1} \rangle \\ & \propto \lim_{N \rightarrow \infty} \exp \left( \phi_N + \bar{n}_0 \phi_0^* - |\phi_0|^2 - \sum_{j=1}^N \Delta t \phi_j^* \partial_t \phi_j \right) \\ & \propto \exp \left( \phi(t_f) + \bar{n}_0 \phi^*(0) - |\phi(0)|^2 - \int_0^{t_f} dt \phi^*(t) \partial_t \phi(t) \right) \end{aligned} \quad (3.38)$$

---

<sup>5</sup> Here we are referring to the projection state for a single lattice site

In the limit  $N \rightarrow \infty$  the set of labels  $t_j = j\Delta t$  become continuous, and the variables  $\phi_j$  are replaced with the continuous function  $\phi(t)$ . The time  $t_f$  in the upper integration limit is the same as the time  $t$  of the observable  $\langle\langle A(t) \rangle\rangle$  in the derivation presented above. However, as shown in the previous section, the final time  $t_f$  is arbitrary, provided  $t_f > t$ . The results would be the same for these terms if the operator  $\hat{A}$  would have been inserted into an earlier time slice.

The final step in the overlap calculation is the generalization to all lattice sites. From the relation (3.32) it follows directly that

$$\begin{aligned} & \lim_{N \rightarrow \infty} \langle |\{\phi\}_N \rangle \langle \{\phi\}_0 | \bar{n}_0 \rangle \prod_{j=1}^N \langle \{\phi\}_j | \{\phi\}_{j-1} \rangle \\ & \propto \exp \left( \sum_i \left[ \phi_i(t_f) + \bar{n}_0 \phi^*(0) - |\phi_i(0)|^2 - \int_0^{t_f} dt \phi_i^*(t) \partial_t \phi_i(t) \right] \right). \end{aligned} \quad (3.39)$$

Next we calculate the function  $H(\{\phi\}_j, \{\phi\}_{j-1})$ . The coherent states are eigenstates of the annihilation operators acting to the right, that is  $a|z\rangle = z|z\rangle$ , which implies that  $\langle z|a^\dagger = \langle z|z^*$ . With these properties and equations (3.9) and (3.29) it follows immediately that

$$\begin{aligned} H(\{\phi\}_j, \{\phi\}_{j-1}) &= -\frac{D}{a^2} \sum_{i,e} \phi_{i,j}^* (\phi_{e,j-1} - \phi_{i,j-1}) \\ &\quad - \lambda \sum_i (1 - (\phi_{i,j}^*)^k) \phi_{i,j-1}^k, \end{aligned} \quad (3.40)$$

where  $e$  is summed over nearest neighbors of  $i$ . Replacing the  $\phi_{i,j-1}$  with  $\phi_{i,j}$  introduces corrections which are higher order in  $\Delta t$ . Therefore we get the limit

$$\begin{aligned} & \lim_{N \rightarrow \infty} \prod_{j=1}^N \left( 1 - H(\{\phi\}_j, \{\phi\}_{j-1}) \Delta t \right) = \\ & \exp \left( \sum_i \int_0^{t_f} dt \left[ \frac{D}{a^2} \sum_e \phi_i^*(t) (\phi_e(t) - \phi_i(t)) + \lambda (1 - \phi_i^*(t)^k) \phi_i(t)^k \right] \right). \end{aligned} \quad (3.41)$$

The expectation value given by (3.30) can now be expressed in terms of a path integral by combining equations (3.30), (3.39), and (3.41), with the result

$$\langle\langle A(t) \rangle\rangle = \mathcal{N}^{-1} \int \left( \prod_i \mathcal{D}\phi_i(t) \mathcal{D}\hat{\phi}_i(t) \right) A(\{\phi\}(t)) e^{-S}, \quad (3.42)$$

where

$$S = \sum_i \left[ \int_0^{t_f} dt \left\{ \hat{\phi}_i \partial_t \phi_i - \frac{D}{a^2} \hat{\phi}_i \sum_e (\phi_e - \phi_i) - \lambda (1 - \hat{\phi}_i^k) \phi_i^k \right\} \right. \\ \left. - \phi_i(t_f) - \bar{n}_0 \hat{\phi}_i(0) + \hat{\phi}(0) \phi(0) \right] \quad (3.43)$$

with the normalization constant

$$\mathcal{N} = \int \left( \prod_i \mathcal{D}\phi_i(t) \mathcal{D}\hat{\phi}_i(t) \right) e^{-S}. \quad (3.44)$$

Here we have substituted  $\hat{\phi}$  for  $\phi^*$ , as we will treat the complex conjugate as an independent field. The functional integration differentials, denoted by  $\mathcal{D}\phi_i(t) \mathcal{D}\hat{\phi}_i(t)$ , are argued to be the limit as  $N \rightarrow \infty$  of the  $N + 1$  differentials  $d\phi_{i,j} d\hat{\phi}_{i,j}$ . This step, as always with the derivation of path integrals, is not rigorous. Henceforth equations (3.42) and (3.44) are implied in the calculation of observables, and we will focus our attention on the action  $S$ .

### 3.3. ACTION FOR THE ONE-SPECIES REACTION

Notice that the action (3.43) is a discrete sum over lattice sites, and contains the same microscopic parameters as the master equation. We can take a continuum limit without coarse graining simply by making the substitutions  $\sum_i \rightarrow \int d^d x / a^d$ ,  $\phi_i \rightarrow \phi(x) / a^d$ ,  $\hat{\phi}_i \rightarrow \hat{\phi}(x)$ ,  $\bar{n}_0 \rightarrow n_0 a^d$ , and  $\sum_e (\phi_e - \phi_i) \rightarrow a^2 \nabla^2 \phi(x)$ . The initial density now has dimension, and is given by  $n_0$ . The diffusion constant exhibits no singular behavior in the renormalization of the theory, so it is absorbed into a rescaling of time, giving the action

$$S = \int d^d x \left[ \int_0^{t_f} dt \left\{ \hat{\phi} (\partial_t - \nabla^2) \phi - \lambda_0 (1 - \hat{\phi}^k) \phi^k \right\} \right. \\ \left. - \phi(t_f) - n_0 \hat{\phi}(0) + \hat{\phi}(0) \phi(0) \right] \quad (3.45)$$

where the coupling  $\lambda_0 = \lambda D^{-1} a^{(k-1)d}$ .

We turn now to the initial conditions. One way to deal with the last two terms in (3.45) is to integrate first over  $\hat{\phi}(0)$ , which has the effect of creating a  $\delta(\phi(0) - n_0)$  term.<sup>6</sup>

---

<sup>6</sup> The integration over  $\hat{\phi}(0)$  can be done rigorously before taking the  $N \rightarrow \infty$  limit of the Trotter formula, as the variable  $\hat{\phi}_{i,j=0}$  appears only in these two terms.

Then integrating over  $\phi(0)$  gives the net result that the two initial terms vanish from (3.45), replaced with an understood constraint of  $\phi(0) = n_0$ . However, the path integral with a constraint is not very useful for perturbation theory.

We would like to find an alternate way of including the initial conditions which is more amenable to a perturbative calculation. To do so, we first address how such a calculation is implemented. Averages are computed with respect to the non-interacting theory, which is in this case given by the  $\hat{\phi}(\partial_t - \nabla^2)\phi$  term. These averages are carried out with standard diagrammatic techniques, in which interactions are connected by a propagator derived from the non-interacting theory. We present in appendix 3.A. the calculation of the propagator, but mention now one of its properties. In wave number-time space, for example, we find

$$\langle \phi(p, t_2) \hat{\phi}(-p, t_1) \rangle = \begin{cases} e^{-p^2(t_2 - t_1)} & t_2 > t_1 \\ 0 & t_2 < t_1, \end{cases} \quad (3.46)$$

That is, the propagator can only connect a  $\phi$  with an earlier  $\hat{\phi}$ .

The interaction terms, labeled  $S_I$ , are included perturbatively by the Taylor expansion of  $\exp(-S_I)$ . Since this expansion includes the initial terms, we consider calculating averages of given powers of  $n_0 \hat{\phi}(0)$  and  $\hat{\phi}(0)\phi(0)$ . As there are no  $\hat{\phi}$  present for  $t < 0$ , the issue we must address is what to do with the  $\phi(0)$ . One idea would be point splitting, that is, we replace last term in (3.45) with

$$\hat{\phi}(0)\phi(0) \rightarrow \lim_{\delta t \rightarrow 0} \hat{\phi}(t = \delta t)\phi(t = -\delta t). \quad (3.47)$$

However, it is arbitrary which way we split the fields, and so we should also consider the effect of splitting the fields in the opposite direction

$$\hat{\phi}(0)\phi(0) \rightarrow \lim_{\delta t \rightarrow 0} \phi(\delta t)\hat{\phi}(-\delta t). \quad (3.48)$$

The results turn out to depend on the point splitting procedure. This must be an artifact of taking the  $N \rightarrow \infty$  limit of the Trotter formula, since the interaction  $\phi_{i,j=0} \hat{\phi}_{i,j=0}$  could be integrated over before with no point splitting, and with finite results. Therefore we need to take the  $N \rightarrow \infty$  limit in such a way that this  $t = 0$  property is maintained.

If we consider a finite number of time slices, using the notation of §3.2, we find for the non-interacting ( $\lambda = 0$ ) action

$$S = \sum_{j=1}^N \sum_i \left\{ \hat{\phi}_{i,j}(\phi_{i,j} - \phi_{i,j-1}) - \frac{D}{a^2} \sum_e \hat{\phi}_{i,j}(\phi_{e,j-1} - \phi_{i,j-1}) \right\}. \quad (3.49)$$

The first term is exact for finite  $\Delta t$ , while the second term contains just the order  $\Delta t$  contribution. The exact expression for finite  $\Delta t$  would involve an expansion with higher powers of  $H(\{\phi\}_j, \{\phi\}_{j-1})$ , but these have no effect on the subsequent analysis. We want to calculate the interaction  $\exp(\hat{\phi}_{i,0}\phi_{i,0})$ , evaluated with the above action. Since there are no terms in  $S$  which are bilinear in  $\hat{\phi}_{i,0}\phi_{i,0}$ , then by Gaussian integration  $\langle \hat{\phi}_{i,0}\phi_{i,0} \rangle = 0$ . We conclude that in taking the  $N \rightarrow \infty$  limit that we must preserve the result that

$$\langle \hat{\phi}(0)\phi(0) \rangle = 0. \quad (3.50)$$

Therefore this interaction term can be dropped from (3.45), as the Taylor expansion of  $\langle \exp(\hat{\phi}(0)\phi(0)) \rangle$  contributes one plus terms which are some power of (3.50).

There is also present in (3.45) the term  $\phi(t_f)$ . This can be eliminated by performing the field shift  $\hat{\phi} = 1 + \bar{\phi}$ . Then

$$S = \int d^d x \left[ \int_0^{t_f} dt \left\{ (1 + \bar{\phi})(\partial_t - \nabla^2)\phi - \lambda_0 \left( 1 - (1 + \bar{\phi})^k \right) \phi^k \right\} - \phi(t_f) - n_0 \left( 1 + \bar{\phi}(0) \right) \right] \quad (3.51)$$

$$= \int d^d x \left[ \int_0^t dt \left\{ \bar{\phi}(\partial_t - \nabla^2)\phi + \sum_{i=1}^k \lambda_i \bar{\phi}^i \phi^k \right\} - n_0 \bar{\phi}(0) \right] + \text{const.},$$

where  $\lambda_i = \binom{k}{i} \lambda_0$ . The integral of  $\partial_t \phi$  in the first line above generates the surface terms  $\phi(t_f) - n_0$ , which has the effect of canceling the  $-\phi(t_f)$  term.<sup>7</sup> This simplifies the perturbative calculations, since one no longer has to consider summing over an expansion of this

---

<sup>7</sup> The same result could be derived by making the shift  $a^\dagger = 1 + \bar{a}^\dagger$  in the second quantized representation, which has the consequence that  $\langle |\bar{a}^\dagger| = 0$ .

end state. The action (3.51) will be used in chapter four to calculate observables for the one-species reaction.

We now address the calculation of observables. Given an observable  $A(\{n\})$ , which is in the original theory some function of the occupation numbers, it is shown in §3.1 how to find the corresponding second quantized operator  $\hat{A}$ . This operator can be expressed in terms of only the  $a_i$ . Then from equation (3.28) the field theory analog  $A(\{\phi\})$  can be found, and is given by the substitution  $a_i \rightarrow \phi_i$ . The expectation value  $A(t)$  is equivalent in all three representations. The field theoretic version is given by equation (3.42), and involves an average of  $A(\{\phi\}, t)$  over the action above. This is denoted by double brackets, and single brackets are used for averages over the part of (3.51) which does not include the initial term. That is,

$$\langle\langle A(x, t) \rangle\rangle = \left\langle A(x, t) e^{n_0 \int d^d x \bar{\phi}(x, 0)} \right\rangle. \quad (3.52)$$

This average is already normalized, since

$$\langle\langle 1 \rangle\rangle = \left\langle e^{n_0 \int d^d x \bar{\phi}(x, 0)} \right\rangle = 1. \quad (3.53)$$

That is, there are no later  $\phi$ 's with which to contract the  $\bar{\phi}$ 's.

Finally, we consider two specific examples. For the density operator, given in the second quantized representation by equation (3.12), we find

$$n(t) = \frac{1}{V} \int d^d x \langle\langle \phi(x, t) \rangle\rangle = \langle\langle \phi(x, t) \rangle\rangle. \quad (3.54)$$

The last equality follows from translational invariance. Also, the correlation function (3.13) is given by

$$C(\mathbf{x}, t) = \langle\langle (\phi(\mathbf{x}, t) + \delta(\mathbf{x})) \phi(0, t) \rangle\rangle. \quad (3.55)$$

### 3.4. ACTION FOR THE TWO-SPECIES REACTION

For the two-species reaction we have a similar model of particles on a lattice of size  $a$ , but now there are two sets of occupation numbers:  $\{n\}$  give the number of  $A$  particles at each lattice site and  $\{m\}$  the number of  $B$  particles. The master equation for the two-species reaction is

$$\begin{aligned} \frac{\partial}{\partial t} P(\{n\}, \{m\}, t) = & \\ & \frac{D_A}{a^2} \sum_{i,e} \left\{ (n_e + 1) P(\dots, n_i - 1, n_e + 1, \dots, \{m\}, t) - n_i P \right\} \\ & + \frac{D_B}{a^2} \sum_{i,e} \left\{ (m_e + 1) P(\{n\}, \dots, m_i - 1, m_e + 1, \dots, t) - m_i P \right\} \\ & + \lambda \sum_i \left\{ (n_i + 1)(m_i + 1) P(\dots, n_i + 1, \dots, m_i + 1, \dots, t) \right. \\ & \quad \left. - n_i m_i P \right\}. \end{aligned} \quad (3.56)$$

As before,  $i$  is summed over lattice sites and  $e$  is summed over nearest neighbors of  $i$ . The first two curly bracket terms describe the diffusion of the  $A$  and  $B$  particles, and the last term the annihilation.

The second quantized representation involves a two sets of creation and annihilation operators,  $a, a^\dagger$  and  $b, b^\dagger$ . These obey the same commutation relations as before, and the two types of operators are mutually commuting. The state of the system at time  $t$  is defined to be

$$|\phi(t)\rangle = \sum_{\{n\}, \{m\}} P(\{n\}, \{m\}, t) \prod_i (a_i^\dagger)^{n_i} (b_i^\dagger)^{m_i} |0\rangle, \quad (3.57)$$

which again obeys the equation of motion (3.6) with the time evolution operator

$$\hat{H} = - \sum_i \sum_e \left\{ \frac{D_A}{a^2} a_i^\dagger (a_e - a_i) + \frac{D_B}{a^2} b_i^\dagger (b_e - b_i) \right\} - \lambda \sum_i (1 - a_i^\dagger b_i^\dagger) a_i b_i. \quad (3.58)$$

The initial state is given by a Poisson distribution of occupation numbers, with averages  $\bar{a}_0$  and  $\bar{b}_0$ . In this thesis we study only the case in which the initial densities are equal, so



that  $\bar{a}_0 = \bar{b}_0 = \bar{n}_0$ , and

$$\begin{aligned}
|\phi(0)\rangle &= C \sum_{\{n\}, \{m\}} \prod_i \frac{\bar{n}_0^{n_i+m_i}}{n_i! m_i!} (a_i^\dagger)^{n_i} (b_i^\dagger)^{m_i} |0\rangle \\
&= C \prod_i \left( \sum_{n_i} \frac{(\bar{n}_0 a_i^\dagger)^{n_i}}{n_i!} \right) \left( \sum_{m_i} \frac{(\bar{n}_0 b_i^\dagger)^{m_i}}{m_i!} \right) |0\rangle \\
&= C \prod_i e^{\bar{n}_0(a_i^\dagger + b_i^\dagger)} |0\rangle.
\end{aligned} \tag{3.59}$$

Similarly, the projection state is given by  $\langle 0 | \prod_i \exp(a_i + b_i)$ .

The derivation of the field theory follows identically, with the coherent states generalized to two fields,  $a$  and  $b$ . The action is

$$\begin{aligned}
S = \int d^d x \left[ \int_0^{t_f} dt \left\{ \hat{a} \left( \partial_t - \frac{D_A}{\bar{D}} \nabla^2 \right) a + \hat{b} \left( \partial_t - \frac{D_B}{\bar{D}} \nabla^2 \right) b \right. \right. \\
\left. \left. - \lambda_0 (1 - \hat{a} \hat{b}) ab \right\} - n_0 \hat{a}(0) - n_0 \hat{b}(0) - a(t_f) - b(t_f) \right].
\end{aligned} \tag{3.60}$$

This result includes a rescaling of time by the average diffusion constant  $\bar{D} = (D_A + D_B)/2$ . The coupling constant is given by  $\lambda_0 = \lambda \bar{D} a^d$ . As before, we can eliminate the final terms by making the field shifts  $\hat{a} = 1 + \bar{a}$  and  $\hat{b} = 1 + \bar{b}$ . This also has the consequence

$$-\lambda_0 (1 - \hat{a} \hat{b}) ab \rightarrow \lambda_0 (\bar{a} + \bar{b}) ab + \lambda_0 \bar{a} \bar{b} ab. \tag{3.61}$$

Since we know the conserved mode of  $a - b$  is important in the dynamics, it is useful to make the transformation to the fields  $\phi, \bar{\phi}, \psi, \bar{\psi}$  defined by

$$\phi = \frac{a+b}{\sqrt{2}} \quad \bar{\phi} = \frac{\bar{a}+\bar{b}}{\sqrt{2}} \quad \psi = \frac{a-b}{\sqrt{2}} \quad \bar{\psi} = \frac{\bar{a}-\bar{b}}{\sqrt{2}}. \tag{3.62}$$

The  $\sqrt{2}$  factors are included so that the non-interacting action maintains a coefficient of unity. The subsequent action is

$$\begin{aligned}
S = \int d^d x \left[ \int_0^{t_f} dt \left\{ \bar{\phi} (\partial_t - \nabla^2) \phi + \bar{\psi} (\partial_t - \nabla^2) \psi - \delta \bar{\psi} \nabla^2 \phi - \delta \bar{\phi} \nabla^2 \psi \right. \right. \\
\left. \left. - \lambda_1 \bar{\phi} (\phi^2 - \psi^2) - \lambda_2 (\bar{\phi}^2 - \bar{\psi}^2) (\phi^2 - \psi^2) \right\} - n_\phi \bar{\phi}(0) \right],
\end{aligned} \tag{3.63}$$

where  $\delta = (D_A - D_B)/(D_A + D_B)$ , the couplings are  $\lambda_1 = \lambda_0/\sqrt{2}$  and  $\lambda_2 = \lambda_0/4$ , and the initial density is  $n_\phi = \sqrt{2}n_0$ . The action (3.63) is the starting point of the analysis in chapter five.

### APPENDIX 3.A. DERIVATION OF THE PROPAGATOR

We show in this appendix how the propagator is derived from the non-interacting action

$$S_0 = \int d^d x \int_0^{t_f} dt \bar{\phi}(\partial_t - \nabla^2)\phi. \quad (3.A.1)$$

In the derivation of the path integral in §3.2 we considered inserting time slices into the operator  $\exp(-\hat{H}t)$  between times  $t = 0$  and  $t = t_f$ . However, we could add time slices from  $-\infty < t < \infty$  with no consequence. Therefore we consider letting the time integral in (3.A.1) run from  $-\infty$  to  $\infty$ . Taking the Fourier transform with respect to time and space gives

$$S_0 = \int d^d p d\omega \bar{\phi}(-\mathbf{p}, -\omega)(-i\omega + p^2)\phi(\mathbf{p}, \omega), \quad (3.A.2)$$

where the transforms are defined by

$$\phi(\mathbf{p}, \omega) = \int \frac{d^d p}{(2\pi)^d} \frac{d\omega}{2\pi} e^{-i(\mathbf{p} \cdot \mathbf{x} - \omega t)} \phi(\mathbf{x}, t) \quad (3.A.3)$$

With this form of the action the propagator can be derived by Gaussian integration, with the result

$$G(\mathbf{p}, \omega) = \frac{1}{-i\omega + p^2}. \quad (3.A.4)$$

Most of the integrals in the following chapter are evaluated using the propagator  $G(\mathbf{p}, t)$ , which is defined by the integral

$$G(\mathbf{p}, t) = \int_{-\infty}^{\infty} \frac{d\omega}{2\pi} \frac{e^{-i\omega t}}{-i\omega + p^2}. \quad (3.A.5)$$

This can be evaluated by contour integration, with a contour which runs along the real axis and is closed at infinity in either the upper or lower half-plane. The only pole is at  $\omega = -ip^2$ . For  $t < 0$  the integral can be closed in the upper half-plane, and therefore gets no contribution from the pole. For  $t > 0$  one finds from the residue theorem

$$G(\mathbf{p}, t) = -2\pi i \lim_{\omega \rightarrow -ip^2} \frac{ie^{-i\omega t}}{2\pi} = e^{-p^2 t} \quad (3.A.6)$$

Therefore, when evaluating the diagrammatic perturbation expansion one can only connect later  $\bar{\phi}$  fields with earlier  $\phi$  fields.

The position space version of the propagator can be evaluated by completing the square in the exponential. That is, for  $t > 0$

$$\begin{aligned}
G(\mathbf{x}, t) &= \int \frac{d^d p}{(2\pi)^d} e^{-i\mathbf{p} \cdot \mathbf{x}} e^{-p^2 t} \\
&= \int \frac{d^d p}{(2\pi)^d} e^{-t(p + ix/2t)^2} e^{-x^2/4t} \\
&= \left( \frac{1}{4\pi t} \right)^{d/2} e^{-x^2/4t}.
\end{aligned} \tag{3.A.7}$$

## Chapter 4. One-Species Reaction $kA \rightarrow \emptyset$

We consider a system described by identical particles moving with diffusion constant  $D$ , and annihilating whenever  $k$  particles meet within a certain capture range  $r_c$ . This is known as the  $kA \rightarrow \emptyset$  reaction-diffusion system. A first approach to this problem is to write the rate equation for the density

$$\frac{\partial}{\partial t}n = -\Gamma n^k, \quad (4.1)$$

where  $\Gamma$  is some rate constant which depends on  $D$  and  $r_c$ . Making the assumption that the diffusion constant acts only to set the scale of time leads to the result that  $\Gamma = Dr_c^{(k-1)d-2}$ , and the asymptotic density

$$n(t) \sim r_c^{-d+2/(k-1)}(Dt)^{-1/(k-1)}. \quad (4.2)$$

While this result is plausible for  $d > 2/(k-1)$ , it can be rejected for the case of  $d < 2/(k-1)$  as the annihilation rate should not decrease with increasing  $r_c$ .

This effect was first noted by Toussaint and Wilczek [31] in the case  $k = 2$ . They identify  $d = 2$  as a critical dimension, below which the random walks of the diffusing particles are reentrant. For  $d < 2$  they argue that the random walk of a single particle which is still present at time  $t$  will have covered a region of linear dimension  $(Dt)^{1/2}$ , and

that no other particles can remain in this region. Therefore the average volume per particle goes as  $(Dt)^{d/2}$ , or equivalently the density

$$n(t) \sim (Dt)^{-d/2}. \quad (4.3)$$

While the generalization of this approach to larger values of  $k$  is not obvious, these arguments do suggest the existence of an upper critical dimension and a mean-field solution. It has been conjectured that the critical dimension for general  $k$  is given by  $d_c = 2/(k-1)$ , and that the density decays as  $n \sim t^{-d/2}$  for  $d < d_c$  [48,49]. The mean field decay of equation (4.2) has been confirmed numerically for  $d = 1$ ,  $k = 3, 4$  [48], as has the  $d < d_c$  result for  $k = 2$ ,  $d = 1, 2$  [31]. When the system is at the critical dimension then it is expected that density will decay with the mean-field exponent, but with logarithmic corrections. There are also exact solutions of these models for  $k = 2$  and  $d = 1$  which are consistent with the predictions above [50–53].

With the field theoretic formulation of the problem developed in chapter three we can apply traditional renormalization group methods to this problem. The existence of the upper critical dimension allows us to calculate an expansion in  $\epsilon = d_c - d$ . The model we consider for this reaction is one of particles on a lattice undergoing continuous-time random walks. Whenever  $k$  particles meet on a lattice site they will react with some rate  $\lambda$  to form an inert particle. In this version of the system, then, the capture radius is replaced with a rate constant. However, since the resulting calculation will demonstrate the universality of the results, the differences between these versions of the system is shown to be irrelevant.

Previous work in applying RG to this system was carried out by Peliti for the case  $k = 2$  [54]. Using the same field theory formulation of this system as is presented in chapter three, Peliti was able to confirm the conjectured decay exponent, and also demonstrate that the reactions  $A + A \rightarrow \emptyset$  and  $A + A \rightarrow A$  are in the same universality class with regard to the decay exponent and the upper critical dimension. However, his results rely on the assumption that the asymptotic density does not depend on the initial conditions.

This assumption turns out to be valid in the one-species reactions, but would not be correct for the reaction  $A + B \rightarrow \emptyset$ , for example. Peliti also made the observations that the coupling constants can be exactly renormalized to all orders and that there is no wave-function renormalization in the theory. The latter has the consequence that simple scaling arguments can be used to extract the decay exponent and the upper critical dimension. However, these scaling arguments are not capable of giving other universal quantities in the system, such as amplitudes or the asymptotic form of the correlation function. For these one must do the complete RG calculation.

Recent work in applying RG to this system includes that of Ohtsuki [55], in which the density is calculated, although with dramatically different results than those presented here. First, Ohtsuki predicts that the amplitude for the asymptotic form of the density has the same reaction rate constant dependence as the mean-field solution,  $n \sim \Gamma^{-1}$  for  $k = 2$ , whereas we find the amplitude to be independent of this rate constant. Second, the leading order term in the  $\epsilon$  expansion for the density amplitude in [55] is of order unity, whereas we find it to be order  $\epsilon^{-1/(k-1)}$ . An RG scheme involving an external source of particles has been developed by Droz and Sasvári [56] which leads to scaling relations which confirm the decay exponent. As with the analysis of Peliti, this approach relies on the irrelevance of the initial conditions, and does not demonstrate it. Friedman *et al.* attempted to calculate the density perturbatively, and concluded that it is necessary to perform a non-perturbative sum of all orders of  $n_0$ , the initial density, when calculating observables [57]. This infinite sum is exactly what we do in our calculation scheme.

A slightly different field theory formalism for this system was developed in analogy with bose condensate calculations [58,59]. This approach leads to a confirmation of the decay exponents as well. However, this method is not as readily generalized to an RG calculation as is the field theory approach of Peliti.

## 4.1. RENORMALIZATION GROUP SCHEME

From the master equation description of the system one can derive the field theory

$$S[\bar{\phi}, \phi, t] = \int d^d x \left[ \int_0^t dt \left\{ \bar{\phi}(\partial_t - \nabla^2)\phi + \sum_{i=1}^k \lambda_i \bar{\phi}^i \phi^k \right\} - n_0 \bar{\phi}(0) \right], \quad (4.4)$$

as was shown in chapter three. The dimensions of the various quantities in (4.4), expressed in terms of wave number, are

$$[t] = p^{-2} \quad [\bar{\phi}(x)] = p^0 \quad [\phi(x)] = p^d \quad [\lambda_i] = p^{2-(k-1)d}. \quad (4.5)$$

The couplings become dimensionless at the traditionally accepted value of the critical dimension,  $d_c = 2/(k-1)$  [48,49]. The relative dimensions of  $\phi$  and  $\bar{\phi}$  are arbitrary, so long as  $[\bar{\phi}\phi] = p^d$ , but the choice above is the most natural, as any other would cause the couplings  $\lambda_i$  to have dimensions which depend on  $i$ .

As demonstrated in chapter three, the density is calculated from the above action by the average of  $\phi$ . That is

$$n(t) = \langle\langle \phi(t) \rangle\rangle = \left\langle \phi(t) \exp \left\{ n_0 \int d^d y \bar{\phi}(y, 0) \right\} \right\rangle, \quad (4.6)$$

where the double brackets denote averages with respect to (4.4), and the single brackets are averages over the bulk action, which is given by the terms in curly braces in (4.4). From this expression a perturbative calculation of  $n(t)$  can be found. The first term in the action gives the diffusion propagator  $G(p, t) = e^{-p^2 t}$  for  $t > 0$  and  $G = 0$  for  $t < 0$ . An expansion in powers of the couplings  $\lambda_i \propto \lambda_0$  can be calculated with the usual perturbation theory techniques. By using the Taylor expansion of the exponential in (4.6) a double expansion in powers of  $\lambda_0$  and  $n_0$  can be obtained. When the renormalization group methods are applied to the system it is found that the coupling  $\lambda_0$  flows to an order  $\epsilon$  fixed point. However, the initial density  $n_0$  flows to a strong coupling limit. Therefore for our perturbation theory to be valid we must find an expansion in powers of the coupling which involves sums over

all powers of  $n_0$ . The development of this expansion and the resultant calculations are the primary results of this chapter.

The scheme developed for renormalizing the theory follows conventional RG analysis [41]. In this vein a renormalized coupling is introduced, and shown to have a stable fixed point of order  $\epsilon$ . The computation of observables requires summing over an infinite set of diagrams, corresponding to all powers of  $n_0$ , and this infinite sum must be grouped into sets of diagrams whose sums give a particular order of the coupling constant. It will be shown below that this grouping is given by the number of loops. That is, the infinite set of tree diagrams sum to give the leading order term in the coupling, the one-loop diagrams the next order term, and so on. However, before addressing the calculation of observables we turn to the renormalization of the theory.

### *Exact Vertex Renormalization*

To renormalize the theory all that is required is coupling constant renormalization. This is because the set of vertices in (4.4) allow no diagrams which dress the propagator, implying there is no wavefunction renormalization. As a consequence the bare propagator is the full propagator for the theory.

To determine which couplings get renormalized one first needs to identify the primitively divergent vertex functions. A general correlation function with  $\ell$   $\phi$ 's and  $m$   $\bar{\phi}$ 's has the dimension

$$[\langle \phi(1) \dots \phi(\ell) \bar{\phi}(\ell+1) \dots \bar{\phi}(\ell+m) \rangle] = p^{d\ell} \quad (4.7)$$

where  $(1) = (x_1, t_1)$ . The Green's function  $G^{(\ell,m)}(p_1, s_1, \dots, p_{\ell+m}, s_{\ell+m})$  is calculated by Fourier and Laplace transforming the correlation function above, and factoring out overall  $p$  and  $s$  conserving  $\delta$  functions. The dimensions of this quantity are

$$[G^{(\ell,m)}] = p^{d+2-2\ell-(d+2)m}. \quad (4.8)$$



The dimensions of the vertex functions  $\Gamma^{(\ell,m)}$  are given by the Green's functions with the  $\ell + m$  external propagators stripped off.

$$[\Gamma^{(\ell,m)}] = [G^{(\ell,m)} / (G^{(1,1)})^{\ell+m}] = p^{2-d(m-1)}. \quad (4.9)$$

The vertex functions with  $m \leq k$  are those which are primitively divergent for  $d \leq d_c$ . Since vertices can only connect  $k$   $\bar{\phi}$ 's to some number less than or equal to  $k$   $\phi$ 's, then it follows that the primitively divergent diagrams have  $m = k$  and  $\ell \leq k$ .

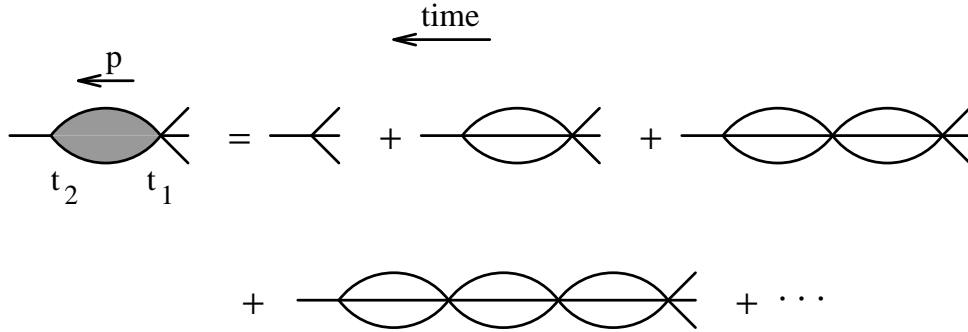


FIGURE 4.1. Sum of all the diagrams which contribute to the vertex function  $\lambda(p, t_2 - t_1)$ . Shown here is the case  $k = 3$ ,  $i = 1$ . These diagrams can be summed exactly, and are the same for all  $i$ .

A general  $\bar{\phi}^i \phi^k$  vertex is renormalized by the set of diagrams shown in fig. 4.1. In these diagrams the propagator is represented by a plain line. Note that this sum is the same for all  $i$ , that is all vertices renormalize identically. This is a reflection of the fact that there is a only one coupling in the theory. These diagrams can be summed to all orders, as noted in [54]. In  $(p, t)$  space the temporally extended vertex function  $\lambda(p, t_2 - t_1)$  is given by

$$\begin{aligned} \lambda(p, t_2 - t_1) = & \lambda_0 \delta(t_2 - t_1) - \lambda_0^2 I(p, t_2 - t_1) \\ & + \lambda_0^3 \int_{t_1}^{t_2} dt' I(p, t_2 - t') I(p, t' - t_1) - \dots \end{aligned} \quad (4.10)$$

where  $I(p, t)$  is the  $k - 1$  loop integral

$$I(p, t) = k! \int \prod_i^k \left( \frac{d^d p_i}{(2\pi)^d} \right) (2\pi)^d \delta(p - \sum_i^k p_i) \exp(-\sum_i^k p_i^2 t). \quad (4.11)$$

The  $\delta$  function can be written in integral form, which turns the integral into a product of  $k$  Gaussian integrals. This gives

$$I(p, t) = B_k t^{-(k-1)d/2} e^{-p^2 t/k} \quad (4.12)$$

where

$$B_k = \frac{k!}{k^{d/2}} \left( \frac{1}{4\pi} \right)^{(k-1)d/2}. \quad (4.13)$$

Taking the Laplace transform,  $\lambda(p, s) = \int_0^\infty dt e^{-st} \lambda(p, t)$ , makes (4.10) a geometric sum:

$$\lambda(p, s) = \frac{\lambda_0}{1 + \lambda_0 B_k \Gamma(\epsilon/d_c) (s + p^2/k)^{-\epsilon/d_c}}, \quad (4.14)$$

where the  $d$  and  $k$  have been exchanged for  $\epsilon$  and  $d_c$ . For a general  $\bar{\phi}^i \phi^k$  vertex the  $\lambda_0$  in the numerator is replaced by  $\lambda_i = \binom{k}{i} \lambda_0$ , and the denominator is unchanged. Therefore the small  $s$  and  $p$  form of the vertex function is independent of  $\lambda_0$  for all  $i$ .

The vertex function (4.14) is used to define a renormalized coupling. Using the wave number  $\kappa$  as a normalization point, we define the dimensionless renormalized coupling to be

$g_R = \kappa^{-2\epsilon/d_c} \lambda(s, p)|_{s=\kappa^2, p=0}$ , and the dimensionless bare coupling

$g_0 = \kappa^{-2\epsilon/d_c} \lambda_0$ . The  $\beta$  function is defined by

$$\beta(g_R) \equiv \kappa \frac{\partial}{\partial \kappa} g_R = -\frac{2\epsilon}{d_c} g_R + \frac{2\epsilon}{d_c} B_k \Gamma\left(\frac{\epsilon}{d_c}\right) g_R^2. \quad (4.15)$$

It is exactly quadratic in  $g_R$  and has a fixed point  $\beta(g_R^*) = 0$  at

$$g_R^* = \{B_k \Gamma(\epsilon/d_c)\}^{-1}. \quad (4.16)$$

The fixed point is of order  $\epsilon$ . From the definition of  $g_R$ , (4.14), and (4.16) it follows that

$g_R^{-1} = g_0^{-1} + g_R^{*-1}$ , or

$$g_0 = \frac{g_R}{1 - g_R/g_R^*} = g_R + \frac{g_R^2}{g_R^*} + \dots \quad (4.17)$$

This will be used to exchange an expansion in  $g_0$ , calculated in perturbation theory, for an expansion in  $g_R$ .

## Calculation of Observables

Next we develop a Callan-Symanzik equation for the theory. Given a correlation function

$$F^{(m)}(t, \lambda_0) \equiv \left\langle \phi(x, t) \left( \int d^d y \bar{\phi}(y, t=0) \right)^m \right\rangle \quad (4.18)$$

The lack of dependence on the normalization scale can be expressed via

$$\left[ \kappa \frac{\partial}{\partial \kappa} + \beta(g_R) \frac{\partial}{\partial g_R} \right] F^{(m)}(t, \kappa, g_R) = 0. \quad (4.19)$$

From dimensional analysis  $[F^{(m)}] = p^{d-md}$ , implying

$$\left[ \kappa \frac{\partial}{\partial \kappa} - 2t \frac{\partial}{\partial t} - d + md \right] F^{(m)} = 0. \quad (4.20)$$

We are interested in the density  $n(t, n_0, g_R, \kappa) = \sum_m n_0^m F^{(m)}/m!$ . Substituting (4.20) into (4.19) and summing to get the density gives the equation

$$\left[ 2t \frac{\partial}{\partial t} - dn_0 \frac{\partial}{\partial n_0} + \beta(g_R) \frac{\partial}{\partial g_R} + d \right] n(t, n_0, g_R, \kappa) = 0. \quad (4.21)$$

This is solved by the method of characteristics, and has the solution

$$n(t, n_0, g_R, \kappa) = (\kappa^2 t)^{-d/2} n(\kappa^{-2}, \tilde{n}_0(\kappa^{-2}), \tilde{g}_R(\kappa^{-2}), \kappa), \quad (4.22)$$

with the characteristic equations for the running coupling and initial density

$$2t \frac{\partial \tilde{n}_0}{\partial t} = -d \tilde{n}_0 \quad \tilde{n}_0(t) = n_0, \quad (4.23)$$

$$2t \frac{\partial \tilde{g}_R}{\partial t} = \beta(\tilde{g}_R) \quad \tilde{g}_R(t) = g_R. \quad (4.24)$$

Because of the simple form of the  $\beta$  function, the running coupling can be found exactly:

$$\tilde{n}_0(t') = (t/t')^{d/2} n_0, \quad (4.25)$$

$$\tilde{g}_R(t') = g_R^* \left( 1 + \frac{g_R^* - g_R}{g_R (t/t')^{\epsilon/d_c}} \right)^{-1}. \quad (4.26)$$

One then sets  $t' = \kappa^{-2}$  and plugs the result into (4.23). Notice that in the large  $t$  limit  $\tilde{g}_R \rightarrow g_R^*$ .

In conventional RG analysis the mechanics developed above is used in the following way: one calculates an expansion in powers of  $g_0$ , and then converts this to an expansion in powers of  $g_R$  via (4.17). As long as the expansion coefficients are non-singular in  $\epsilon$ , then the  $g_R$  expansion can be related to an  $\epsilon$  expansion via (4.22). That is, we substitute  $t \rightarrow \kappa^{-2}$ ,  $n_0 \rightarrow \tilde{n}_0$ ,  $g_R \rightarrow \tilde{g}_R$ , in the  $g_R$  expansion, and multiply by the overall factor shown in (4.22). Then for large  $t$ ,  $\tilde{g}_R \rightarrow g_R^*$  giving  $n(t, n_0, \lambda_0)$  as an expansion in powers of  $\epsilon$ . For a given coefficient in the  $g_R$  expansion we keep only the leading term for large  $n_0$ , since  $\tilde{n}_0 \sim t^{d/2}$  and so the subleading terms in  $\tilde{n}_0$  will correspond to sub-leading terms in  $t$ .

The identification of the leading terms in  $g_0$  is less straightforward than it is in conventional RG calculations, since the sum over all powers of  $n_0$  must be taken into account. For the density, tree diagrams are of order  $g_0^i n_0^{1+i(k-1)}$  for integer  $i$ . Diagrams with  $j$  loops are of order  $g_0^i n_0^{1+i(k-1)-j}$ . Since the addition of loops makes the power of  $g_0$  higher relative to the power of  $n_0$ , we hypothesize that the number of loops will serve as an indicator of the order of  $g_0$ . This will be shown to be the case via explicit calculation.

## 4.2. TREE DIAGRAMS

To calculate all possible diagrams of a given number of loops it is necessary to develop two tree-level quantities: the classical density and the classical response function. The term classical means averaged with respect to the classical action, which is the action (4.4), but with only the  $\bar{\phi}\phi^k$  vertex. The classical density is given by sum of all tree diagrams which terminate with a single propagator, as shown in fig. 4.2, and is represented graphically by a wavy line. These diagrams are evaluated in wave number space. From (4.6) it follows that the  $\bar{\phi}(t=0)$  in the initial state all have  $p=0$ , so all diagrams at tree level have  $p=0$ .

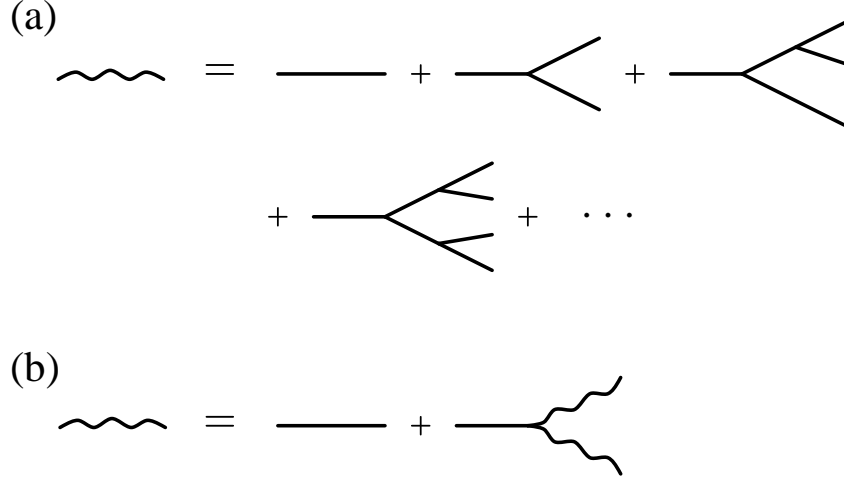


FIGURE 4.2. The classical density, represented as a wavy line, is given by (a) the complete sum of tree diagrams, and (b) an integral equation. The latter is equivalent to the mean-field rate equation. Shown here is the case  $k = 2$ .

Shown also in fig. 4.2 is an exact graphical relation for the infinite sum, which is equivalent to the mean-field rate equation (4.1). This can be seen by considering the diagram in position space, and acting with  $(\partial_t - \nabla^2)$ , the inverse of the Green's function  $G_0$ , on either side of the diagrammatic equation. Note that the combinatoric factors involved in attaching the full density lines to vertices is different than for propagators, which is discussed in appendix 4.A. This equation has the exact and asymptotic solutions

$$\begin{aligned}
 n_{cl}(t) &= \frac{n_0}{(1 + k(k-1)n_0^{k-1}\lambda_0 t)^{1/(k-1)}} \\
 &\sim \left( \frac{1}{k(k-1)\lambda_0} \right)^{1/(k-1)} t^{-1/(k-1)}.
 \end{aligned}
 \tag{4.27}$$

The asymptotic solution depends on the coupling strength, but not the initial density.

The response function is defined by

$$G(p, t_2, t_1) \equiv \langle\langle \phi(-p, t_2) \bar{\phi}(p, t_1) \rangle\rangle,
 \tag{4.28}$$

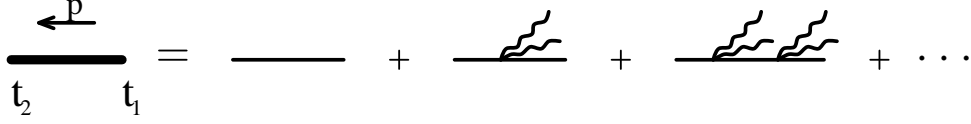


FIGURE 4.3. The response function, shown as a heavy line, is given as a sum of the bare propagator plus a term with a single vertex connecting  $k - 1$  full density lines, plus a term with two vertices, and so on. Shown here is  $k = 3$ . These diagrams can be summed exactly.

and the classical response function is the above quantity with only tree diagrams included in the averaging. It is represented graphically by a heavy line, and is given by the sum of diagrams as shown in fig. 4.3. Note that the only  $p$ -dependence is that of the bare propagator. That is, the density lines all carry zero wave number. The time dependence of the propagators connecting the vertices cancels to leave only overall dependence on  $t_1, t_2$ . The vertices are now symmetric under interchange, so we can trade the requirement that they be ordered for a factor of  $1/n_v!$  where  $n_v$  is the number of vertices. The sum of diagrams is then identified as the Taylor expansion of an exponential, giving

$$\begin{aligned}
 G_{cl}(p, t_2, t_1) &= e^{-p^2(t_2-t_1)} \exp \left\{ -k^2 \lambda_0 \int_{t_1}^{t_2} dt n_{cl}(t)^{k-1} \right\} \\
 &= e^{-p^2(t_2-t_1)} \left( \frac{1 + k(k-1)n_0^{k-1}\lambda_0 t_1}{1 + k(k-1)n_0^{k-1}\lambda_0 t_2} \right)^{k/(k-1)}.
 \end{aligned} \tag{4.29}$$

The extra factor of  $k$  associated with each  $-k\lambda_0$  vertex is a consequence of the combinatorics (see Appendix 4.A). From (4.6) it follows that  $\langle\langle\phi(t)\bar{\phi}(0)\rangle\rangle = \partial\langle\phi(t)\rangle/\partial n_0$  or  $G(p=0, t, 0) = \partial n(t)/\partial n_0$ . This relation should also hold for the classical density and response function, as is the case for the solution above.

### 4.3. DENSITY CALCULATION

With the classical or tree-level solutions of the previous section, and the renormalization scheme developed above, the asymptotic form of the density can now be calculated.

The solution for the tree diagrams in terms of  $g_0$ , or  $\lambda_0$ , is given by (4.27). To leading order in  $g_R$  one just replaces  $\lambda_0$  with  $g_R \kappa^{2\epsilon/d_c}$ . For large  $t$  the running coupling  $\tilde{g}_R \rightarrow g_R^*$ , which gives

$$n^{(0)}(t) = \frac{n_0}{(1 + k(k-1)n_0^{k-1}g_R^* t^{(k-1)d/2})^{1/(k-1)}}. \quad (4.30)$$

The superscript on the density refers to the number of loops in the calculation. The asymptotic form of this expression is

$$n^{(0)}(t) \sim \left( \frac{(k-2)!}{2\pi(k-1)k^{1/(k-1)}\epsilon} \right)^{1/(k-1)} t^{-d/2} + O(\epsilon^{1-1/(k-1)}). \quad (4.31)$$

The term in parentheses is the leading order term in  $A_k$ , the amplitude of the  $t^{-d/2}$  component of the density.

#### *Amplitude Corrections for $k = 2$*

Next the corrections from the higher loop diagrams are calculated. It will be shown that adding a loop makes the sum of diagrams an order  $g_R^{1/(k-1)}$  higher. At  $k-1$  loops the diagrams will contain a singularity in  $\epsilon$ , caused by the appearance of the first primitively divergent diagram. However this singularity is cancelled when the  $g_R^2$  correction to  $g_0$  in (4.17) is included in the tree diagram sum. In general the higher order terms in (4.17) will cancel all divergences in the coefficients of the  $g_R$  expansion. This will be illustrated in the one-loop corrections for  $k = 2$ .

The infinite sum of all one-loop diagrams can be written in terms of the classical response function found above. The sum of diagrams is shown in fig. 4.4(a). Expressing this graph in integral form

$$n^{(1)}(t, n_0, g_0, \kappa) = 2 \int dt_2 dt_1 \frac{d^d p}{(2\pi)^d} G_{cl}(0, t, t_2) (-2\lambda_0) G_{cl}(p, t_2, t_1)^2 (-\lambda_0) n_{cl}(t_1)^2, \quad (4.32)$$

where the time integrals are over  $0 < t_1 < t_2 < t$ . Taking the large  $n_0$  limit of (4.32) to extract the asymptotic part gives

$$n^{(1)}(t, n_0, g_0, \kappa) = \frac{1}{t^2} \int dt_2 dt_1 \frac{d^d p}{(2\pi)^d} t_2^{-2} e^{-2p^2(t_2-t_1)} t_1^2 + O(n_0^{-1}). \quad (4.33)$$

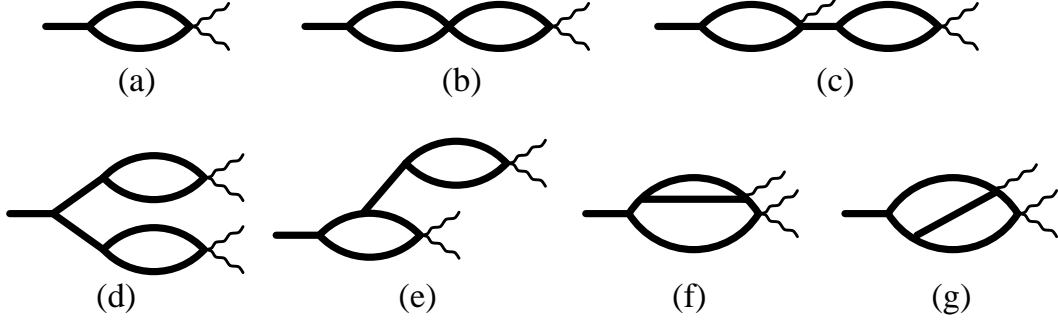


FIGURE 4.4. One- and two-loop diagrams for  $k = 2$ . By using the response function all such diagrams are included. Diagram (a) is used to calculate the amplitude correction.

Notice that this is independent of  $g_0$ , consistent with the prediction that the one-loop diagrams are of order  $g_R^0$  and provide a correction to the leading term in (4.31). The integral can be done exactly. Expressing the leading piece in terms of  $g_R^*$ , and the rest as an expansion in  $\epsilon$ :

$$n^{(1)}(t, n_0, g_0, \kappa) = t^{-d/2} \left( \frac{1}{2g_R^*} - \frac{2C + 5}{16\pi} + O(\epsilon) \right), \quad (4.34)$$

where  $C$  is Euler's constant. The correction to the tree-level component due to the sub-leading term in  $g_0(g_R)$  is

$$n^{(0)}(t, g_R) = \frac{1}{2g_R} t^{-d/2} - \frac{1}{2g_R^*} t^{-d/2} + O(g_R). \quad (4.35)$$

The singular parts of the  $g_R^0$  coefficient cancel as advertised. Combining (4.34) and (4.35) and making use of the Callan-Symanzik solution (4.22) gives

$$A_2 = \frac{1}{4\pi\epsilon} + \frac{2 \ln 8\pi - 5}{16\pi} + O(\epsilon). \quad (4.36)$$

The two-loop diagrams are also shown in fig. 4.4. They all contribute to order  $g_R^1$ . Unfortunately we are unable to evaluate diagrams (f,g) due to the complicated time dependence of the vertices, which prohibits calculation of the  $O(\epsilon)$  term in  $A_2$ . The most



singular of the diagrams, (b-d), are of order  $\epsilon^{-2}$ . These diagrams can be calculated and the singular pieces cancel as expected.

Note that the asymptotic, or large  $n_0$ , limits of the classical density and the classical response function are of order  $n_0^0$ , which implies that the asymptotic time dependence of the density, calculated to any number of loops, will be  $t^{-d/2}$ . Therefore the decay exponent is exact to all orders in  $\epsilon$ .

The cancellation of the singularities which appear in the  $g_R$  expansion can be most easily understood by viewing the correction terms in (4.17) as counterterms introduced to cancel primitive divergences. That is, considering  $\delta g_R = g_R^2/g_R^* + O(g_R^3)$ , and calculating the first order term in  $\delta g_R$  at tree level gives a diagram similar to fig. 4.4(a), but with the counterterm in place of the loop. This diagram, when added to the one-loop diagram, cancels the singularity in the  $g_R^0$  coefficient. Two-loop diagrams (b-f) can be viewed as primitively divergent loops added to the one-loop diagram (a). The order  $\delta g_R$  terms in the one-loop diagram are equivalent to diagrams (b-f) with a counterterm in place of the additional loop, and will cancel the divergences in these diagrams. Diagram (g) differs in that it is not a primitively divergent loop ‘added on’ to diagram (a), but it is also non-singular.

### *Amplitude Corrections for $k = 3$*

The one- and two-loop diagrams for  $k = 3$  are shown in fig. 4.5. The one-loop diagram contains no singularity, and gives the order  $g_R^0$  correction to (4.31). The asymptotic piece is given by the integral

$$n^{(1)}(t, n_0, g_0, \kappa) = \frac{3}{2t^{3/2}} \int dt_2 dt_1 \frac{d^d p}{(2\pi)^d} t_2^{-2} e^{-2p^2(t_2-t_1)} t_1^{3/2} + O(n_0^{-1}). \quad (4.37)$$

Performing the integral and using (4.22) we find the amplitude

$$A_3 = \left( \frac{\sqrt{3}}{12\pi\epsilon} \right)^{1/2} + \frac{9\sqrt{2\pi}}{64} + O(\epsilon^{1/2}). \quad (4.38)$$

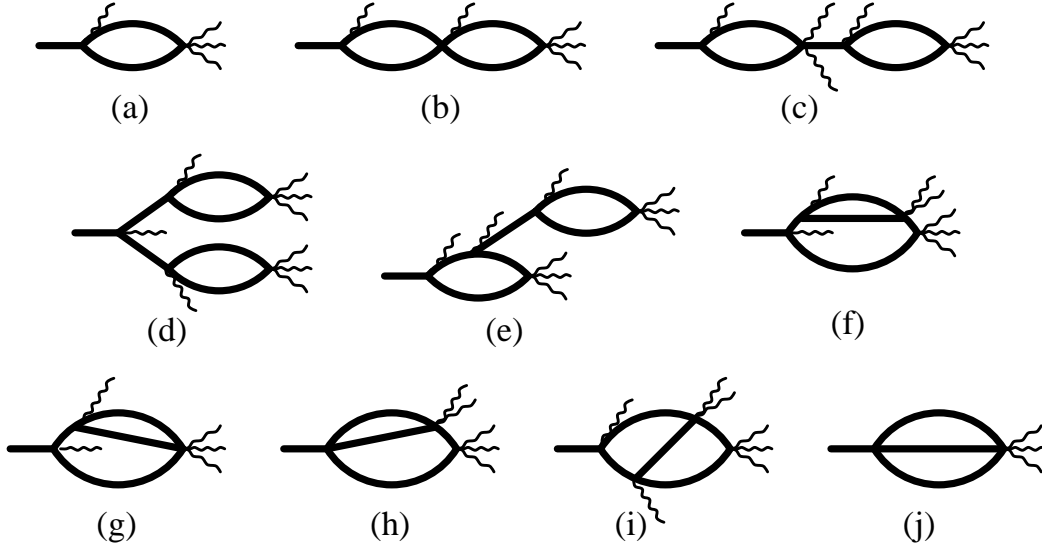


FIGURE 4.5. One- and two-loop diagrams for  $k = 3$ . Diagram (a) contains no  $\epsilon$  singularity, and is used to calculate the amplitude correction.

The two-loop diagrams are of order  $g_R^{1/2}$ , although, similar to the case of  $k = 2$ , we are unable to calculate diagrams (f-i). The only diagram with a singularity is (j), which can be calculated to demonstrate that the  $g_R^{1/2}$  coefficient is non-singular as expected.

#### *Dressed Tree Calculation*

There exists an alternate method for calculating the leading order amplitude of the density which does not require using the RG formalism. However, there is a discrepancy between this method, the dressed tree sum, and the RG in the case  $k = 2$ . We present the dressed tree calculation below, and an explanation for why we believe the RG to be correct for  $k = 2$ .

Consider summing the most divergent diagrams for each power of  $\lambda_0$  and  $n_0$ . This is equivalent to summing the dressed tree diagrams, which are tree diagrams with all the vertices replaced by the temporally extended vertex function (4.10).

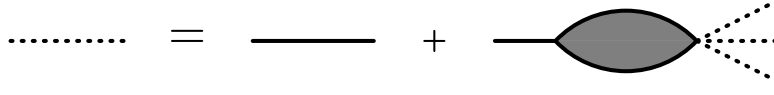


FIGURE 4.6. Exact diagrammatic equation for  $n_{dt}(t)$ , the sum of the dressed tree diagrams.

The sum of these diagrams,  $n_{dt}(t)$ , satisfies the diagrammatic equation shown in fig. 4.6, where  $n_{dt}$  is represented by a dotted line. As with the tree diagram sum, acting on this equation with the propagator inverse  $(\partial_t - \nabla^2)$  gives a differential equation

$$\partial_t n_{dt}(t) = n_0 \delta(t) - k \int_0^t dt' \lambda(p=0, t-t') n_{dt}(t')^k. \quad (4.39)$$

Laplace transforming the equation gives

$$sn(s) - n_0 = -k\lambda(0, s)n^k(s), \quad (4.40)$$

where  $n(s) = \int_0^\infty dt e^{-st} n_{dt}(t)$  and  $n^k(s) = \int_0^\infty dt e^{-st} n_{dt}(t)^k$ . The transform of the vertex function  $\lambda(0, s)$  is known exactly, and is given by (4.14). However, the equation is not algebraic in  $n(s)$ , making it difficult to obtain an exact solution. To proceed, we assume  $n_{dt} \sim \tilde{A}t^{-\alpha}$ , so that for small  $s$ ,  $n(s) \sim \tilde{A}\Gamma(1-\alpha)s^{\alpha-1}$ . Also,  $n^k(s) \sim \tilde{A}^k\Gamma(1-k\alpha)s^{k\alpha-1}$ , and  $\lambda(0, s) \sim s^{\epsilon/d_c}/(B_k\Gamma(\epsilon/d_c))$ . The transform of  $n_{dt}(t)^k$  is calculated by imposing a small  $t$  regulator, which is justified as the transform of the exact solution does exist, and then taking the small  $s$  limit. The amplitude which results is independent of the regulator. Substituting these in to (4.40) and taking the small  $s$  limit of the equation gives  $\alpha = d/2$ , and the amplitude

$$\tilde{A}^{k-1} = \frac{B_k \Gamma\left(\frac{2\epsilon}{k-1}\right) \Gamma\left(\frac{k-2}{k-1} + \frac{\epsilon}{2}\right) \left(\frac{1}{k-1} - \frac{k\epsilon}{2}\right)}{k \Gamma\left(\frac{k-2}{k-1} + \frac{k\epsilon}{2}\right)}. \quad (4.41)$$

For  $k \neq 2$  the non-singular  $\Gamma$  functions cancel to leading order in  $\epsilon$ , with the result  $\tilde{A} = A_k + O(\epsilon^0)$ . However, for  $k = 2$  all the  $\Gamma$  functions are singular, which has the consequence

that  $\tilde{A}_2 = 2A_2 + O(\epsilon^0)$ . In light of this, it seems necessary to find an explanation why this particular set of diagrams sums to give the proper leading order term for general  $k$ , but not for  $k = 2$ , if indeed the RG is giving the correct leading order term.

Consider the set of dressed one-loop diagrams. That is, the set of diagrams given in fig. 4.4(a) and fig. 4.5(a), but again with each vertex replaced by the temporally extended vertex function. While it would be difficult to calculate this sum, it is possible to see a property specific to  $k = 2$  that they have. The analog of the classical densities in these diagrams is the dressed tree density  $n_{dt} \propto t^{-d/2}$ . Therefore for general  $k$  there is a time integral over  $t^{-kd/2}$ , or  $t^{-k/(k-1)-k\epsilon/2}$ . This time integral will be in the form of a Laplace convolution integral, similar to (4.39). Using a regulated transform as before, the amplitude of the small  $s$  limit will be proportional to  $\Gamma((k-2)/(k-1) + k\epsilon/2)$ . For  $k \neq 2$  this is non-singular at  $\epsilon = 0$ , but for  $k = 2$  it is of order  $\epsilon^{-1}$ . Therefore these diagrams are part of the leading order amplitude for  $k = 2$ . As a result, it would appear that the discrepancy is a consequence of the failure of the dressed tree method, and not of the RG.

### *Crossovers*

There are two crossover time scales in this system, one given by  $n_0$  and one by  $\lambda_0$ . For the coupling constant crossover we consider the large  $t$  expansion of (4.26)

$$\tilde{g}_R = g_R^* \left( 1 - \lambda_0^{-1} t^{-\epsilon/d_c} + O(t^{-2\epsilon/d_c}) \right). \quad (4.42)$$

Including the correction term in the density calculation will generate a  $\lambda_0$  dependent term proportional to  $t^{-d/2-\epsilon/d_c}$ . From (4.42) it follows that the characteristic crossover time is given by  $t_{\lambda_0} \sim (\epsilon/\lambda_0)^{d_c/\epsilon}$ . In terms of the constants in the master equation,  $t_\lambda \sim a^2 D^{-1} (\epsilon D/a^2 \lambda)^{d_c/\epsilon}$ . For small  $\epsilon$ , or large  $\lambda_0$ , the time required to reach the fluctuation dominated regime becomes small.

The  $n_0$  crossover is calculated by keeping the order  $n_0^{-1}$  terms in the integrals performed above. These terms will pick up an extra factor of  $t^{-d/2}$  when put into (4.22), so

the exponent of the leading  $n_0$  dependent term in the density is  $t^{-d}$ . The characteristic crossover time is only weakly  $\epsilon$  dependent, and is given by  $t_{n_0} \sim D^{-1} n_0^{-2/d} = a^2 D^{-1} \bar{n}_0^{-2/d}$ .

If the  $n_0$  crossover occurs first, then for intermediate times  $t_{n_0} \ll t \ll t_{\lambda_0}$  one would expect the system to obey the asymptotic form of the mean-field solution. That is,  $n \sim [k(k-1)\lambda_0 t]^{-1/(k-1)}$ . If the  $\lambda_0$  crossover occurs first it is less clear what the behavior in the intermediate regime will be. The contribution from the tree diagrams will be exactly (4.30), which does not become a power law until the  $n_0$  crossover is reached. This is complicated even further by the higher order diagrams.

#### 4.4. CORRELATION FUNCTION CALCULATION

The density correlation function is given by

$$C(x, t) = \langle\langle (\phi(x, t) + \delta^d(x)) \phi(0, t) \rangle\rangle. \quad (4.43)$$

where the  $\delta$  function is a consequence of the second quantized operators developed in chapter three. A Callan-Symanzik equation for the correlation function can be developed in a similar fashion as before. Consider the function

$$F^{(m)}(p, t, \lambda_0) \equiv \int d^d x e^{-ip \cdot x} \left\langle (\phi(x, t) + \delta^d(x)) \phi(0, t) \left( \int d^d y \bar{\phi}(y, t=0) \right)^m \right\rangle. \quad (4.44)$$

Dimensional analysis gives  $[F^{(m)}] = p^{d-md}$ . The correlation function  $C(p, t)$  is given by  $\sum_m n_0^m F^{(m)}/m!$ . This leads to the equation

$$\left[ 2t \frac{\partial}{\partial t} - p \frac{\partial}{\partial p} - dn_0 \frac{\partial}{\partial n_0} + \beta(g_R) \frac{\partial}{\partial g_R} + d \right] C(p, t, n_0, g_R, \kappa) = 0 \quad (4.45)$$

which has the solution

$$C(p, t, n_0, g_R, \kappa) = (\kappa^2 t)^{-d/2} C(\tilde{p}(\kappa^{-2}), t = \kappa^{-2}, \tilde{n}_0(\kappa^{-2}), \tilde{g}_R(\kappa^{-2}), \kappa), \quad (4.46)$$

with  $\tilde{g}_R$  and  $\tilde{n}_0$  given by (4.25) and (4.26), and

$$\tilde{p}(t') = p\sqrt{\frac{t}{t'}}. \quad (4.47)$$

Again the calculation of the right hand side of (4.46) is divided into the number of loops. First the connected and disconnected pieces are separated

$$C(p, t) = n(t) + g(p, t) + \delta^d(p)n(t)^2. \quad (4.48)$$

The first term on the right hand side is a consequence of the  $\delta$  function in (4.43), and is considered part of the connected correlation function. The disconnected tree-level graphs are of the order  $g_0^i n_0^{2+i(k-1)}$ , and represent the leading order terms in the correlation function. This is reasonable, as the classical solution of this system corresponds to the absence of correlations. The connected tree-level diagrams, which are the leading terms in  $g(p, t)$ , are of order  $g_0^i n_0^{1+i(k-1)}$ , and represent the leading corrections due to fluctuations. The tree-level and one-loop diagrams for  $g(p, t)$  in the case  $k = 2$  are shown in fig. 4.7. Diagram (a) can be calculated explicitly to give the leading term

$$\begin{aligned} g(p, t) &= -\frac{1}{4\pi\epsilon} t^{-d/2} f_2(p^2 t) + O(\epsilon^0) \\ f_2(x) &= -\frac{e^{-2x}}{4x^3} + \frac{1}{4x^3} - \frac{1}{2x^2} + \frac{1}{2x}. \end{aligned} \quad (4.49)$$

The function  $f_2(x)$  is regular at  $x = 0$ , with  $f_2(0) = 1/3$ . For large  $x$ ,  $f_2(x) \sim 1/(2x)$ .

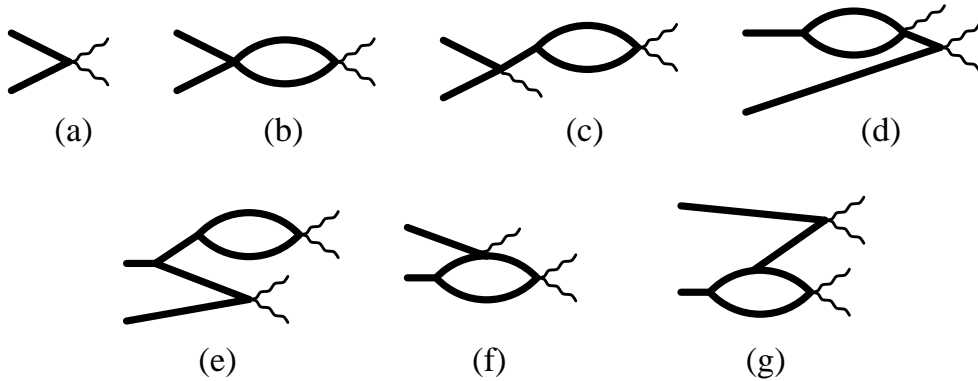


FIGURE 4.7. The diagrams for the connected correlation function at tree level and one loop, for  $k = 2$ .

We are unable to evaluate the one-loop diagrams analytically for general  $p$ , although it is possible to calculate an expansion in  $p^2$ , which we have done to order  $p^2$ . For the connected correlation function,

$$\begin{aligned}\bar{C}(p, t) &= n(t) + g(p, t) \\ &= \left[ \frac{1}{6\pi\epsilon} + \frac{9\ln 8\pi - 26}{108\pi} + \left( \frac{1}{24\pi\epsilon} + \frac{15\ln 8\pi - 19}{720\pi} \right) p^2 t + \dots \right] t^{-d/2} \\ &\quad + O(\epsilon).\end{aligned}\tag{4.50}$$

With the expansion above it is possible to calculate the second moment of  $\bar{C}(x, t)$ , giving a length scale for the correlations. For  $\bar{C}(p, t) = A + Bp^2 + \dots$  the second moment  $-\xi^2 \equiv \int d^d x x^2 \bar{C}(x, t) / \int d^d x \bar{C}(x, t) = -2B/A$ . The negative sign in the definition of  $\xi$  is required since the second moment is negative, indicating that the particles are negatively correlated at larger distances. For  $k = 2$  the length  $\xi$  is given by

$$\xi_2 = \sqrt{t} \left( \frac{\sqrt{2}}{2} + \frac{73\sqrt{2}}{360}\epsilon + O(\epsilon^2) \right).\tag{4.51}$$

The correlation function can be used to calculate the fluctuations in the density. For example, the fluctuations in the local density are given by integrating  $C(p, t)$  over  $p$ . However, the  $p$ -independent term causes this integral to diverge. One can consider the fluctuations of the average particle number within a fiducial volume  $v$ . This is given by

$$(\delta N_v)^2 = v \int_v dx \bar{C}(x, t) = vn(t) + O(v^2),\tag{4.52}$$

where translational invariance is assumed. The order  $v$  contribution originates from the  $\delta$  function in (4.43). For small  $v$  the fluctuations go as  $\delta N_v \sim \sqrt{vn(t)}$ , which is universal. Also,  $\delta N_v/N_v \sim 1/\sqrt{vn(t)}$ , which diverges as  $v$  goes to zero, consistent with the local fluctuations being divergent.

The fluctuations in the total number of particles is given by  $V\bar{C}(p = 0, t)$  where  $V$  is the volume of the system. When divided by the square of the average number of particles,  $V^2 n(t)^2$ , this gives

$$\frac{(\delta N)^2}{N^2} V = \left( \frac{8\pi}{3}\epsilon - \frac{18\pi \ln 8\pi - 38\pi}{3}\epsilon^2 + O(\epsilon^3) \right) t^{-d/2}.\tag{4.53}$$

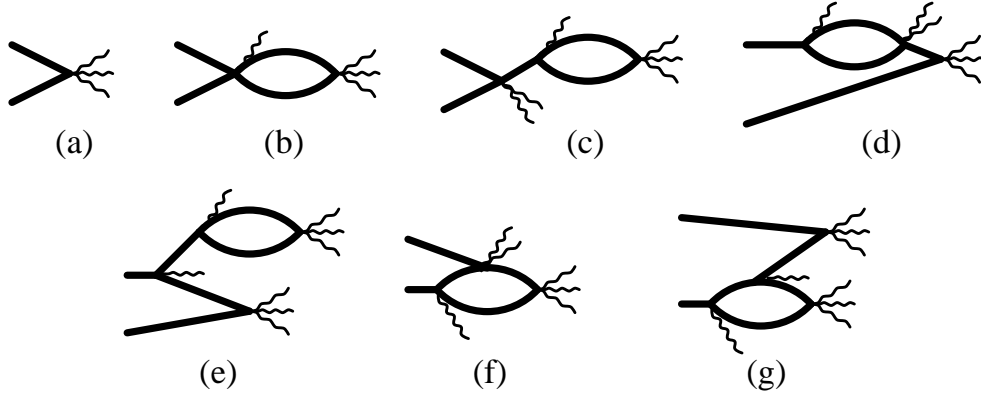


FIGURE 4.8. The diagrams for the connected correlation function at tree level and one loop, for  $k = 3$ .

Note that all these fluctuation terms would be negative if the  $\delta$  function term were neglected. That is,  $\langle\langle\phi(x)^2\rangle\rangle < 0$ , a demonstration that the fields introduced via the path integral formulation of [28] are complex.

The diagrams contributing to  $g(p, t)$  for  $k = 3$  are shown in fig. 4.8. The leading order term for the connected part is

$$g(p, t) = - \left( \frac{\sqrt{3}}{12\pi\epsilon} \right)^{1/2} t^{-d/2} f_3(x) + O(\epsilon^0) \quad (4.54)$$

$$f_3(x) = \frac{e^{-2x} 3\sqrt{\pi} \operatorname{erfi}(\sqrt{2x})}{16\sqrt{2}x^{5/2}} - \frac{3}{8x^2} + \frac{1}{2x}$$

where  $\operatorname{erfi}(x) = -i \operatorname{erf}(ix) = (2/\sqrt{\pi}) \int_0^x dy e^{y^2}$ . The function  $f_3(x)$  is also regular, with  $f_3(0) = 2/5$  and  $f_3(x) \sim 1/(2x)$  for large  $x$ .

The one-loop diagrams can be calculated as an expansion in  $p^2$ , with the net result

$$\bar{C}(p, t) = \left[ \frac{3}{10} \left( \frac{\sqrt{3}}{3\pi\epsilon} \right)^{1/2} + \frac{81\sqrt{2\pi}}{1600} + \frac{288}{875} \sqrt{\frac{2}{\pi}} \right. \\ \left. + \left( \frac{4}{35} \left( \frac{\sqrt{3}}{3\pi\epsilon} \right)^{1/2} + \frac{9\sqrt{2\pi}}{98} - \frac{27546}{42875} \sqrt{\frac{2}{\pi}} \right) p^2 t + \dots \right] t^{-d/2} \quad (4.55)$$



plus terms of order  $\epsilon^{1/2}$ . In this case the sign of the second moment of the correlation function depends on  $\epsilon$ . For  $\epsilon < 0.4$  the second moment is negative, and the resulting length scale is given by

$$\xi_3 = \sqrt{t} \left( \frac{4}{\sqrt{21}} + \left( \frac{2\sqrt{3}}{21} \right)^{1/2} \left( \frac{711\pi}{2240} - \frac{2217}{490} \right) \epsilon^{1/2} + O(\epsilon) \right). \quad (4.56)$$

The fluctuations in total particle number are given by

$$\frac{(\delta N)^2}{N^2} V = \left( \frac{6\sqrt{\pi}}{5} \epsilon^{1/2} + (2\pi\sqrt{3})^{1/2} \left( \frac{1152}{875} - \frac{189\pi}{400} \right) \epsilon \right) t^{-d/2}. \quad (4.57)$$

plus terms of order  $\epsilon^{3/2}$ .

#### 4.5. LOGARITHMIC CORRECTIONS FOR $d = d_c$ .

In general, when  $d < d_c$ , certain relevant parameters determine the critical exponents of the system. When  $d = d_c$  these parameters become marginally irrelevant. In such a case the exponents are given by mean-field theory, but with logarithmic corrections. In our system the marginally irrelevant parameter is the coupling  $\lambda_0$ .

When  $d = d_c$  the Callan-Symanzik solution (4.22) still holds, although with a different running coupling. The  $\beta$  function can be calculated either with a cutoff which is taken to infinity or by taking  $\epsilon \rightarrow 0$  in (4.15) with the same result:  $\beta(g_R) = 2B_k g_R^2$ . This gives the running coupling

$$\tilde{g}_R(\kappa^{-2}) = \frac{g_R}{1 + g_R B_k \ln(\kappa^2 t)}. \quad (4.58)$$

For large  $t$  the coupling goes to zero, which is the only fixed point of the  $\beta$  function. Using the asymptotic form  $\tilde{g}_R \sim \{B_k \ln(\kappa^2 t)\}^{-1}$  in the tree-level sum gives

$$n(t) \sim \left( \frac{(k-2)!}{4\pi k^{1/(k-1)}} \right)^{1/(k-1)} \left( \frac{\ln t}{t} \right)^{1/(k-1)} \left[ 1 + O((\ln t)^{-1/(k-1)}) \right]. \quad (4.59)$$

Higher order terms in  $\tilde{g}_R$  will give sub-leading time dependence, so this represents the full leading order amplitude. Notice that the correction terms are only an order  $(\ln t)^{-1/(k-1)}$  smaller, which will make time required to reach the asymptotic regime large.

The same procedure gives an exact expression for the leading term in the correlation function as well. For  $k = 2$

$$\bar{C}(p, t) = \frac{1}{8\pi} \left(1 - f_2(p^2 t)\right) \left(\frac{\ln t}{t}\right) [1 + O((\ln t)^{-1})] \quad (4.60)$$

and for  $k = 3$

$$\bar{C}(p, t) = \left(\frac{\sqrt{3}}{12\pi}\right)^{1/2} \left(1 - f_3(p^2 t)\right) \left(\frac{\ln t}{t}\right)^{1/2} [1 + O((\ln t)^{-1/2})]. \quad (4.61)$$

#### 4.6. GENERALIZATION TO THE REACTION $kA \rightarrow \ell A$

Our results can be immediately generalized to a coagulation reaction  $kA \rightarrow \ell A$ ,  $\ell < k$ . The only change in the field theory is the vertices  $\lambda_i$  in (4.4):

$$\lambda_i = \begin{cases} \lambda_0 \binom{k}{i} - \lambda_0 \binom{\ell}{i}, & i \leq \ell \\ \lambda_0 \binom{k}{i}, & i > \ell. \end{cases} \quad (4.62)$$

The renormalization follows identically. For example, the leading term in the amplitude, given by (4.31), is generalized to

$$A_{k,\ell} = \left(\frac{k}{k-\ell}\right)^{1/(k-1)} A_k + O(\epsilon^0). \quad (4.63)$$

This proportionality is not generally true for all terms in the  $\epsilon$  expansion, although it does happen to hold when  $k = 2$ . To see this, consider a rescaling  $\phi \rightarrow b\phi$ ,  $\bar{\phi} \rightarrow \bar{\phi}/b$ , and  $n_0 \rightarrow bn_0$  in the action (4.4). The only terms changed by such a rescaling are the couplings  $\lambda_i \rightarrow b^{i-k}\lambda_i$ , which for  $k = 2$  is only the coupling  $\lambda_1$ . Starting from the theory  $A + A \rightarrow \emptyset$  and making the scale transformation with  $b = 2$  gives exactly the theory for  $A + A \rightarrow A$ . As a consequence, the density for  $A + A \rightarrow A$ , starting from an initial density of  $n_0$ , will for all times be exactly twice the density of the system  $A + A \rightarrow \emptyset$  with initial density of  $n_0/2$ . This result agrees with the recent exact solution of a particular model of  $A + A \rightarrow (\emptyset, A)$  in  $d = 1$  [53], although it should be noted that this relation is not truly universal for all times, as it only holds when the irrelevant couplings are excluded. The

asymptotic amplitude is universal, and so the relation  $A_{2,1} = 2A_{2,0}$  is exact to all orders in  $\epsilon$ , and independent of the initial densities.

For  $k = 3$  such a simple relation does not hold. We can consider all three theories,  $\ell = 0, 1, 2$ , combined with relative strengths  $r_0, r_1, r_2$ , where  $\sum_i r_i = 1$ . The rescaling defined above will relate two systems with different  $r_\ell$  in that the densities will be identical up to a rescaling. However this rescaling only removes one degree of freedom from the two independent variables, so unlike  $k = 2$ , one cannot necessarily scale one theory into another. Considering  $r_0$  and  $r_1$ , we find

$$r_0(b) = (1 - b)^2 + b(2b - 1)\bar{r}_0 + b(1 - b)\bar{r}_1 \quad (4.64)$$

$$r_1(b) = (3 - b)(b - 1) + 2b(1 - b)\bar{r}_0 + b^2\bar{r}_1 \quad (4.65)$$

where  $\bar{r}_0, \bar{r}_1$  are the values of  $r_0, r_1$  prior to rescaling. Consider the system which is purely  $\ell = 0$ , or  $\bar{r}_0 = 1, \bar{r}_1 = \bar{r}_2 = 0$ . For any  $b \neq 1$  then  $r_1(b) < 0$ , which implies that there is no combination of systems with different  $\ell$  which is equivalent to  $\ell = 0$  up to a rescaling. This is not the case for the pure  $\ell = 1$  system. This system can be rescaled from  $b = 1$  to  $b = 3/4$ . At the latter point one has  $r_0 = 1/4, r_1 = 0$ , and  $r_2 = 3/4$ , so this combination of systems, with an initial density of  $3n_0/4$ , will give exactly  $3/4$  the density of the  $\ell = 1$  system at all times. Similarly, starting with  $\bar{r}_2 = 1$  the system can be rescaled from  $b = 1$  to  $b = 3/2$ . At the latter point  $r_0 = 1/4, r_1 = 3/4$ , and  $r_2 = 0$ .

The correlation function will not be identical up to a rescaling for any of the systems described above. This is a consequence of the fact that the correlation function contains both  $\phi$  and  $\phi^2$  pieces.

When  $d = d_c$  the density amplitudes for  $\ell \neq 0$  are given exactly by the relation

$$A_{k,\ell} = \left( \frac{k}{k - \ell} \right)^{1/(k-1)} A_k. \quad (4.66)$$

This is because the amplitude is given by the same diagrams which contribute the leading order term in  $\epsilon$  for  $d < d_c$ . These amplitudes have recently been measured numerically

for the reactions  $3A \rightarrow A$  and  $3A \rightarrow 2A$  in one dimension with the results  $A_{3,1} \approx 0.76$  and  $A_{3,2} \approx 0.93$  [60]. Our calculations yield instead  $A_{3,1} \approx 0.26$  and  $A_{3,2} \approx 0.37$ . The magnitude of this discrepancy is somewhat disturbing. One possible explanation is that it is from the diffusion constant, as one can easily make errors of factors of two with the analytical and numerical definitions of this quantity. We have checked our calculations and believe them to be correct. It is quite difficult to measure numerically the amplitudes of logarithmic terms, and the correction terms in this case are predicted to be of order  $(\ln t)^{-1/2}$ . The data in [60] becomes dominated by noise around a value of  $\ln t = 10$ , so the correction terms could still be contributing. It is also worth noting that (4.66) predicts that  $A_{3,2}/A_{3,1} = \sqrt{2}$ , which is independent of possible errors in deriving the diffusion constant or evaluating the loop integrals. The numerical amplitudes have a ratio  $A_{3,2}/A_{3,1} \approx 1.22$ .

## APPENDIX 4.A. SYMMETRY FACTORS

Diagrams which contain the classical density or the classical response function are representations of infinite sums of diagrams. While they resemble ordinary perturbation theory diagrams, they differ in combinatorics. When calculating the Wick contraction combinatorics one treats propagators as distinguishable, although the resulting combinatoric factor is then cancelled by a factor which is absorbed into the definition of the coupling constant. Our diagrams differ from this in two ways. First, the classical density is attached to vertices as an indistinguishable object. This will be demonstrated below. Second, we have chosen to introduce in the coupling constants no pre-adjusted combinatoric factor. This is merely a matter of convention, and is motivated by the indistinguishability mentioned above, and by the direct relation of the coupling constant to the parameters used in the master equation.

The indistinguishability of the density lines can be demonstrated by considering the contraction of  $k$   $\phi$ 's, representing a vertex, with the infinite sum which is the initial state.

$$\begin{aligned}\langle\langle\phi^k\rangle\rangle_{cl} &= \sum_{m=0}^{\infty} \frac{n_0^m}{m!} \langle\phi^k \bar{\phi}^m\rangle_{cl} \\ &= \sum_{m=0}^{\infty} \frac{1}{m!} \sum_{\substack{m_1, \dots, m_k \\ m_1 + \dots + m_k = m}} C_{m_1, \dots, m_k}^m \prod_{i=1}^k \left( n_0^{m_i} \langle\phi \bar{\phi}^{m_i}\rangle_{cl} \right).\end{aligned}\tag{4.A.1}$$

where  $C_{m_1, \dots, m_k}^m = m!/(m_1! \dots m_k!)$  is the number of ways to partition  $m$  objects into  $k$  distinct boxes. The sums can be replaced with unrestricted sums over  $m_1 \dots m_k$ , and the above expression factors completely, giving

$$\langle\langle\phi^k\rangle\rangle_{cl} = \langle\langle\phi\rangle\rangle_{cl}^k\tag{4.A.2}$$

The significance of (4.A.2) is that there is no  $k!$  prefactor. The  $k$  classical density lines which are connected to the vertex are effectively indistinguishable.

In calculating the classical response function it is necessary to consider attaching one propagator and  $k - 1$  density lines to a  $\phi^k$  vertex. This brings in a factor of  $k$ , for the number of distinguishable ways the propagator can be attached. The remaining  $k - 1$  densities follow through the same combinatorics as that shown above, and contribute a factor of 1.

In general, where the classical response function appears in a diagram it can be treated as a propagator for combinatorics. The exception to this situation is in diagrams such as fig. 4.4 and fig. 4.5, diagrams (d). Here the symmetry of the two disconnected branches will result in the branches attaching as indistinguishable objects.

## Chapter 5. Two-Species Reaction $A + B \rightarrow \emptyset$

Consider a model with two types of particles,  $A$  and  $B$ , each undergoing continuous-time random walks on a lattice. These particles will, whenever they meet on a lattice site, react with some rate to form an inert particle, or equivalently to annihilate. The particles may have equal or unequal diffusion constants. We will assume that the particles are initially randomly distributed, and also that they have equal initial densities.

The first approach this problem is to assume the particles are uniformly distributed at all times. Then the system can be described by the mean-field rate equations

$$\frac{\partial}{\partial t}a = \frac{\partial}{\partial t}b = -\Gamma ab, \quad (5.1)$$

where  $a, b$  are the densities of  $A, B$  particles, and  $\Gamma$  is a rate constant. These rate equations would be valid for a rapidly stirred system, in which the densities  $a, b$  are driven to remain homogeneous. With equal initial densities they have the asymptotic solution  $a, b \sim 1/(\Gamma t)$ . In the absence of mixing there are fluctuations in the densities, which then modify the decay of the density. Note that the mean-field solution for the density in the two-species reaction is the same as that of  $A + A \rightarrow \emptyset$  (see chapter four). However, the density behaves quite differently when fluctuations are included, which is a consequence of a conservation law present in the two-species reaction.

The reaction  $A + B \rightarrow \emptyset$  does not change the number difference of  $A$  and  $B$  particles. Therefore fluctuations in  $a - b$  can only evolve diffusively, giving a slow mode for the two-species reaction which does not exist in the one-species case. This conserved quantity is set equal to zero under the assumption of uniformity above, but a random initial distribution of  $A$  and  $B$  particles will contain non-zero fluctuations of  $a - b$ , which will dominate the asymptotic dynamics.

A scaling argument can be used to predict the time dependence of the density based on the fluctuations in  $a(0) - b(0)$  for a random initial distribution. The total number of  $A$  or  $B$  particles initially present in a volume of size  $\ell_D$ , assuming that both species have an initial density of  $n_0$ , goes as

$$N \approx n_0 \ell_D^d \pm \sqrt{n_0 \ell_D^d}. \quad (5.2)$$

Therefore the absolute value of the number difference is given by

$$|N_{A-B}| \propto \sqrt{n_0 \ell_D^d} = \ell_D^d \sqrt{n_0 / \ell_D^d}. \quad (5.3)$$

Dividing both sides by  $\ell_D^d$  gives the density of the excess of the majority species in this region,  $n_{\text{maj}} \propto \sqrt{n_0 / \ell_D^d}$ . Next one argues that by a time  $t \propto \ell_D^2 / D$ , where  $D$  is the usual diffusion constant, all the particles in this region have had a chance to interact, and therefore all that will remain is the initial excess of  $A$  or  $B$  particles. This leads to the prediction that asymptotically

$$a, b \propto \sqrt{n_0} (Dt)^{-d/4}. \quad (5.4)$$

For  $d < 4$  this process gives a slower decay than the mean-field  $t^{-1}$ , and is therefore dominant. When  $d > 4$  one expects a crossover, then, to the mean-field power law  $t^{-1}$ , and an amplitude which is independent of the initial density.

## 5.1. PREVIOUS ANALYTICAL AND NUMERICAL WORK

The importance of these fluctuations was first noted by Ovchinnikov and Zeldovich [61]. Later Toussaint and Wilczek [31] developed a calculation scheme for the density which predicted the exponent  $t^{-d/4}$  and the crossover at  $d = 4$  from mean-field theory. They also calculated the amplitude of the density explicitly. Their method was to use the central limit theorem to calculate the strength of the fluctuations in the field  $f = a - b$ , given random initial conditions for particles on a lattice. Then they assumed this field would obey a classical diffusion equation, from which they concluded that  $f(t)$  has a normal distribution with a calculable width. Their final assumption was that at late times the regions of  $A$  particles and  $B$  particles would be completely segregated, from which they concluded that  $\langle a \rangle, \langle b \rangle = \langle |f| \rangle / 2$ , where the angle brackets denote averages over the initial conditions. That is, if the local minority species is completely absent, then  $|f|$  represents the density of the local majority species, which will be  $A$  in half of the segregated regions and  $B$  in the other half. Their result<sup>8</sup> was that for  $d < 4$  (henceforth denoting the behavior of both species by that of  $a$ )

$$\langle a \rangle \sim \frac{\sqrt{n_0}}{\pi^{1/2}(8\pi)^{d/4}} (Dt)^{-d/4}. \quad (5.5)$$

This result is confirmed, at least for  $d > 2$  and  $n_0$  small, by our calculation. We find that the  $\sqrt{n_0}$  term above can be regarded as the leading term in a small  $n_0$  expansion, and that there are higher order corrections. We also demonstrate that the segregation occurs, rather than assuming it as input for the calculation. For  $d \leq 2$  we believe the amplitude may be the same as above, at least to leading order in  $\epsilon = 2 - d$ . In this case there are non-trivial noise effects due to the diffusion which were neglected in Toussaint and Wilczek's calculation, which can be treated with RG methods.

A different approach to the problem was pursued by Bramson and Lebowitz [46,47], which is a refinement of the simple scaling arguments presented above that led to (5.4).

---

<sup>8</sup> There is a misprint in the quoted value for the  $d = 3$  amplitude in equation (19c) of [31].



They start with particles on a lattice with Poissonian initial conditions for the occupation number of each species, with the average per site given by  $\bar{n}_0$ . Then they consider a continuous time diffusion of the particles, with the rule that  $A$  and  $B$  will annihilate whenever they are simultaneously occupying a lattice site. This definition of the model has a shortcoming in that it does not have an input parameter with which to vary the rate of reaction, and therefore cannot predict the dependence on such a parameter. They consider a region of a given size of the reacting model, and compare it to an auxiliary model, which is defined to have the same initial configuration of particles, but to evolve with the reaction turned off. They provide a lengthy proof in [46] that the asymptotic density has the upper and lower bounds

$$\begin{aligned} c_d &\leq \langle a \rangle \frac{t^{d/4}}{\sqrt{\bar{n}_0}} \leq C_d & d < 4 \\ c_4 &\leq \langle a \rangle \frac{t}{\max(\sqrt{\bar{n}_0}, 1)} \leq C_4 & d = 4 \\ c_d &\leq \langle a \rangle t \leq C_d & d > 4, \end{aligned} \tag{5.6}$$

where  $c_d$  and  $C_d$  are constants. Furthermore, they state a theorem in their more recent paper [47] that the quantities above are not just bounded by constants, but are in fact asymptotically equal to constants. This is a stronger statement than we are able to make in the case  $d = 4$ , as they are predicting a discontinuity in the first derivative of the amplitude with respect to  $n_0$  at some value of the initial density  $n_0^c$ , which is equal to one in their treatment, but likely dependent on the lattice size and the reaction rate. For initial densities greater or lesser than this value the amplitude goes as  $\sqrt{n_0}$  or is independent of  $n_0$ , respectively. We can derive upper and lower bounds on the amplitude for  $d = 4$  which have these limits asymptotically for large and small  $n_0$ , but we have no means of predicting or ruling out this intermediate singular dependence. The proof of the theorem in [47] has, to our knowledge, not yet been published.

The two-species reaction has been simulated in  $d = 1, 2, 3$ , with the simulations giving convincing confirmation of the power law  $t^{-d/4}$ . However, the amplitude of this power law

has received little attention, and seems to vary dramatically between simulations. The original simulations were performed by Toussaint and Wilczek [31] for  $d = 1$  and  $d = 2$ . They considered a low density limit, with initial densities of 0.05 and 0.1, in units where the lattice spacing is unity. They also did not allow multiple occupancy at a given site, which introduces hard sphere correlations in the particles. They found that the amplitude in one dimension went like  $A_1\sqrt{n_0}$  with an amplitude  $A_1 = 0.28$ , which differs from their calculated value of 0.25. Their two-dimensional simulations used only  $n_0 = 0.05$ , and so did not test the  $n_0$  dependence. Using the  $\sqrt{n_0}$  prediction to calculate  $A_2$  gives a value of  $A_2 = 0.17$  from the simulations, in contrast to the calculated value 0.11. Simulations were later performed by Kang and Redner [49,62] in which they also observed the  $t^{-1/4}$  power law in one-dimension.

More recent simulations involve those of Schnörer, *et al.* [63]. They also simulated one- and two-dimensional systems, and also with the hard sphere correlations introduced by allowing only single occupancy. They start from a nearly filled lattice, the initial density of each species  $n_0 = 0.4$  in one dimension, and a completely filled lattice in two dimensions. Their results do not test the  $\sqrt{n_0}$  dependence of the amplitude, but if it is assumed then their simulations give values for  $A$  which are twice that given by (5.5) in one dimension, and a factor of five larger in two dimensions. However, their plots do not show a convincing asymptotic regime. Still, it is probable that starting with such a strongly lattice dependent initial condition has a dramatic effect on the amplitude of the power law. The amplitude is, in this sense, a less universal quantity.

The square-root dependence on the initial density has been tested in two dimensions by Cornell, *et al.* [64]. They find, in the regime where the  $t^{-1/2}$  power law is convincing, that the amplitude seems to go as  $n_0^{1/4}$  rather than the predicted square root. This is difficult to reconcile with any of the previous approaches, although we predict corrections to the square root dependence of  $n_0$  which could become quite large in the strong lattice limit, that is, the limit of a nearly filled lattice with only single occupancy allowed.

The only three dimensional simulation was performed by Leyvraz [30], in which again only single occupancy was allowed. Various initial densities (per individual species) between 0.025 and 0.5 were simulated, with only the initially completely filled lattice giving a good power law regime. For this initial density, the power law  $t^{-3/4}$  is convincingly demonstrated. Assuming the amplitude has the form  $A_3\sqrt{n_0}$  leads to a value of  $A_3 = 0.3$ , which is much larger than the prediction (5.5) of  $A_3 = 0.05$ . For smaller values of the initial density the simulations fail to reach the asymptotic regime before finite size effects dominate. This can be understood by considering that in approaching the asymptotic regime there is a subleading mean-field component of the density which is independent of  $n_0$ . That is

$$\langle a \rangle \propto \sqrt{n_0} t^{-3/4} + (\text{constant}) t^{-1}, \quad (5.7)$$

so that lowering the initial density enhances the strength of the subleading term. The crossover time can be found from above to scale like  $t \sim 1/n_0^2$ .

To summarize, the power law  $t^{-d/4}$  is confirmed in all simulations, but the amplitude prediction (5.5), which we will show is really a small  $n_0$  prediction, does not agree with the simulations in two and three dimensions. In these cases a strong lattice limit has been used in order to obtain an asymptotic regime.

There has been recently interest in studying the microscopic distribution of particles. For example, it is found from scaling arguments that the nearest neighbor distance distribution function for like particles scales differently than that of unlike particles [32]. The characteristic length of the nearest neighbor distribution for like particles goes as  $\ell_{AA} \sim t^{1/4}$  for  $d < 4$ , which is the same as the average interparticle spacing given by the density  $\bar{\ell} = \langle a \rangle^{-1/d}$ . This length scale is already present in the problem, and so this result is considered trivial. In contrast, if one considers the separation distance when the nearest neighbors are of the opposite species, then this distribution has a characteristic length in  $d = 1$  of  $\ell_{AB} \sim t^{3/8}$ . This exponent is argued also to be non-trivial in  $d = 2$  [32], with  $\ell_{AB} \sim t^{1/3}$ . These exponents have been verified numerically, with an algorithm that uses

some fixed number of nearest neighbors in order to improve the statistics of the distribution. In three dimensions it is found numerically that  $\ell_{AB} \sim t^{1/4}$  [30,32], which is claimed to hold for all  $d > 2$ . We disagree with this result, and argue that this length scale will be non-trivial for all  $d < 4$ , as will be demonstrated in §5.7.

Generally it is assumed that the two species of particles have equal diffusion constants, which would not necessarily be the case when considering a chemical reaction. In all the simulations mentioned above the diffusion constants were set equal. While it seems plausible that the density power law  $t^{-d/4}$  should be independent of a difference in the diffusion constants, this has never been explicitly demonstrated. Also, there has been no previous calculation of the amplitude when  $D_A \neq D_B$ . We have calculated this amplitude for  $d > 2$ .

## 5.2. FIELD THEORY

In our approach to the two-species reaction we consider a master equation which describes particles on a lattice undergoing a continuous time random walks. Multiple occupancy is allowed. When at least one particle of each species is present on a lattice site, then these particles have some rate of annihilation. This master equation is shown in chapter three to have a corresponding field theory, given by the action

$$S = \int d^d x \left[ \int_0^t dt \left\{ \bar{\phi}(\partial_t - \nabla^2)\phi + \bar{\psi}(\partial_t - \nabla^2)\psi - \bar{\psi}\delta\nabla^2\phi - \bar{\phi}\delta\nabla^2\psi \right. \right. \\ \left. \left. + \lambda_1\bar{\phi}(\phi^2 - \psi^2) + \lambda_2(\bar{\phi}^2 - \bar{\psi}^2)(\phi^2 - \psi^2) \right\} - n_\phi\bar{\phi}(0) \right]. \quad (5.8)$$

This action is written in terms of the fields  $\phi = (a + b)/\sqrt{2}$  and  $\psi = (a - b)/\sqrt{2}$ , and is what we will refer to as the full theory. It provides the complete description of the system for all dimensions  $d$ . It should be noted that  $n_\phi = \sqrt{2}n_0$ , where  $n_0$  is the initial density of each individual species, and the relations of the other parameters to those of the master equation can be found in chapter three. The parameter  $\delta$  is dimensionless and is given by  $\delta = (D_A - D_B)/(D_A + D_B)$ .

One can calculate various quantities given by this action via perturbation theory. We will treat the  $\delta$  vertices as two-point interactions, and so the propagators for  $\phi, \psi$  are given by the first two terms in (5.8), and are the usual diffusion propagators:  $G_{\bar{\phi}\phi}(p, t) = G_{\bar{\psi}\psi}(p, t) = e^{-p^2 t}$  when  $t > 0$ , and  $G_{\bar{\phi}\phi} = G_{\bar{\psi}\psi} = 0$  for  $t < 0$ . These propagators are represented by solid and dashed lines respectively. The three- and four-point vertices, which correspond to the annihilation reaction, are shown in fig. 5.1. When  $\delta \neq 0$  then there are two-point vertices which connect a  $\phi$  propagator to a  $\psi$  propagator, and vice versa. These vertices are wave number dependent, with magnitude  $p^2$ . In addition there is a source term for  $\phi$  at  $t = 0$ , similar to the one-species reaction of the previous chapter.

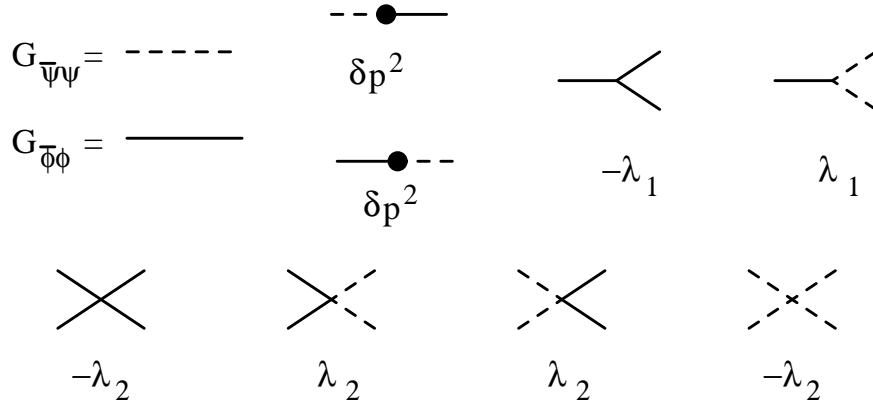


FIGURE 5.1. Propagators and vertices for the full theory in the two-species reaction-diffusion system.

With these tools one can construct a perturbation expansion which, if summed exactly, would give the complete description of the system. It is useful to introduce the classical density and response function, as derived in §4.2. These quantities, constructed with only  $\phi$  propagators, are defined and calculated exactly as before. The classical density is denoted by a wavy line, and the response function by a heavy line.

We can perform dimensional analysis on this action in the following way. There is a rigid constraint that  $[\bar{\phi}\phi] = [\bar{\psi}\psi] = p^d$ , where  $p$  is a wave number. We can consider

rescaling the fields by dimensionful parameters, as long as the conjugate fields are rescaled accordingly. Under such a rescaling the couplings  $\lambda_1$  and  $\lambda_2$  behave differently, although originally they are both proportional to  $\lambda_0$ . In particular, we could rescale the fields

$$\phi \rightarrow \phi/\lambda_1 \quad \bar{\phi} \rightarrow \lambda_1 \bar{\phi} \quad \psi \rightarrow \psi/\lambda_1 \quad \bar{\psi} \rightarrow \lambda_1 \bar{\psi}, \quad (5.9)$$

which has the result of setting the  $\bar{\phi}(\phi^2 - \psi^2)$  coupling to unity, while leaving  $\lambda_2$  unchanged. The rescaling (5.9) also results in  $n_\phi \rightarrow \lambda_1 n_\phi$ . This is the proper quantity to study when addressing issues of relevance and irrelevance, which can be seen by studying the diagrams generated by the action (5.8): whenever an additional  $t = 0$  line is added with weight  $n_\phi$ , there is an additional  $\lambda_1$  required to connect it. In this system of units, then, one finds that

$$[\lambda_2] = p^{2-d} \quad [\lambda_1 n_\phi] = p^2 \quad [\delta] = p^0. \quad (5.10)$$

Therefore there exists a critical dimension  $d_c = 2$ , above which  $\lambda_2$  flows to zero. Doing the complete power counting method with vertex functions, as was done in chapter four, yields the same result. Also, as before, the initial density is a strongly relevant parameter. The diffusion constant difference  $\delta$  is always marginal whenever it is not zero.

One approach to studying this problem is to integrate out the conjugate fields  $\bar{\psi}$  and  $\bar{\phi}$ . This leads to the equations of motion

$$\frac{\partial}{\partial t} \phi = \nabla^2 \phi - \lambda_1 \phi^2 + \lambda_1 \psi^2 + \eta_\phi \quad (5.11)$$

$$\frac{\partial}{\partial t} \psi = \nabla^2 \psi + \eta_\psi, \quad (5.12)$$

where  $\eta_\phi, \eta_\psi$  are noise terms with non-trivial distributions, but with average zero. In fact, the  $\eta_\phi$  noise is purely imaginary. It is important to note that the physical density is not the field  $\phi$ , but rather the average of  $\phi$  over the noise terms. These equations, without the noise terms included, are often taken as the starting point for analysis, but this approach is not generally valid. It is correct for  $d > 2$  at least, as will be shown below. One can

simplify equation (5.12) in any dimension, since it is a linear equation, by averaging over the noise. This is an average over the stochastic process of diffusion, and not over the initial conditions. Then the field  $\langle\psi\rangle_{\text{diff}}$  obeys the simple diffusion equation, for any given initial configuration.

### 5.3. EFFECTIVE FIELD THEORY FOR $d > 2$

From the dimensional analysis and power counting above it follows that for  $d > 2$  the full theory given by (5.8) can be replaced by an effective theory in which  $\lambda_2 = 0$  and  $\lambda_1 \rightarrow \lambda_{\text{eff}}(\lambda_1, \lambda_2, \Lambda)$ , where  $\Lambda$  is a wave number cutoff, necessary to regulate the theory. However, in constructing such an effective theory one has to consider all possible relevant terms, consistent with the symmetry of the theory, which might be generated. In order to identify these terms we note that this problem is analogous to that of a semi-infinite system in equilibrium statistical mechanics, with the analog of the boundary being the hyperplane  $t = 0$ . While one finds, in the semi-infinite equilibrium case, that the bulk critical properties do not depend on the surface terms, nonetheless one expects surface terms to contribute to correlation functions which involve fields on the boundary [65]. All observables in our problem are given by such correlation functions, since all diagrams originate with the  $n_\phi \bar{\phi}(0)$  term. Therefore we must check for all relevant *initial* terms, the  $t = 0$  analog of the surface terms, which might be generated, as well as those of the bulk. As mentioned above, the only relevant bulk term is that of  $\lambda_1$ .

The proper framework for determining which terms are relevant is via the rescaled fields (5.9). Therefore, for an initial term of the type  $(\Delta^{(m,n)}/m!n!)\bar{\phi}^m\bar{\psi}^n|_{t=0}$  added to (5.8) we consider the dimensions of the coupling  $[\lambda_1^{m+n}\Delta^{(m,n)}] = p^{(n+m)(2-d)+d}$ . This power of  $\lambda_1$  also follows from calculating the number of vertices required to attach a  $t = 0$  vertex of  $\Delta^{(m,n)}$  to a given diagram. These terms are relevant when

$$d < \frac{2(n+m)}{n+m-1}. \quad (5.13)$$

If  $m + n = 1$  then the initial term is relevant for all  $d$ . The case  $m = 1$  corresponds to the initial density, which has already been demonstrated to be relevant. For the case  $n = 1$  we first address the symmetry of the theory. When starting with equal initial densities the system is invariant under exchanging  $A \leftrightarrow B$  and  $D_A \leftrightarrow D_B$ . Therefore the action must be invariant under the transformation  $(\phi, \bar{\phi}, \psi, \bar{\psi}, \delta) \rightarrow (\phi, \bar{\phi}, -\psi, -\bar{\psi}, -\delta)$ . For what follows we will consider only the case  $\delta = 0$ , or  $D_A = D_B$ , in which case the symmetry forbids the generation of a initial term  $\Delta^{(0,1)}\bar{\psi}$ . In §5.8 the case  $\delta \neq 0$  will be discussed, and it will be demonstrated that again no  $n = 1$  initial term is generated.

For  $m + n = 2$  symmetry allows only the generation of  $\Delta^{(2,0)}$  and  $\Delta^{(0,2)}$ . Below we will address the calculation of these quantities, and demonstrate that  $\Delta^{(0,2)} = -\Delta^{(2,0)} \equiv \Delta$ . These terms are relevant whenever  $d < 4$ , as can be seen by equation (5.13), and therefore must be considered when constructing an effective theory for  $2 < d \leq 4$ . In fact, it will be shown that the term  $(\Delta/2)\bar{\psi}^2$  is solely responsible for determining the asymptotic decay of the density. This is an important point. This system is dominated by initial terms, as opposed to the one-species reaction studied in chapter four. Therefore techniques which utilize homogeneous source terms and look for a bulk steady state will not work for this problem. Since this initial term dominates the asymptotic behavior of the density, we identify  $d_c^* = 4$  as a second critical dimension of the system.

Higher order initial terms will also be relevant in the range  $2 < d \leq 3$ . In fact, as  $d \rightarrow 2$  one finds that all initial terms become relevant. While this seems to be an extreme complication, it is in fact possible to calculate exactly the asymptotic density for  $2 < d \leq 4$  and demonstrate that it is independent of such terms. This will be presented in the next section. We now turn to the calculation of the parameter  $\Delta$ .

The diagrams which must be considered in calculating an effective initial term  $(\Delta/2)\bar{\psi}^2$  are all those in which two  $\psi$  lines exit from the left, as shown in fig. 5.2(a). The sum of these diagrams gives rise to an effective term  $f(t)\bar{\psi}(t)^2$  in the action. If the function  $f(t)$  goes to zero for large  $t$ , and is sharply peaked enough that  $\int_0^\infty dt f(t)$  is finite, then a coarse-graining in time gives  $f(t)\bar{\psi}(t)^2 \sim (\Delta/2)\delta(t)\bar{\psi}(0)^2$ , where both quantities are understood



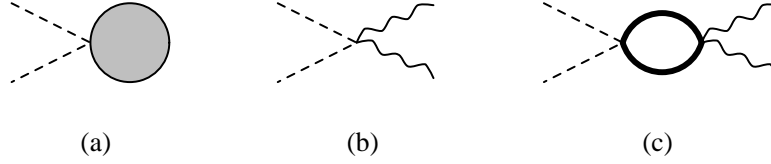


FIGURE 5.2. The initial term  $\Delta$  is generated by diagrams of the form (a). The tree diagrams in (b) give the leading order contribution for small  $n_0$ . The leading order corrections come from the diagrams (c). The classical density and response functions are defined in §4.2. For  $\Delta^{(2,0)}$  the same diagrams would be used, but with the opposite sign for the  $\lambda_2$  vertex on the left.

to be integrated over  $t$ , and  $\Delta = 2 \int_0^\infty dt' f(t')$ . To calculate this parameter  $\Delta$  we consider first the subset of diagrams given by the tree diagrams, as shown in fig. 5.2(b). These diagrams sum to give  $f_0(t) = -\lambda_2/(1 + n_\phi \lambda_1 t)^2$ , and so

$$\Delta_0 = -2\lambda_2 \int_0^\infty dt \frac{1}{(1 + n_\phi \lambda_1 t)^2} = 2n_\phi \frac{\lambda_2}{\lambda_1}. \quad (5.14)$$

Therefore we conclude that this set of diagrams generates an effective initial term  $\Delta_0 = 2n_\phi \lambda_2/\lambda_1$ , or, in terms of the parameters in the master equation (3.56),  $\Delta_0 = n_0$ , the initial density of each species. This will be shown to be the leading order term for a small  $n_0$  expansion of  $\Delta$ . The width of the function  $f_0(t)$  is given by  $(n_\phi \lambda_1)^{-1}$ , and therefore we expect this coarse-grained picture to be valid for times  $t \gg (n_\phi \lambda_1)^{-1}$ .

We can group all the diagrams in the full theory (5.8) which are of the form specified in fig. 5.2(a) in the following way. There is a vertex  $\lambda_2$  which is the leftmost vertex in the diagram. The lines coming into this vertex from the right can either come from mutually distinct or connected diagrams. The tree diagrams are a subset of the former group, and we argue that by letting  $\lambda_1$  go to some bulk effective coupling  $\lambda_{\text{eff}}$  all diagrams of the former group are included. The connected diagrams can be grouped by the number of times they are connected, and shown in fig. 5.2(c) are a set of diagrams which are connected exactly once. Again we argue that by taking  $\lambda_1 \rightarrow \lambda_{\text{eff}}$  the diagrams of fig. 5.2(c) give

the entire contribution of the set which are connected exactly once. The sum of these diagrams can be evaluated, and is found to contribute to  $\Delta$  a term which is higher order in  $n_0$  than that given by the tree diagrams. It can be shown in general that the groups with more connections will contribute correspondingly higher order terms, and therefore this classification scheme gives rise to an expansion for  $\Delta$ .

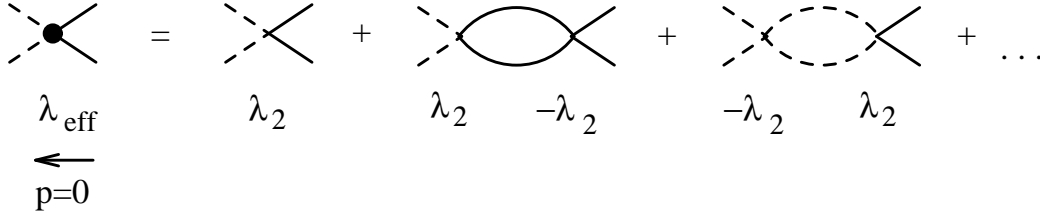


FIGURE 5.3. The expansion for the effective coupling constant.  
The wave number integrals are regulated by a cutoff  $\Lambda$ .

In order to calculate the next order of correction terms to the expansion  $\Delta = \Delta_0 + \dots$  we must first comment on the bulk diagrams which generate  $\lambda_{\text{eff}}$ . The effective coupling can be calculated as an expansion in the bare couplings, via the diagrams shown in fig. 5.3. The loop integrals in this expansion require the cutoff  $\Lambda$ , and one finds

$$\lambda_{\text{eff}} = \lambda_2 - \lambda_2^2 \frac{4\Lambda^{d-2}}{(8\pi)^{d/2}(d-2)} + O(\lambda_2^3). \quad (5.15)$$

If the response functions in the loop of fig. 5.2(c) were instead just propagators, then this set of diagrams would be included into those of fig. 5.2(b) when the substitution  $\lambda_2 \rightarrow \lambda_{\text{eff}}$  is made via (5.15). Therefore, the terms which are new and constitute a correction to  $\Delta_0$  are those in fig. 5.2(c) with the propagator loop subtracted out. We define the large  $t$  limit of these diagrams to be  $\Delta_1$ , that is

$$\Delta_1 = 4\lambda_2^2 n_\phi^2 \int_0^\infty dt_2 \left[ \int_0^{t_2} dt_1 \frac{d^d p}{(2\pi)^d} \left\{ \frac{e^{-2p^2 t} (1 + n_\phi \lambda_1 t_1)^2}{(1 + n_\phi \lambda_1 t_2)^4} - \frac{\Lambda^{d-2}}{(8\pi)^{d/2}(d-2)(1 + n_\phi \lambda_1 t_2)^2} \right\} \right]. \quad (5.16)$$

Performing the wave number integral with the  $\Lambda$  cutoff imposed in the same manner as in (5.15) gives

$$\Delta_1 = \frac{4\lambda_2^2 n_\phi^2}{(8\pi)^{d/2}} \int_0^\infty \frac{dt_2}{(1 + n_\phi \lambda_1 t_2)^4} \left[ \int_0^{t_2} dt_1 \left\{ \frac{(1 + n_\phi \lambda_1 t_1)^2}{(t_2 - t_1 - \Lambda^{-2})^{d/2}} - \frac{\Lambda^{d-2}}{d-2} (1 + n_\phi \lambda_1 t_2)^2 \right\} \right]. \quad (5.17)$$

The  $t_1$  integral can be evaluated as a Laplace convolution integral, and the cutoff dependent terms cancel. The remaining  $t_2$  integral is

$$\Delta_1 = \frac{-8\lambda_2^2 n_\phi^2}{(8\pi)^{d/2}(d-2)} \int_0^\infty \frac{dt_2 t_2^{1-d/2}}{(1 + n_\phi \lambda_1 t_2)^4} \left[ 1 + \frac{4n_\phi t_2}{4-d} + \frac{8n_\phi^2 t_2^2}{(4-d)(6-d)} \right]. \quad (5.18)$$

This integral can be done exactly, giving

$$\Delta_1 = \frac{\lambda_2^2}{\lambda_1^2} (n_\phi \lambda_1)^{d/2} \frac{(d+2)(d+4)}{48(8\pi)^{d/2-1} \sin(\pi d/2)}. \quad (5.19)$$

In terms of the initial density  $n_0$  and the effective coupling then

$$\Delta = n_0 - (n_0 \lambda_{\text{eff}})^{d/2} \frac{(d+2)(d+4)}{384(8\pi)^{d/2-1} \sin(\pi(d-2)/2)} + \dots \quad (5.20)$$

Evaluating the diagrams such as those in fig. 5.2(c), but containing more loops will then give the higher order terms in this small  $n_0$  expansion of  $\Delta$ .

In summary of the discussion above, we conclude that for  $2 < d \leq 4$  and for large times one can replace the full theory with a simpler action

$$S = \int d^d x \left[ \int_0^t dt \left\{ \bar{\phi}(\partial_t - \nabla^2)\phi + \bar{\psi}(\partial_t - \nabla^2)\psi - \lambda_{\text{eff}} \bar{\phi}(\phi^2 - \psi^2) \right\} - n_\phi \bar{\phi}(0) - \frac{\Delta}{2} \bar{\psi}(0)^2 + \text{other initial terms} \right], \quad (5.21)$$

where  $\Delta$  is given by (5.20). Since the bulk theory is linear in  $\bar{\phi}$  and  $\bar{\psi}$  these fields can be integrated out to yield the equations of motion

$$\frac{\partial}{\partial t} \phi = \nabla^2 \phi - \lambda_{\text{eff}} \phi^2 + \lambda_{\text{eff}} \psi^2 \quad (5.22)$$

$$\frac{\partial}{\partial t} \psi = \nabla^2 \psi. \quad (5.23)$$

These are equations for classical fields with fluctuations in the initial conditions. They are often taken to be the continuum limit of the master equation (3.56), but we stress that only for  $d > 2$  and large times are these equations valid.

## 5.4. DENSITY CALCULATION FOR $2 < d < 4$

Starting with the action (5.21) one can calculate exactly the leading time dependence of the density, as well as correlation functions. We begin with a comment about notation. For this section and the next, where we deal with only the effective field theory, averages over the initial conditions will be denoted by angular brackets. The averages over the bulk action have already been taken implicitly. That is, the classical fields  $\phi, \psi$  represent bulk averages, or equivalently, averages over diffusion, of the same fields as written in (5.8). Also, the effective coupling is abbreviated to be  $\lambda = \lambda_{\text{eff}}$ . With this notation, then, the average of equation (5.22) over the translationally invariant initial conditions is

$$\frac{d}{dt}\langle\phi\rangle = -\lambda\langle\phi^2\rangle + \lambda\langle\psi^2\rangle, \quad (5.24)$$

since  $\nabla^2\langle\phi\rangle = 0$ .

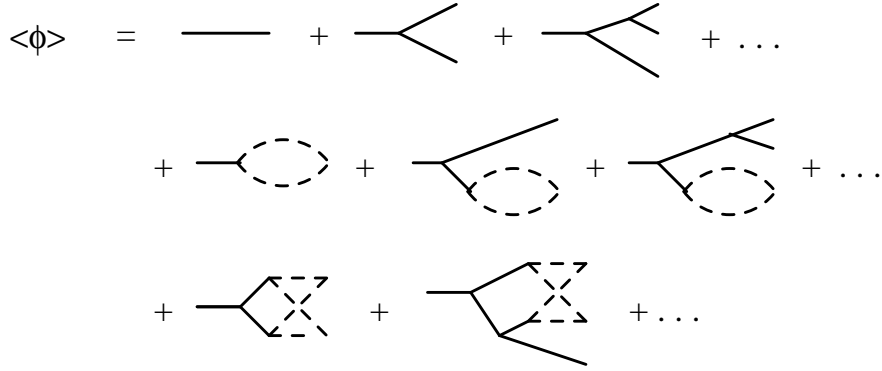


FIGURE 5.4. Diagrammatic expansion for  $\langle\phi\rangle$ . Diagrams which contain initial terms other than  $n_\phi$  and  $\Delta$  are not shown, but are included in the sum. The only diagram in which the leftmost vertex is connected to  $\psi$  fields is that of the single  $\psi$  loop.

A diagrammatic expansion for  $\langle\phi\rangle$  is shown in fig. 5.4. Operating on both sides of this expansion with  $(\partial_t - \nabla^2)$ , the inverse of the Green's function propagator, gives equation (5.24). While exactly summing these diagrams appears not to be possible, nonetheless

by use of non-perturbative methods we are able to find the asymptotic form of this sum. Acting on this sum with the inverse propagator turns the left side into  $\partial_t \langle \psi \rangle$ , and on the right side it has the effect of removing the propagator on the left and setting the leftmost vertex to time  $t$ . Out of this infinite sum, then, there is only one diagram contributing to the value of  $\langle \psi^2 \rangle$  in equation (5.24), which is the single  $\psi$  loop. Evaluating this loop gives  $\langle \psi^2 \rangle = \Delta / (8\pi t)^{d/2}$ . It is important to note that this result holds even when all possible higher order initial terms are included.

Next, consider as an approximation replacing  $\langle \phi^2 \rangle$  in (5.24) by  $\langle \phi \rangle^2$ , which is equivalent to including only the diagrams in fig. 5.4 which are disconnected to the right of the leftmost vertex. This partial sum satisfies a differential equation known as Ricatti's equation, which, though non-linear, can be solved. Let  $f$  denote the function which satisfies this equation, that is,

$$\frac{d}{dt}f = -\lambda f^2 + \lambda \frac{\Delta}{(8\pi)^{d/2}} t^{-d/2}. \quad (5.25)$$

It will be shown below that this function  $f$  provides a upper bound for the actual density, but first we will discuss the solution of this equation. It is integrable for certain values of  $d$ , specifically  $d = 4$  and  $d = 4 \pm 4/(2s + 1)$  where  $s$  is a non-negative integer, with a solution which can be expressed in terms simple functions. For general values of  $d$  a solution can be obtained<sup>9</sup> by transforming the equation via the substitution  $f = \dot{u}/(\lambda u)$ , which gives

$$\ddot{u} = \frac{\lambda^2 \Delta}{(8\pi)^{d/2}} t^{-d/2} u, \quad (5.26)$$

a linear, second order equation whose solution can be expressed in terms of confluent hypergeometric functions. Therefore the asymptotic behavior of  $f$  is rigorously obtained, and is in fact what one naively obtains by assuming  $f \sim A t^{-\alpha}$  and plugging it in to (5.25):

$$f \sim \begin{cases} \Delta^{1/2} (8\pi t)^{-d/4} & d < 4 \\ A_4^u t^{-1} & d = 4 \\ (\lambda t)^{-1} & d > 4 \end{cases} . \quad (5.27)$$

---

<sup>9</sup> For an interesting presentation of the properties and history of this equation, see [66].

When  $d < 4$  the asymptotic behavior comes from balancing the two terms on the right hand side of (5.25), whereas for  $d > 4$  it comes from balancing the  $f^2$  and the  $\dot{f}$  terms. For  $d = 4$  all three terms contribute, and the amplitude is

$$A_4^u = \frac{1}{2\lambda} + \sqrt{\frac{1}{(2\lambda)^2} + \frac{\Delta}{(8\pi)^2}}. \quad (5.28)$$

The case of  $d = 4$  will be discussed in more detail in §5.5. Notice that the asymptotic behavior of the solution  $f$  is independent of the initial conditions. In fact, the initial conditions must be specified at some  $t_0 > 0$ , since the equation is singular at  $t = 0$ . A natural choice for this initial time is that given by the coarse-graining time scale of the effective initial conditions, that is  $t_0 = (n_\phi \lambda)^{-1}$ .

Now we show that  $f$  provides an upper bound for the actual density  $\langle \phi \rangle$ . Our method is to derive an equation for  $\chi = f - \langle \phi \rangle$  and show that asymptotically  $\chi \geq 0$ . Since  $\phi$  is a real field in the effective theory, then  $h(t) \equiv \langle \phi^2 \rangle - \langle \phi \rangle^2 \geq 0$ . Equation (5.24) can be rewritten

$$\frac{d}{dt} \langle \phi \rangle = -\lambda h(t) - \lambda \langle \phi \rangle^2 + \lambda \langle \psi^2 \rangle, \quad (5.29)$$

and then substituting  $\langle \phi \rangle = f - \chi$  gives

$$\frac{d}{dt} \chi = \lambda h + \lambda(\chi - 2f)\chi. \quad (5.30)$$

Assume that  $\chi(t_0) = 0$ , that is we choose the initial condition for  $f$  such that  $f(t_0) = \langle \phi(t_0) \rangle$ . As mentioned above, the asymptotic value of  $f$  is independent of the choice of initial conditions. Since the solution of  $f$  is known and is positive for all  $t > t_0$ , then from equation (5.30) we know that  $\dot{\chi} > 0$  whenever  $\chi < 0$ . Now we make the assumption that there exists some  $t_1 > t_0$  for which  $\chi(t_1) < 0$ . Since  $\chi(t)$  is a continuous function then it follows that there must be some intermediate time  $t_0 < t < t_1$  for which  $\chi(t) < 0$  and  $\dot{\chi}(t) < 0$ . This is in contradiction with equation (5.30), and therefore our assumption that there exists  $\chi(t_1) < 0$  for  $t_1 > t_0$  is false.

We can also find a lower bound for  $\langle \phi \rangle$  by noting that  $\phi(\mathbf{x}, t) \geq |\psi(\mathbf{x}, t)|$  at all points  $(\mathbf{x}, t)$ . This is equivalent to the statement that  $a(\mathbf{x}, t), b(\mathbf{x}, t)$  are at all points non-negative, when starting from any initial condition in which  $a, b$  are everywhere non-negative. While this result is somewhat intuitive, it can be made more rigorous by considering the field equations (5.22), (5.23) expressed in terms of  $a = (\phi + \psi)/\sqrt{2}$  and  $b = (\phi - \psi)/\sqrt{2}$ :

$$\frac{\partial}{\partial t}a = \nabla^2 a - \sqrt{2}\lambda ab \quad \frac{\partial}{\partial t}b = \nabla^2 b - \sqrt{2}\lambda ab. \quad (5.31)$$

Given that the fields  $a, b$  are initially everywhere non-negative, then for the fields to have a negative value at a later time  $t_1$  there must be an intermediate time  $0 < t_0 < t_1$  for which both  $a(t_0) = 0$  and  $\partial_t a(t_0) < 0$ . However, in the case where  $a = 0$  at a single point in space, then  $a > 0$  locally around the point, implying that it is a local minimum and  $\partial_t a > 0$ . For a region of  $a = 0$  equation (5.31) gives  $\partial_t a = 0$  in the region and  $\partial_t a > 0$  on the boundary. Therefore the fields cannot pass through zero, and will remain non-negative.

Since  $\phi \geq |\psi|$  it follows that  $\langle \phi \rangle \geq \langle |\psi| \rangle$ . At late times  $\psi$  has a normal distribution, independent of the initial distribution, which follows from the fact that  $\psi$  obeys the simple diffusion equation (5.23). Therefore the asymptotic value of  $\langle |\psi| \rangle$  can be computed directly. The asymptotic distribution of  $\psi$  is given by

$$P[\psi(t)] \propto \exp \left\{ -\frac{\psi(t)^2}{2\langle \psi(t)^2 \rangle} \right\}, \quad (5.32)$$

from which it follows that

$$\langle |\psi(t)| \rangle = \sqrt{\frac{2}{\pi} \langle \psi(t)^2 \rangle} = \frac{(2\Delta)^{1/2}}{\pi^{1/2}(8\pi)^{d/4}} t^{-d/4}. \quad (5.33)$$

Given the upper bound  $f \sim t^{-d/4}$  it can be shown that  $\langle \phi \rangle \sim \langle |\psi| \rangle$ , that is, that the lower bound gives exactly the density. Using again  $\phi \geq |\psi|$ :

$$\begin{aligned} \langle \phi - |\psi| \rangle^2 &\leq \langle (\phi - |\psi|)^2 \rangle \\ &= \langle \phi^2 \rangle + \langle \psi^2 \rangle - 2\langle \phi|\psi| \rangle \\ &\leq \langle \phi^2 \rangle - \langle \psi^2 \rangle \\ &= -\frac{1}{\lambda} \langle \dot{\phi} \rangle = O(t^{-1-d/4}). \end{aligned} \quad (5.34)$$

Therefore  $\langle \phi \rangle = \langle |\psi| \rangle + O(t^{-1/2-d/8})$ , which gives  $\langle \phi \rangle \sim \langle |\psi| \rangle$  for  $d < 4$ . This is actually a statement about segregation in the system, implying that to leading order the density of  $a + b$  is the same as  $|a - b|$ , or equivalently, that the minority species in each region decays faster than the majority. The densities  $\langle a \rangle, \langle b \rangle$  are given by  $\langle a \rangle = \langle b \rangle = \langle \phi \rangle / \sqrt{2}$ . For  $2 < d < 4$  then, we find

$$\langle a \rangle = \frac{\Delta^{1/2}}{\pi^{1/2}(8\pi)^{d/4}} t^{-d/4}, \quad (5.35)$$

with  $\Delta$  given by (5.20). Substituting the leading order term in the expansion  $\Delta = n_0 + O(n_0^{d/2})$  then gives the result of Toussaint and Wilczek [31]. In fact, our method is very similar to theirs, with two exceptions. First, they use a central limit argument to calculate  $\Delta$ , whereas we can compute it directly from the full field theory. It is reassuring that the answers agree, to leading order in  $n_0$ . The other difference is that they calculate  $\langle |\psi| \rangle$ , and then hypothesize the asymptotic segregation, saying  $\langle \phi \rangle \sim \langle |\psi| \rangle$ . The methods developed here can be used to show rigorously that these quantities are asymptotically the same.

## 5.5. DENSITY FOR $d \geq 4$

When  $d = 4$  the upper and lower bounds for the density from §5.4 still hold:  $\langle |\psi| \rangle \leq \langle \phi \rangle \leq f$ . However, it is no longer necessarily true that  $\langle \phi \rangle \sim \langle |\psi| \rangle$ , since the bound on the corrections, which is of order  $O(t^{-1/2-d/8})$ , is the same order as the density. The upper bound  $f \sim A_4^u/t$  is given by (5.27) and (5.28). Notice that for small  $\lambda$  or small  $\Delta$  that  $A_4^u \rightarrow 1/\lambda$ . Also, when  $\lambda$  is large or  $\Delta$  is large then  $A_4^u \rightarrow \Delta^{1/2}/(8\pi)$ . However, in the intermediate region there is a smooth crossover in the upper bound from the  $\lambda$  dependent asymptote to the  $\Delta$  dependent asymptote.

The lower bound is given by  $\langle \phi \rangle \geq \langle |\psi| \rangle = A_4^\ell/t$  with  $A_4^\ell = \Delta^{1/2}/8\pi^{3/2}$ . For large  $\Delta$ , then, the upper and lower bounds differ by a factor of  $\sqrt{\pi}$ . The lower bound continues to decrease with  $\Delta$ , and therefore is not very useful in the small  $\Delta$  limit. However, since the parameter  $\Delta$  is dimensionless in  $d = 4$  one can do a perturbative expansion for small  $\Delta$ , which results in a better lower bound. It follows from equation (5.24) that the zeroth



order term in this expansion is a constant, and is in fact equal to the small  $\Delta$  limit of the upper bound,  $\lambda^{-1}$ . To the next order one has

$$\langle a \rangle = \frac{1}{\lambda t} + \frac{\lambda \Delta}{t} + O(\Delta^2), \quad (5.36)$$

and it is plausible to conjecture that the amplitude is monotonically increasing with  $\Delta$ .

The conjectured form of the amplitude given by Bramson and Lebowitz [47], has the form

$$A_4 \propto \begin{cases} \text{constant} & \Delta < \Delta_c \\ \Delta^{1/2} & \Delta > \Delta_c. \end{cases} \quad (5.37)$$

Their result seems to be at odds with our small  $\Delta$  calculation. However, one possible explanation is that in the model they consider the reaction occurs immediately if one of each species occupy the same lattice site. Thus, they allow multiple occupation, but only of the same particle type. In our model the reaction occurs at a given rate, but not immediately. Given the non-universal nature of the amplitude, this could be the cause of the discrepancy.

When  $d > 4$  then it follows from the power counting of §5.3 that the  $(\Delta/2)\bar{\psi}^2$  initial term is irrelevant. In this case the density is given asymptotically by  $\langle a \rangle \sim (\lambda t)^{-1}$ . The power law of the density decay is independent of the dimension of space. The amplitude  $\lambda^{-1}$  will depend on the dimension and the microscopic details, but it is independent of initial terms, or equivalently initial conditions.

## 5.6. RENORMALIZATION FOR $d \leq 2$

When  $d \leq 2$  one has to consider the full theory as given by the action (5.8). In calculating the diagrams generated by this theory one encounters divergences, just as in the one-species case. The primitively divergent vertex functions can be identified by power counting, and are found to be those with two lines coming in and two or fewer lines going out. This is identical to the situation in the  $A + A \rightarrow \emptyset$ . In order to calculate the density,

or other quantities such as correlation functions, it is then necessary to introduce the renormalized coupling and Callan-Symanzik equation as was done in chapter four.

The renormalization of the coupling follows quite similarly to that of the one-species reaction. There are now four  $\lambda_2$  couplings, shown in fig. 5.1, which contribute to the bubble sums. However, it is still true that all of the vertex functions renormalize identically, since they have the same sum of bubble diagrams. The temporally extended vertex function  $\lambda_i(p, t)$  is defined to be the sum of the bubble diagrams shown in fig. 5.5. The subscript  $i = 1, 2$  refers to the number of exiting lines.

$$\lambda(p, t) = \text{tree} + \text{bubble}_1 + \text{bubble}_2 + \text{bubble}_3 + \text{bubble}_4 + \text{bubble}_5 + \text{bubble}_6 + \dots$$

FIGURE 5.5. The sum of diagrams which contribute to the primitively divergent vertex function  $\lambda_i(p, t)$ . Shown here is the case  $i = 1$ , with the  $\psi$  propagators for the incoming external legs.

To each order in the number of loops there are more diagrams than in the one-species case, because the loops can be composed of  $\psi$  or  $\phi$  propagator pairs in all possible combinations. These different combinations come in with the same sign, since replacing a  $\phi$  loop with a  $\psi$  loop, for example, introduces always two negative signs (see fig. 5.1). For a bubble diagram with  $n$  loops there are  $2^n$  diagrams, all contributing identically, whereas in the one-species reaction there is just one. As a result, the sum is the same as that

performed in equation (4.10), except that at the order of  $n$  loops there is a new factor of  $2^n$ . Taking the Laplace transform  $\lambda_i(p, s) = \int_0^\infty dt e^{-st} \lambda_i(p, t)$  gives a geometric sum

$$\lambda(p, s) = \frac{\pm \lambda_i}{1 + 2\lambda_2 B_2 \Gamma(\epsilon/2)(s + p^2/2)^{-\epsilon/2}}, \quad (5.38)$$

where  $\epsilon = 2 - d$ , and the overall sign is positive when the incoming and outgoing external lines are of the same type, and negative if they differ. The constant  $B_2 = 2(8\pi)^{-d/2}$  is calculated in §4.1.

As before, this vertex function is used to define a renormalized coupling. For a given wave number scale  $\kappa$  we define  $g_R \equiv \lambda(p = 0, s = \kappa^2)$ . The rest of the analysis follows identically to that in chapter four, which leads to the solution of the Callan-Symanzik equation for the density

$$n(t, n_0, g_R, \kappa) = (\kappa^2 t)^{-d/2} n\left(\kappa^{-2}, \tilde{n}_0(\kappa^{-2}), \tilde{g}_R(\kappa^{-2}), \kappa\right), \quad (5.39)$$

where  $n = \langle a \rangle = \langle b \rangle$ . The running coupling  $\tilde{g}_R$  flows to an order  $\epsilon$  fixed point as  $t \rightarrow \infty$ .

The difference between the two- and one-species reactions lies in determining which diagrams to put into the right hand side of (5.39) in order to get an exact or perturbative answer from the left hand side. In the one-species case the answer was relatively simple: by using on the right hand side the infinite sum of diagrams containing a given number  $n$  loops, one generates the  $n$ th order term in the perturbative calculation. A scheme was developed which allowed one, in principle, to calculate these sums, and was sufficient to show that to all orders the exponent of the density decay was exact. The state of affairs is less convincing for the two-species case.

In the one-species case it was shown that the leading order in  $\epsilon$  contribution to the amplitude comes from putting the tree diagrams into the right hand side of the Callan-Symanzik solution. This was shown explicitly, but it was motivated first by observing that the mean-field diagrams, those which contain no  $\lambda_2$  vertices, have the lowest power of the coupling relative to  $n_0$ . In the two-species case the analog of these diagrams are those

with no  $\lambda_2$  vertices, but with the effective initial terms included. These effective terms are generated for  $d \leq 2$  as well as  $d > 2$ . They arise from including certain  $\lambda_2$  vertices, as shown in fig. 5.2. While it might appear arbitrary to include these  $\lambda_2$  vertices in calculating the lowest order term for the right hand side of (5.39), this is motivated by the fact that these terms give rise to the “classical” density for  $d > d_2 = 2$ , and are therefore the analog of the usual tree diagram expansion. From here we make the conjecture that, as before, the sum over all powers of  $n_0$  for a given power of  $\lambda_2$  gives a term higher order in the coupling. Then, from the Callan-Symanzik solution, these diagrams contribute to higher order in  $\epsilon$  terms. Plugging the previous solution into (5.39) gives

$$\langle a \rangle = \frac{\Delta^{1/2}}{\pi^{1/2}(8\pi)^{d/4}} t^{-d/4} + O(\epsilon). \quad (5.40)$$

The value of  $\Delta$  is yet to be determined. The set of diagrams in fig. 5.2(b) can still be evaluated, and gives  $\Delta = n_0$  as before. However, when  $d \leq 2$  we cannot proceed to calculate the correction terms as we did in §5.3. It seems plausible that any correction terms would be higher order in the coupling when calculated, and therefore higher order in  $\epsilon$ . If this is correct, then  $\Delta$  can be replaced with  $n_0$  in the equation above. This result is in good agreement with the simulations of Toussaint and Wilczek [31] for  $d = 1$ .

When  $d = 2$  the running coupling goes to zero as  $(\ln t)^{-1}$  for  $t \rightarrow \infty$ , rather than to an order  $\epsilon$  fixed point. Therefore the leading order terms for an  $\epsilon$  expansion of the amplitude become the exact asymptotic amplitude, with correction terms which go as  $(\ln t)^{-1}$ . As a result, the amplitude predicted above should be exact in the truly asymptotic limit. However, these logarithmic corrections are likely to persist for the time scales accessible to simulation.

## 5.7. REACTION ZONES

It was shown in §5.4 that for  $d < 4$  the particles segregate asymptotically into regions of purely  $A$  or  $B$  particles. As a result of this segregation there exist interfaces between

the two species, and all reactions occur in the interfacial regions. These reaction zones have interesting scaling properties. For example, the width of the interface goes as  $t^\alpha$  with the exponent  $\alpha < 1/2$ . Also one can study the nearest neighbor distance distribution of the particles in the reaction zone, and show that the characteristic length  $\ell_{rz}$  also goes as a power of  $t$  with a non-trivial exponent for  $d < 4$ . By non-trivial we mean that the characteristic separation distance in the reaction zone differs from that of the bulk system, in which  $\bar{\ell} \sim \langle a \rangle^{-1/d} \sim t^{1/4}$ . To derive these properties we begin with the related and well-studied problem of a single interface.

Consider an initial configuration in which the  $A$  and  $B$  particles are completely segregated, so that for some spatial coordinate  $x$  there are only  $A$  particles where  $x < 0$  and only  $B$  particles where  $x > 0$ . At later times one expects the densities  $\langle a \rangle$  and  $\langle b \rangle$  to be continuous functions of  $x$  with a cross-section as pictured in fig. 5.6. The angle brackets in this case correspond to averages over the stochastic process of diffusion, and also any randomness in the initial state—for example, the particles can be taken to be randomly distributed throughout their semi-infinite region. The reaction rate profile is defined to be  $R(x, t) = \langle ab \rangle$ . One way to visualize this function  $R$  is to consider the reaction  $A + B \rightarrow C$ , with  $C$  particles inert. Then  $R(x, t)$  represents the rate of production of  $C$  particles at time  $t$  and position  $x$ .

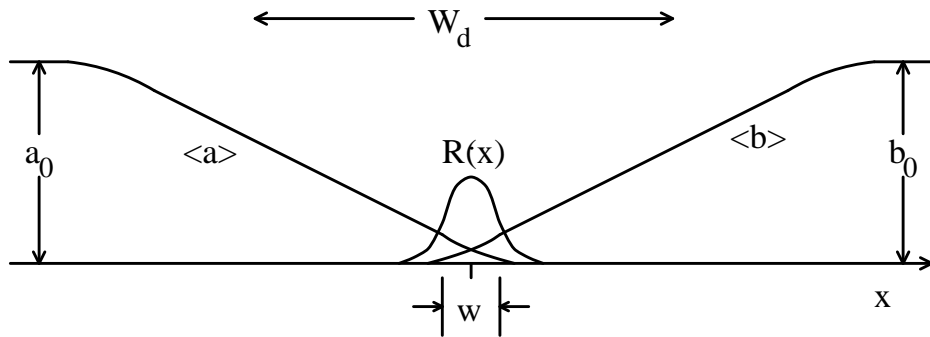


FIGURE 5.6. The cross-section of a reaction zone. The reaction profile  $R(x, t) = \langle ab \rangle$  has the characteristic width  $w$ . The depletion region  $W_d \sim t^{1/2}$ .

The field equations for this reaction are given by

$$\begin{aligned}\frac{\partial}{\partial t}\langle a \rangle &= \nabla^2 \langle a \rangle - \sqrt{2}\lambda \langle ab \rangle \\ \frac{\partial}{\partial t}\langle b \rangle &= \nabla^2 \langle b \rangle - \sqrt{2}\lambda \langle ab \rangle.\end{aligned}\tag{5.41}$$

The functions  $\langle a \rangle$  and  $\langle b \rangle$  will depend on  $x$ , and so  $\nabla^2 \langle a \rangle \neq 0$ , unlike in the case of the translationally invariant initial conditions. If one makes the mean-field approximation that  $\langle ab \rangle = \langle a \rangle \langle b \rangle$  then the equations above become partial differential equations for the functions  $\langle a \rangle$ ,  $\langle b \rangle$ . From these equations it has been demonstrated that the densities and the reaction profile exhibit scaling, that is

$$\langle a \rangle = t^{-\beta/2} f(xt^{-\alpha}) \quad \langle b \rangle = t^{-\beta/2} g(xt^{-\alpha}) \quad R = t^{-\beta} h(xt^{-\alpha}), \tag{5.42}$$

with the exponents  $\alpha = 1/6$  and  $\beta = 2/3$  [67]. Here  $x$  refers to the distance from the center of the interface. From these scaling relations it follows that width  $w$  of the profile  $R$  goes as  $w \sim t^{1/6}$ .

It is important to observe that the reaction front is highly localized relative to the depletion zone. The densities will be depleted from their initial values out to a range  $W_d \sim t^{1/2}$ , since particles within this range will have had a chance to diffuse into the reaction region. The reaction zone goes as  $t^\alpha$ , and it is generally assumed that  $\alpha < 1/2$ , and then demonstrated self-consistently. The significance of this localization is that there is a diffusion zone, defined by the range of  $x$  where  $w \ll |x| \ll W_d$ , in which the density has simply a linear profile. This follows from the solution of Laplace's equation with the boundary conditions being  $\langle a \rangle \approx a_0$  at  $x = -W_d$  and  $\langle a \rangle \approx 0$  at  $x = 0$ . The slope of this linear profile is denoted by  $\pm J$ , and is given by  $J \approx a_0/W_d \sim t^{-1/2}$ . In this diffusion region the density is  $\langle a \rangle = -Jx$ , so the current  $\mathbf{J} = -\nabla \langle a \rangle = J\hat{\mathbf{x}}$ . Now we observe that the reaction front in this dynamic case is equivalent to the steady state reaction front created by incoming currents  $J \sim t^{-1/2}$ . This correspondence to a steady state problem is very useful for simulations of the front [33], and is also important in generalizing the results of a

single reaction front to the case of the reaction zones formed in the homogeneous system, as will be shown below.

It is possible to derive the exponent characterizing the width of the reaction front from the field theory version of the problem. For example, the current  $J$  is given by an operator  $\bar{a}\partial_x a$ , where  $a = (\phi + \psi)/\sqrt{2}$ . From dimensional analysis one has  $[J] = p^{d+1}$ . The width of the reaction zone can in principle depend on the current  $J$  and the reaction rate  $\lambda_0$ . However, we have demonstrated that for  $d < 2$  the coupling  $\lambda_0$  flows to an order  $\epsilon$  fixed point, and so all observables are independent of the initial value of the coupling. Therefore, for  $d < 2$ ,  $w \sim J^{-1/(d+1)}$ .<sup>10</sup> When  $d > 2$  the coupling enters back in to the scaling analysis, and we expect the dependence of  $w$  on  $J$  to be independent of dimension, that is  $w \sim J^{-1/3}$ . This last result can be made rigorous by the scaling analysis of [67]. Making the correspondence  $J \sim t^{-1/2}$  then gives

$$w \sim \begin{cases} t^{1/2(d+1)} & d \leq 2 \\ t^{1/6} & d \geq 2 \end{cases} \quad (5.43)$$

While there is still controversy regarding the situation for  $d < 2$  [68], there is a reasonable amount of theoretical and numerical work [33] which indicates that  $w \sim t^{1/4}$  for  $d = 1$ , consistent with the results above.<sup>11</sup>

A similar argument can be made for the density within the reaction region. That is, since lengths scale as  $J^{-1/(d+1)}$  for  $d < 2$ , then

$$\langle a \rangle = \begin{cases} J^{d/(d+1)} f(xJ^{1/(d+1)}) & d \leq 2 \\ J^{2/3} f(xJ^{1/3}) & d > 2. \end{cases} \quad (5.44)$$

The scaling form for  $d > 2$  follows from [67]. If we assume that the distribution of particles in the reaction zone is roughly uniform, which would be equivalent to saying that

---

<sup>10</sup> This result holds even if the diffusion constants of the two species are not equal, since the new parameter which is introduced,  $\delta = (D_A - D_B)/(D_A + D_B)$ , is dimensionless.

<sup>11</sup> It is actually found that  $w \sim t^\alpha$  with  $\alpha \approx 0.30$  in the time-dependent case. However, it is very difficult to get into the asymptotic regime, and the analogous steady state simulation yields  $w \sim J^{-\nu}$  with  $\nu = 0.497 \pm 0.008$ , in excellent agreement with the analysis.

the function  $f(xJ^{1/(d+1)})$  can be replaced by a constant, then the characteristic distance between nearest neighbors in the reaction zone would go like

$$\ell_{rz} \sim \langle a \rangle^{-1/d} \sim \begin{cases} J^{-1/(d+1)} & d \leq 2 \\ J^{-2/3d} & d \geq 2. \end{cases} \quad (5.45)$$

While the density is not truly uniform, we argue that non-uniformities do not affect the scaling analysis, or equivalently, that there is just one length scale characterizing this non-uniform distribution. Making the correspondence  $J \sim t^{-1/2}$  gives

$$\ell_{rz} \sim \begin{cases} t^{1/2(d+1)} & d \leq 2 \\ t^{1/3d} & d \geq 2. \end{cases} \quad (5.46)$$

The results above are for the case of a single reaction front created by inhomogeneous initial conditions. However, we can extend this analysis to the reaction zones which form for  $d < 4$  when starting from homogeneous initial conditions with equal initial densities of each species. Asymptotically the segregated domains of  $A$  and  $B$  particles will form a percolated network as shown in fig. 5.7. We are interested in the cross-section of an interface, which will look roughly like fig. 5.6. Since these reaction zones will be confined within a diffusion depleted region as before, then again the analogy to the steady state system can be made.

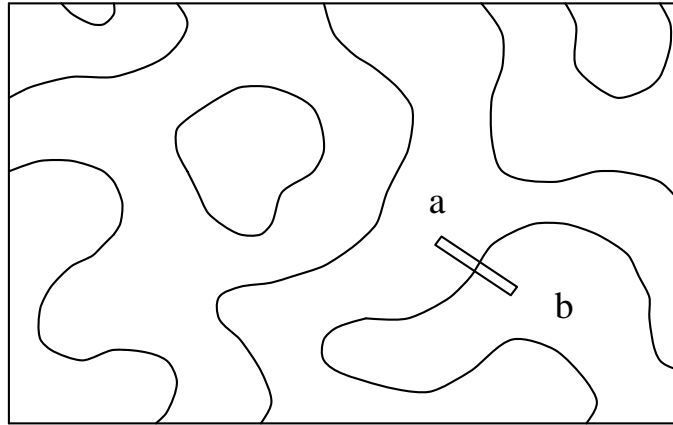


FIGURE 5.7. A two-dimensional picture of the segregated domains. The cross-section labeled by the rectangle will resemble fig. 5.6.



The scaling dependence of  $w$  and  $\ell_{rz}$  on  $J$  is unchanged. The difference in the reaction zones between the homogeneous case and that of the single front lies in how the  $J$  scales with  $t$ . The width of the diffusion depleted region is still given by  $W_d \sim t^{1/2}$ . However, the height of the non-depleted density now scales as  $\langle a \rangle \sim t^{-d/4}$ , instead of being time independent as in the single reaction front case. Since the slope of the depletion region determines the current  $J$  in the steady state analog, then we have  $J \sim t^{-(d+2)/4}$  for  $d < 4$ . The width of the reaction zone, for the homogeneous case, is then

$$w \sim \begin{cases} t^{(d+2)/4(d+1)} & d \leq 2 \\ t^{(d+2)/12} & 2 \leq d < 4 \end{cases} \quad (5.47)$$

These exponents are new results. Note that as  $d \rightarrow 4$ ,  $w \rightarrow t^{1/2}$ . That is, the width of the reaction zone is of the same order as the size of the segregated regions, consistent with the loss of segregation at  $d = 4$ .

Making the substitution  $J \sim t^{-(d+2)/4}$  into the scaling results (5.45) for  $\ell_{rz}$ , gives

$$\ell_{rz} \sim \begin{cases} t^{(d+2)/4(d+1)} & d \leq 2 \\ t^{(d+2)/6d} & 2 \leq d < 4. \end{cases} \quad (5.48)$$

The scaling of this quantity has been studied by Leyvraz and Redner, and also measured numerically [30,32]. What they actually study is the length scale of the unlike nearest neighbor distribution function,  $\ell_{AB}$ . This distribution is for the separation lengths of nearest neighbors when they are of the opposite species, and should not be confused with the distribution of distances to the nearest unlike neighbor. If the nearest neighbor is an unlike particle then the particles must be in the reaction zone, and therefore  $\ell_{AB} \propto \ell_{rz}$ .

Comparing our results we find that  $\ell_{rz} \sim t^{3/8}$  in  $d = 1$  and  $\ell_{rz} \sim t^{1/3}$  in  $d = 2$ , in agreement with the scaling arguments and numerical results of Leyvraz and Redner. However, they argue that for  $d > 2$  that  $\ell_{AB} \sim t^{1/4}$ , that is, that the reaction zone no longer contains a non-trivial length scale. They report numerical results for  $d = 3$  consistent with this prediction. We find instead that  $\ell_{rz}$  is non-trivial for all  $d < 4$ , and

that  $\ell_{rz} \sim t^{5/18}$  in  $d = 3$ . This value for the exponent is close to  $1/4$ , and appears to provide an equally good, if not better, fit to their data.

It is interesting to use the scaling results above to test the standard assumption that the segregated regions are of length  $t^{1/2}$ . If we integrate the field equations (5.41) over the entire volume  $V$ , we find  $\int d^d x \partial_t \langle a \rangle \propto - \int d^d x \langle ab \rangle$ , or

$$V t^{-1-d/4} \propto A \int dx_{\perp} R(x_{\perp}, t) \quad (5.49)$$

where  $A$  represents the volume of the  $d-1$  dimensional hypersurface given by the interfaces, which are the only regions which give a contribution to  $\langle ab \rangle$ . The coordinate  $x_{\perp}$  is locally defined to be perpendicular to the surface of the interface. If  $d > 2$  then we can assume  $R = \langle a \rangle \langle b \rangle$ , and therefore  $R \sim J^{4/3} f(x J^{1/3})$  and  $\int dx R(x) \sim J \sim t^{-1/2-d/4}$ . Substituting this into (5.49) we find for  $d > 2$  that the characteristic length of the segregated domains  $\bar{\ell}_{\text{seg}} = V/A \sim t^{1/2}$ . When  $d \leq 2$  one cannot assume that  $\langle ab \rangle$  and  $\langle a \rangle \langle b \rangle$  scale in the same way. In fact, it can be shown via RG arguments [69] that

$$\frac{\langle ab \rangle}{\langle a \rangle \langle b \rangle} \sim J^{(2-d)/(d+1)}. \quad (5.50)$$

Recalling that  $J^{1/(d+1)}$  scales as the wave number  $p$ , then this anomalous dimension is just  $p^{\epsilon}$  where  $\epsilon = 2 - d$ . The scaling form of  $R$  for  $d < 2$  is then

$$R = J^{(d+2)/(d+1)} f(x J^{1/(d+1)}), \quad (5.51)$$

and so  $\int dx_{\perp} R(x_{\perp}) \sim J \sim t^{-1/2-d/4}$ , just as before. As a result, the size of the segregated domains goes as  $\bar{\ell}_{\text{seg}} \sim t^{1/2}$  for  $d \leq 2$  as well.

## 5.8. UNEQUAL DIFFUSION CONSTANTS, $D_A \neq D_B$ , FOR $d > 2$

When the two species of particles no longer have equal diffusion constants, then the vertices which depend on  $\delta$  must be included in the full theory. Then for  $d > 2$  an effective theory can be developed, just as before, with the resulting action

$$S = \int d^d x \left[ \int_0^t dt \left\{ \bar{\phi}(\partial_t - \nabla^2) \phi + \bar{\psi}(\partial_t - \nabla^2) \psi - \bar{\psi} \delta \nabla^2 \phi - \bar{\phi} \delta \nabla^2 \psi \right. \right. \\ \left. \left. + \lambda \bar{\phi}(\phi^2 - \psi^2) \right\} - n_{\phi} \bar{\phi}(0) - \frac{\Delta}{2} \bar{\psi}(0)^2 + \dots \right]. \quad (5.52)$$

The effective theory describes classical fields which evolve via the deterministic equations of motion

$$\frac{\partial}{\partial t}\phi = \nabla^2\phi + \delta\nabla^2\psi - \lambda\phi^2 + \lambda\psi^2 \quad (5.53)$$

$$\frac{\partial}{\partial t}\psi = \nabla^2\psi + \delta\nabla^2\phi, \quad (5.54)$$

which follows from integrating out the  $\bar{\phi}, \bar{\psi}$  degrees of freedom in the bulk component of (5.52). From these equations the density can be calculated exactly by using the same methods as before. First, equation (5.53) is averaged over the initial conditions to yield equation (5.24), just as in the  $\delta = 0$  case. The solution to Ricatti's equation again provides an upper bound  $f \sim \sqrt{\langle\psi(t)^2\rangle}$ , although the value of  $\langle\psi(t)^2\rangle$  is changed. It will be shown that  $\langle\psi^2\rangle \propto t^{-d/2}$ , so the upper bound decays with the same exponent as before. Since the fields are real and  $\phi \geq |\psi|$ , it then follows that  $\langle\phi\rangle \sim \langle|\psi|\rangle$  for  $d < 4$ , as shown in (5.34). Furthermore, it will be shown that asymptotically  $\psi(t)$  has a normal distribution, so the density is given exactly by  $\langle a \rangle = \langle\phi\rangle/\sqrt{2} \sim \sqrt{\langle\psi^2\rangle}/\pi$ . Therefore the only change in the asymptotic density from the  $\delta = 0$  case is due to the change in the value of  $\langle\psi(t)^2\rangle$ .

### *Calculation of $\langle\psi(t)^2\rangle$*

The initial terms in the effective theory are in general changed by the presence of  $\delta$  in the full theory, and therefore must be computed again. One can show that, as before, no  $\Delta^{(0,1)}\bar{\psi}$  initial term is generated. For any diagram which ends with a single  $\psi$  line, the last vertex (first from the left) must be a  $\delta p^2$  vertex. However, this external line has  $p = 0$ , and so all of these diagrams have no contribution. To leading order  $\Delta = n_0$  is unchanged, as can be seen from the diagrams in fig. 5.2: the leading order contribution to  $\Delta$  comes from diagrams composed of no loops, and so all lines carry wave number  $p = 0$  and are unaffected by the  $\delta p^2$  vertex. The correction terms to the small  $n_0$  limit of  $\Delta$  will likely be of the same order as before,  $O(n_0^{d/2}\lambda^{d/2})$ , but with a different amplitude. This amplitude could be calculated, although it would require a generalization of the response functions

discussed below. It will be shown the asymptotic value of  $\langle \psi^2 \rangle$  depends only on  $\Delta$ , and so the other surface terms can be neglected.

There are new response functions generated in the bulk theory. With  $\delta = 0$  there was just a bare  $\psi$  propagator and a  $\phi$  response function. In this theory there are instead four response functions, which connect  $\phi, \psi$  to  $\bar{\phi}, \bar{\psi}$  in each possible way, as shown in fig. 5.8. Each of these response functions, represented by double lines, is an infinite sum over all possible numbers of  $\delta p^2$  vertices inserted.

$$\begin{aligned}
\text{F} & \text{====} = \text{---} + \text{---} \text{---} + \dots \\
\text{G} & \text{=====} = \text{---} + \text{---} \text{---} + \text{---} \text{---} \text{---} + \dots \\
\text{H} & \text{=====} = \text{---} + \text{---} \text{---} + \text{---} \text{---} \text{---} + \dots \\
\text{J} & \text{=====} = \text{---} \text{---} + \text{---} \text{---} \text{---} + \dots
\end{aligned}$$

$\begin{array}{c} t_2 \quad t_1 \\ \leftarrow \\ p \end{array}$

$$\begin{aligned}
\text{(a)} \quad & \text{=====} = \text{---} + \text{---} \bullet \text{=====} \\
& \text{====} = \text{---} \bullet \text{=====} \\
\text{(b)} \quad & \text{=====} = \text{---} + \text{---} \bullet \text{=====} \\
& \text{=====} = \text{---} \bullet \text{=====}
\end{aligned}$$

FIGURE 5.8. The response functions for the case  $\delta \neq 0$ , and the coupled equations they satisfy.

These response functions can be found exactly via the coupled integral equations, also shown in fig. 5.8. For our purposes we need to know only the form of the response functions

when the earlier time argument is set to zero.<sup>12</sup> Setting  $t_2 = t$ ,  $t_1 = 0$  in the equations represented by diagrams (a) gives

$$\begin{aligned} G(p, t) &= e^{-p^2 t} + \delta p^2 \int_0^t dt' e^{-p^2(t-t')} F(p, t') \\ F(p, t) &= \delta p^2 \int_0^t dt' e^{p^2(t-t')} \left( \frac{1 + n_\phi \lambda t'}{1 + n_\phi \lambda t} \right)^2 G(p, t'), \end{aligned} \quad (5.55)$$

or, in terms of  $f, g$  defined by  $G(p, t) = e^{-p^2 t} g(p, t)$  and  $F(p, t) = e^{-p^2 t} f(p, t)$

$$\begin{aligned} g(p, t) &= 1 + \delta p^2 \int_0^t dt' f(p, t') \\ f(p, t) &= \delta p^2 \int_0^t dt' \left( \frac{1 + n_\phi \lambda t'}{1 + n_\phi \lambda t} \right)^2 g(p, t'). \end{aligned} \quad (5.56)$$

Differentiating both equations in (5.56) with respect to  $t$  gives

$$f(p, t) = \frac{1}{\delta p^2} \dot{g}(p, t) \quad (5.57)$$

$$\frac{\partial}{\partial t} [(1 + n_\phi \lambda t)^2 f(p, t)] = \delta p^2 (1 + n_\phi \lambda t)^2 g(p, t) \quad (5.58)$$

Substituting for  $f$  into the lower equation and manipulating the expression gives a remarkably simple equation for  $g$

$$\frac{\partial^2}{\partial t^2} [(1 + n_\phi \lambda t) g] = \delta^2 p^4 [(1 + n_\phi \lambda t) g] \quad (5.59)$$

which has the general solution

$$g(p, t) = \frac{1}{1 + n_\phi \lambda t} [A \cosh(\delta p^2 t) + B \sinh(\delta p^2 t)]. \quad (5.60)$$

From the integral equation (5.56) one finds the conditions  $g(p, 0) = 1$ , which implies  $A = 1$ , and  $g(0, t) = 1$ , which then implies  $B = n_0 \lambda / (\delta p^2)$ . Therefore the explicit form of  $G(p, t)$ , and from (5.57)  $F(p, t)$ , is known

$$G(p, t) = \frac{e^{-p^2 t}}{1 + n_\phi \lambda t} \left[ \cosh(\delta p^2 t) + \frac{n_\phi \lambda}{\delta p^2} \sinh(\delta p^2 t) \right] \quad (5.61)$$

---

<sup>12</sup> To calculate the higher order terms in the expansion  $\Delta = n_0 + \dots$  one needs to derive these response functions with  $t_1 \neq 0$ .

$$F(p, t) = \frac{e^{-p^2 t}}{(1 + n_\phi \lambda t)^2} \left[ \left( 1 + n_\phi \lambda t - \frac{n_\phi^2 \lambda^2}{\delta^2 p^4} \right) \sinh(\delta p^2 t) + \frac{n_\phi^2 \lambda^2 t}{\delta p^2} \cosh(\delta p^2 t) \right]. \quad (5.62)$$

The other response functions,  $H(p, t)$  and  $J(p, t)$ , defined in diagram fig. 5.8, can be found via similar methods. The coupled integral equations shown in fig. 5.8(b), written in terms of  $h = e^{p^2 t} H$  and  $j = e^{p^2 t} J$ , are

$$\begin{aligned} h(p, t) &= \frac{1}{(1 + n_\phi \lambda t)^2} + \delta p^2 \int_0^t dt' \left( \frac{1 + n_\phi \lambda t'}{1 + n_\phi \lambda t} \right)^2 j(p, t') \\ j(p, t) &= \delta p^2 \int_0^t h(p, t'). \end{aligned} \quad (5.63)$$

Differentiating both equations with respect to  $t$  and substituting to eliminate  $h$  gives the equation

$$\frac{\partial^2}{\partial t^2} [(1 + n_\phi \lambda t) j] = \delta^2 p^4 [(1 + n_\phi \lambda t) j] \quad (5.64)$$

which has the general solution

$$j(p, t) = \frac{1}{1 + n_\phi \lambda t} [A \cosh(\delta p^2 t) + B \sinh(\delta p^2 t)]. \quad (5.65)$$

The condition that  $j(p, 0) = 0$  implies  $A = 0$ . The general solution of  $h$  can be found from (5.65), and then the condition that  $h(p, 0) = 1$  implies  $B = 1$ . Therefore  $H$  and  $J$  are given by

$$H(p, t) = \frac{e^{-p^2 t}}{(1 + n_\phi \lambda t)^2} \left[ (1 + n_\phi \lambda t) \cosh(\delta p^2 t) - \frac{n_\phi \lambda}{\delta p^2} \sinh(\delta p^2 t) \right] \quad (5.66)$$

$$J(p, t) = \frac{e^{-p^2 t}}{(1 + n_\phi \lambda t)} \sinh(\delta p^2 t). \quad (5.67)$$

In §5.4 the value of  $\langle \psi^2 \rangle$  was calculated from the simple loop shown in fig. 5.4. The generalization of this calculation is given by the diagrams shown in fig. 5.9, which are composed of the  $G(p, t)$  and  $J(p, t)$  response functions. The surface couplings  $\Delta^{(0,2)} \neq -\Delta^{(2,0)}$  beyond the leading small  $n_0$  terms, and so the couplings are labeled  $\Delta$  and  $\Delta'$  respectively. It should be noted that unlike the  $\delta = 0$  case, these are not the only diagrams

$$\begin{aligned}
\langle \psi^2 \rangle = & \text{ (dashed loop) } \Delta + \text{ (double loop) } \Delta' \\
& + \text{ irrelevant terms}
\end{aligned}$$

FIGURE 5.9. The generalization of the simple  $\psi$  loop of fig. 5.4 to the case of  $\delta \neq 0$ .

which contribute to  $\langle \psi^2 \rangle$ . Examples of other diagrams, and arguments for why they are irrelevant, will be given below. First, we compute those of fig. 5.9, which give

$$\langle \psi(t)^2 \rangle = \int \frac{d^d p}{(2\pi)^d} [\Delta G(p, t)^2 - \Delta' J(p, t)^2]. \quad (5.68)$$

Substituting (5.61) and (5.67) into the equation above, and rewriting the integral in terms of the variable  $u = p^2 t$  gives

$$\begin{aligned}
\langle \psi(t)^2 \rangle = & \frac{\Delta t^{-d/2}}{(4\pi)^{d/2} \Gamma(d/2) (1 + n_\phi \lambda t)^2} \int_0^\infty du u^{d/2-1} e^{-2u} \left[ \Delta \cosh^2(\delta u) \right. \\
& \left. - \Delta' \sinh^2(\delta u) + \frac{n_\phi \lambda t}{\delta u} \sinh(2\delta u) + \left( \frac{n_\phi \lambda t}{\delta u} \right)^2 \sinh(\delta u)^2 \right]. \quad (5.69)
\end{aligned}$$

Each term in the square brackets gives a convergent integral for  $d > 0$ . Therefore we can take the large  $t$  limit before integrating, and only calculate the leading term in  $t$ . This term, on the far right in the brackets, depends only on  $\Delta$ , and so the value of  $\Delta'$  is unimportant.

Evaluating this integral gives

$$\langle \psi^2 \rangle = \frac{\Delta}{(8\pi)^{d/2}} Q(d, \delta) t^{-d/2} \quad (5.70)$$

where

$$Q(d, \delta) = 4 \frac{(1 + \delta)^{2-d/2} + (1 - \delta)^{2-d/2} - 2}{\delta^2 (d - 2)(d - 4)}. \quad (5.71)$$

From (5.70) it follows that  $Q = \langle \psi^2 \rangle_\delta / \langle \psi^2 \rangle_0$ , to the extent that  $\Delta$  is independent of  $\delta$ . This function  $Q$  is non-singular at  $\delta = 0$ , and satisfies  $Q(d, 0) = 1$ . While  $Q$  appears to be divergent at  $d = 2, 4$ , it is actually finite everywhere except  $d \geq 4$  and  $\delta = \pm 1$ . It is likely that the limits of  $t \rightarrow \infty$  and  $\delta \rightarrow \pm 1$  do not necessarily commute, and that a separate treatment for the case of an immobile species, at least in this singular case, would be required. For  $d < 4$  this function has finite values as  $\delta \rightarrow \pm 1$ , but the slope at  $\delta = \pm 1$  is infinite for  $d \geq 2$ .

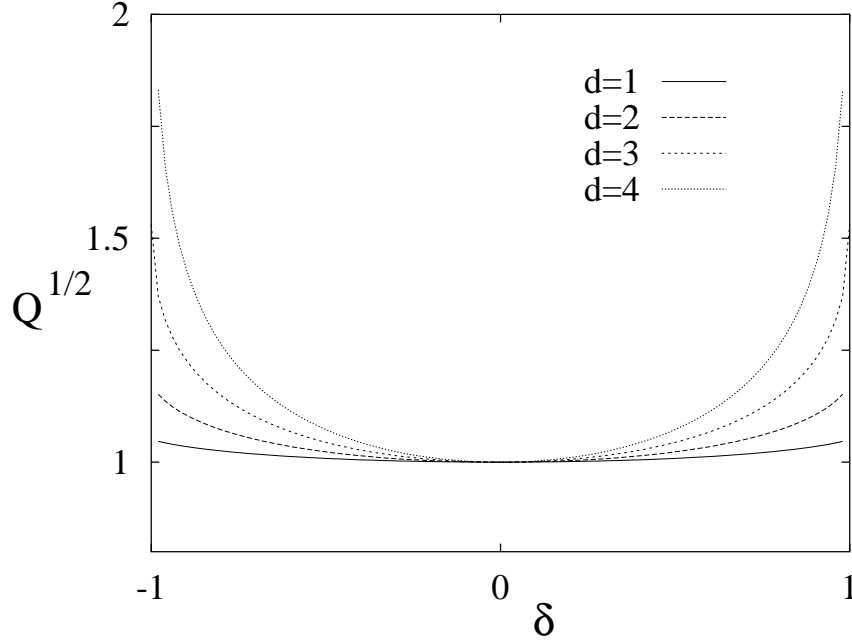


FIGURE 5.10. A plot of  $\sqrt{Q} = \langle a \rangle_\delta / \langle a \rangle_0$  for integer values of  $d$ .

While the calculation of  $Q(d, \delta)$  is only strictly valid for  $2 < d < 4$ , it is nonetheless interesting to consider its limits for the integer dimensions from  $d = 1$  to  $d = 4$ , motivated by §5.6 on  $d \leq 2$ , in which it was conjectured that the “classical” amplitude is also the



leading term in an  $\epsilon$  expansion for  $d = 2 - \epsilon$ . From (5.71)

$$Q(d, \delta) = \begin{cases} \frac{4}{3\delta^2} [(1 + \delta)^{3/2} + (1 - \delta)^{3/2} - 2] & d = 1 \\ \frac{(1 - \delta) \ln(1 - \delta) + (1 + \delta) \ln(1 + \delta)}{\delta^2} & d = 2 \\ \frac{4}{\delta^2} [2 - \sqrt{1 + \delta} - \sqrt{1 - \delta}] & d = 3 \\ \frac{-\ln(1 - \delta^2)}{\delta^2} & d = 4 \end{cases} \quad (5.72)$$

Since the density goes as  $\sqrt{\langle \psi^2 \rangle}$ , the function  $\sqrt{Q(d, \delta)}$  is plotted in fig. 5.10 for integer values of  $d$ . The density amplitude increases monotonically with  $|\delta|$ , but is not changed remarkably for modest values of  $\delta$ .

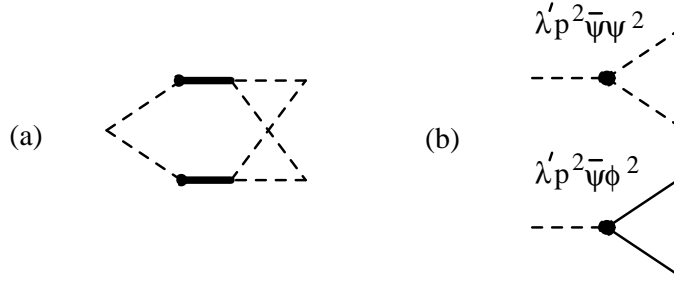


FIGURE 5.11. (a) An example of one of the diagrams besides those of fig. 5.9 which contribute to  $\langle \psi^2 \rangle$ , and (b) the effective bulk vertices that all such diagrams contain.

There are other diagrams which give contributions to  $\langle \psi^2 \rangle$ , unlike the  $\delta = 0$  case. Some of these are shown in fig. 5.11(a). All of these diagrams have the similar feature that they contain one of the two sub-diagrams in fig. 5.11(b). These sub-diagrams give rise to effective vertices of the form  $\lambda' \bar{\psi} \nabla^2 \psi^2$  and  $\lambda' \bar{\psi} \nabla^2 \phi^2$  in the bulk theory. However, such vertices are irrelevant, which follows from power counting, and so the diagrams which arise from them must be sub-leading in time. Therefore we conclude that asymptotically the value of  $\langle \psi^2 \rangle$  is given by (5.70) and (5.71).

### *Demonstration that $\psi(t)$ has a Normal Distribution*

In order for the calculation of  $\langle \psi^2 \rangle$  to give the amplitude of the density it is necessary that  $\psi(t)$  have a normal distribution. When  $\delta = 0$  this follows directly from the simple diffusion equation satisfied by  $\psi$ , or equivalently, from central limit arguments. However,  $\psi$  evolves via equation (5.54) for  $\delta \neq 0$ , and so it needs to be shown that it still flows to a normal distribution. What we will show is that the random variable  $t^{d/4}\psi$  flows to a static normal distribution, the width of which was calculated above.

Consider  $\langle \psi^n \rangle$ , where  $n$  is even. There is one diagram in which  $n$  response functions  $G(p, t)$  are connected in pairs to  $n/2$  initial terms  $(\Delta/2)\bar{\psi}^2$ . This diagram contains  $n/2$  loops, and is therefore of order  $t^{-nd/4}$ . It was shown above replacing any of the  $G(p, t)$  loops with  $J(p, t)$  response functions connected to  $(\Delta'/2)\bar{\phi}^2$  gives a lower order contribution. Similarly, any other diagrams, which would originate from considering higher order surface terms, will involve more than  $n/2$  loops, and will therefore decay faster in time. For  $n$  odd one finds that there are no diagrams for  $\langle \psi^n \rangle$  which decay as slowly as  $t^{-nd/4}$ . That is, for  $n$  odd,  $\lim_{t \rightarrow \infty} \langle (t^{d/4}\psi)^n \rangle = 0$ . The distribution of the variable  $t^{d/4}\psi$  has only even moments as  $t \rightarrow \infty$ , and these moments are just multiples of  $\langle (t^{d/4}\psi)^2 \rangle$ , generated by all possible pair contractions. Therefore the distribution is normal.

## 5.9. CORRELATION FUNCTIONS FOR $2 < d < 4$

When  $d > 2$ , one can use the classical action to calculate the correlation functions. Unfortunately, these correlation functions are averaged quantities, and therefore much of the microscopic information about the distribution of particles is lost. However, there are interesting parallels between these correlation functions and those of the phase ordering systems with scalar order parameter.

Consider the distribution of the random variable  $t^{d/4}\phi(\mathbf{x}, t)$  with  $2 < d < 4$ . From §5.4 we know that  $\langle t^{d/4}\phi - t^{d/4}|\psi| \rangle \rightarrow 0$  as  $t \rightarrow \infty$ . Furthermore, from equation (5.34) it follows that, as  $t \rightarrow \infty$ ,  $\langle (t^{d/4}\phi - t^{d/4}|\psi|)^2 \rangle \rightarrow 0$ . This suggests that the joint probability

distribution of the non-negative random variable  $t^{d/4}\phi(\mathbf{x}, t) - t^{d/4}|\psi(\mathbf{x}, t)|$  goes to a  $\delta$  function, or that the distribution  $P[t^{d/4}\phi] \rightarrow P[t^{d/4}|\psi|]$  as  $t \rightarrow \infty$ . The latter distribution is known exactly, as  $t^{d/4}\psi$  is at late times given by a static normal distribution.

It is not correct to say that asymptotically  $\phi$  and  $|\psi|$  are everywhere equal, since this would imply that there are no regions in which the densities  $a$  and  $b$  are both non-zero. However, the reaction regions, those in which both densities are non-zero, become negligibly small for large  $t$ , and the corrections to setting  $\phi$  equal to  $|\psi|$  in calculating correlation functions will be subleading in time. Stated another way, the leading term in both  $\langle\phi_1\phi_2\rangle$  and  $\langle|\psi_1||\psi_2|\rangle$  is of order  $t^{-d/2}$ . To this order the two random variables  $\phi$  and  $|\psi|$  have identical distributions. This is in contrast to a quantity such as  $\phi^2 - \psi^2$ , which is measuring a subleading term relative to  $t^{-d/2}$ .

We can use the property that  $t^{d/4}\phi$  is given by the absolute value of a Gaussian random field to calculate correlation functions. This is similar to what is done in the dynamics of phase ordering, where the order parameter field can be mapped to an auxiliary field which is assumed to be a Gaussian random field. This analogy will be discussed further below.

Since  $\phi$  and  $|\psi|$  are given by the same distribution, we conclude  $\langle\phi_1\phi_2\rangle \sim \langle|\psi_1||\psi_2|\rangle$ , where the labels indicate the positions  $\mathbf{x}_1$  and  $\mathbf{x}_2$  at time  $t$ . The correlation function  $\langle|\psi_1||\psi_2|\rangle$  can be calculated exactly by using the fact that, asymptotically,  $\psi(t)$  has a normal distribution. The joint probability distribution  $P[\psi_1, \psi_2]$  is then also normal, so

$$P[\psi_1, \psi_2] = \frac{\sqrt{4\alpha^2 - \beta^2}}{2\pi} \exp \left\{ -\alpha\psi_1^2 - \alpha\psi_2^2 - \beta\psi_1\psi_2 \right\}, \quad (5.73)$$

where we have used translational invariance to set  $\langle\psi_1^2\rangle = \langle\psi_2^2\rangle$ . The constants  $\alpha$  and  $\beta$  are determined by the values of  $\langle\psi^2\rangle$  and  $\langle\psi_1\psi_2\rangle$ , which are evaluated from the diagrams. The latter we have only calculated for  $\delta = 0$ , or equal diffusion constants, so we consider that case first. For notational convenience we define  $\langle\psi^2\rangle \equiv C(t) = \Delta/(8\pi t)^{d/2}$ . The diagram shown in fig. 5.12(a) is used to calculate the correlation function  $\langle\psi(\mathbf{p})\psi(-\mathbf{p})\rangle$ , from which one finds

$$\langle\psi_1\psi_2\rangle = \int \frac{d^d p}{(2\pi)^d} e^{i\mathbf{p}\cdot(\mathbf{x}_1 - \mathbf{x}_2)} \langle\psi(\mathbf{p})\psi(-\mathbf{p})\rangle. \quad (5.74)$$

When  $\delta = 0$  then  $\langle \psi(\mathbf{p})\psi(-\mathbf{p}) \rangle = \Delta e^{-2p^2 t}$ , and

$$\langle \psi_1 \psi_2 \rangle = C(t) \exp(-r^2/8t) \equiv C(t)f(r^2/t) \quad (5.75)$$

where  $r = |\mathbf{x}_1 - \mathbf{x}_2|$ . In terms of (5.75) we find for  $\alpha, \beta$

$$\alpha = \frac{1}{2C(1-f^2)} \quad \beta = \frac{f}{C(1-f^2)}. \quad (5.76)$$

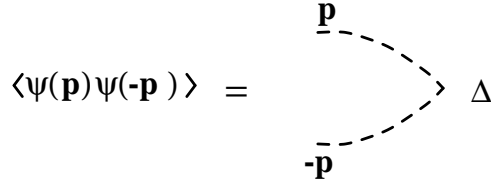


FIGURE 5.12. The diagram for  $\langle \psi(\mathbf{p})\psi(-\mathbf{p}) \rangle$ , when  $\delta = 0$ .

With these values substituted into (5.73), one can calculate

$$\begin{aligned} \langle \phi_1 \phi_2 \rangle &\sim \langle |\psi_1| |\psi_2| \rangle = \int_{-\infty}^{\infty} d\psi_1 \int_{-\infty}^{\infty} d\psi_2 |\psi_1| |\psi_2| P[\psi_1, \psi_2] \\ &= \frac{2C}{\pi} \left[ \sqrt{1-f^2} + f \arctan \left( \frac{f}{\sqrt{1-f^2}} \right) \right]. \end{aligned} \quad (5.77)$$

This correlation function can be used to find the correlation functions  $\langle a_1 a_2 \rangle$  and  $\langle a_1 b_2 \rangle$ .

Specifically

$$\langle a_1 a_2 \rangle = \frac{1}{2} \langle \phi_1 \phi_2 + \psi_1 \psi_2 \rangle, \quad (5.78)$$

which gives for the connected part  $\langle a_1 a_2 \rangle_c = \langle a_1 a_2 \rangle - \langle a \rangle^2$ ,

$$\langle a_1 a_2 \rangle_c = \frac{\Delta}{\pi(8\pi t)^{d/2}} \left[ \frac{\pi}{2} f - 1 + \sqrt{1-f^2} + f \arctan \left( \frac{f}{\sqrt{1-f^2}} \right) \right] \quad (5.79)$$

For large  $r$ ,  $f = \exp(-r^2/8t)$  is small, giving

$$\langle a_1 a_2 \rangle_c \sim \frac{\Delta}{2(8\pi t)^{d/2}} e^{-r^2/8t}. \quad (5.80)$$

Similarly,  $\langle a_1 b_2 \rangle = \langle \phi_1 \phi_2 - \psi_1 \psi_2 \rangle / 2$ , so that

$$\langle a_1 b_2 \rangle_c = \frac{\Delta}{\pi(8\pi t)^{d/2}} \left[ -\frac{\pi}{2} f - 1 + \sqrt{1-f^2} + f \arctan \left( \frac{f}{\sqrt{1-f^2}} \right) \right] \quad (5.81)$$

which for large  $r$  goes as

$$\langle a_1 b_2 \rangle_c \sim -\frac{\Delta}{4(8\pi t)^{d/2}} e^{-r^2/8t}. \quad (5.82)$$

A plot of these connected correlation functions is shown in fig. 5.13. The signs of these,  $\langle a_1 a_2 \rangle > 0$  and  $\langle a_1 b_2 \rangle < 0$ , can be understood for short distances to be a consequence of the segregation. Given an  $A$  particle at a particular point, there is an increased probability that a nearby particle is also an  $A$ , and a decreased probability that it is a  $B$ .

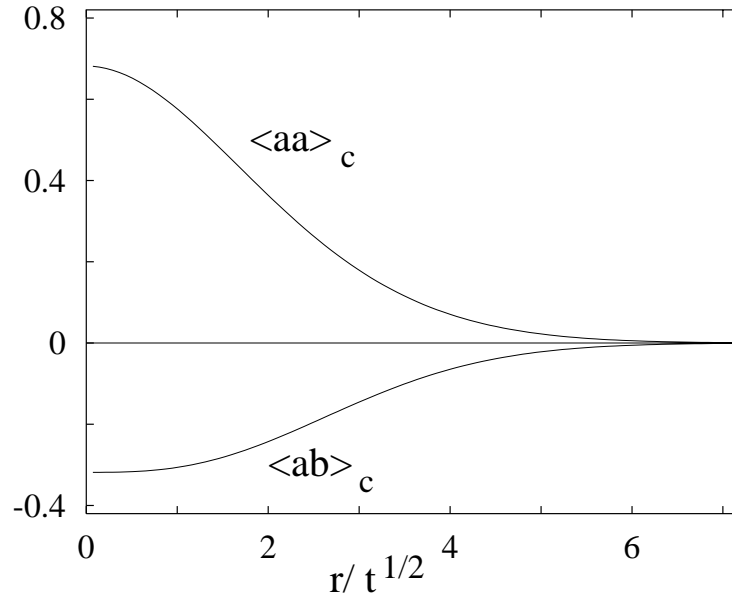


FIGURE 5.13. The correlation functions  $\langle a(r, t) a(0, t) \rangle_c$  and  $\langle a(r, t) b(0, t) \rangle_c$  plotted as functions of  $r/\sqrt{t}$ . The vertical axis is given in units of  $\Delta(8\pi t)^{-d/2}$ .

For the case  $\delta \neq 0$  one has  $\langle \psi^2 \rangle = C(t)Q(d, \delta)$ , as given by (5.70). The generalization of  $\langle \psi(\mathbf{p}) \psi(-\mathbf{p}) \rangle$ , shown in fig. 5.12, behaves for small  $p$  the same as when  $\delta = 0$ . Therefore, for large  $r$  one still has  $\langle \psi_1 \psi_2 \rangle = Cf$ . When this is put in the expressions for  $\langle a_1 a_2 \rangle$  and

$\langle a_1 b_2 \rangle$  one finds that the large  $r$  behavior is given by (5.80) and (5.82) is unaffected by  $\delta \neq 0$ .

While these correlation functions and other quantities can be calculated, they ultimately rely on the stronger statement that  $\psi$  is a Gaussian random field, and that  $\phi \sim |\psi|$ . The topology of the domains is determined by the random field, with the boundaries between  $a$  regions and  $b$  regions given by the zeroes of  $\psi$ . This topology is completely equivalent to an analogous situation in phase ordering. It has been suggested in the phase ordering of a scalar order parameter that an invertible, non-linear mapping from the order parameter field to an auxiliary field results in the latter being a Gaussian random field [70]. Usually this mapping is chosen to be the solution of a single kink, for example the hyperbolic tangent profile. While this method is no longer believed quantitatively to be correct [71], it does provide a qualitative picture of the structure of the domains. Again, the zeroes of this Gaussian random field determine the boundaries between the equilibrated phase.

The difference between these systems lies in how correlation functions are calculated from this random field. In the reaction-diffusion case one is interested in the correlation functions of the field itself, and of the absolute value of the field. Neither of these quantities exhibit remarkable behavior. In the phase ordering one argues that at late times the mapping between the order parameter field and the Gaussian field goes to a step function, and therefore order parameter correlations are given by the correlations of the sign of the random field. These sharp boundaries have generally more interesting features than in the present case. In particular they give rise to non-analytic terms in the small  $r$  limit of the correlation function, or correspondingly power law tails for large wave number in the Fourier transform.

# References

- [1] B. P. Lee and J. L. Cardy, Phys. Rev. E **48**, 2452 (1993).
- [2] B. P. Lee, J. Phys. A, **27**, 2633 (1994).
- [3] J. D. Gunton, M. San Miguel, and P. S. Sahni, in *Phase Transitions and Critical Phenomena*, edited by C. Domb and J. L. Lebowitz (Academic, New York, 1983), Vol. 8.
- [4] H. Furukawa, Adv. Phys. **34**, 703 (1985).
- [5] K. Binder, Rep. Prog. Phys. **50**, 783 (1987).
- [6] J. S. Langer, in *Solids Far From Equilibrium*, edited by C. Godrèche (Cambridge, Cambridge, 1992).
- [7] B. D. Gaulin, S. Spooner, and Y. Morii, Phys. Rev. Lett. **59**, 668 (1987).
- [8] A. P. Y. Wong, P. Wiltzius, and B. Yurke, Phys. Rev. Lett. **68**, 3583 (1992).
- [9] N. Mason, A. N. Pargellis, and B. Yurke, Phys. Rev. Lett. **70**, 190 (1993).
- [10] I. M. Lifshitz and V. V. Slyozov, J. Phys. Chem. Solids **19**, 35 (1961).
- [11] Y. Oono and S. Puri, Phys. Rev. A **38**, 434 (1988); S. Puri and Y. Oono, Phys. Rev. A **38**, 1542 (1988).
- [12] G. Mazenko and O. T. Valls, Phys. Rev. Lett. **59**, 680 (1987);  
G. Mazenko, O. T. Valls, and M. Zannetti, Phys. Rev. B **38**, 520 (1988).
- [13] C. Roland and M. Grant, Phys. Rev. Lett. **60**, 2657, (1988);  
C. Roland and M. Grant, Phys. Rev. B **39**, 11971 (1989).
- [14] A. J. Bray, Phys. Rev. Lett. **62**, 2841 (1989); A. J. Bray, Phys. Rev. B **41**, 6724 (1990).
- [15] F. J. Dyson, Comm. Math. Phys. **12**, 91 (1969); F. J. Dyson, Comm. Math. Phys. **12**, 212 (1969).
- [16] P. W. Anderson, G. Yuval, and D. R. Hamann, Phys. Rev. B **1**, 4464 (1970).
- [17] J. L. Cardy, J. Phys. A **14**, 1407 (1981).
- [18] A. J. Bray, Phys. Rev. E **47**, 3191 (1993).

- [19] A. D. Rutenberg and A. J. Bray, unpublished.
- [20] S. A. Rice and M. J. Pillig, *Prog. React. Kinetics* **9**, 93 (1978).
- [21] J. K. Baird and S. P. Escott, *J. Chem. Phys.* **74**, 6993 (1981).
- [22] W. A. Noyes, *Prog. React. Kinetics* **1**, 129 (1961).
- [23] V. Kuzovkov and E. Kotomin, *Rep. Prog. Phys.* **51**, 1479 (1988).
- [24] A. A. Ovchinnikov, S. F. Timashev, and A. A. Belyy, *Kinetics of Diffusion Controlled Chemical Processes*, (Nova Science, New York, 1989).
- [25] Y. E. Koo, L. Li, and R. Kopelman, *Mol. Cryst. Liq. Cryst.* **183**, 187 (1990).
- [26] V. Castets, *et al.* *Phys. Rev. Lett.* **64**, 2953 (1990).
- [27] I. R. Epstein, *et al.* *Physica A* **188**, 26 (1992).
- [28] L. Peliti, *J. Physique* **46**, 1469 (1985).
- [29] A. A. Lushnikov, *Phys. Lett. A* **120**, 135 (1987).
- [30] F. Leyvraz, *J. Phys. A* **25**, 3205 (1992).
- [31] D. Toussaint and F. Wilczek, *J. Chem. Phys.* **78**, 2642 (1983).
- [32] F. Leyvraz and S. Redner, *Phys. Rev. Lett.* **66**, 2168 (1991);  
F. Leyvraz and S. Redner, *Phys. Rev. A* **46**, 3132 (1992).
- [33] S. Cornell and M. Droz, *Phys. Rev. Lett.* **70**, 3824 (1993).
- [34] H. Hayakawa, Z. Rácz, and T. Tsuzuki, *Phys. Rev. E* **47**, 1499 (1993).
- [35] I. M. Lifshitz, *Sov. Phys. JETP* **15**, 939 (1962).
- [36] S. M. Allen and J. W. Cahn, *Acta Metall.* **27**, 1085 (1979).
- [37] M. K. Phani, *et al.*, *Phys. Rev. Lett.* **45**, 366 (1980); P. S. Sahni, *et al.*, *Phys. Rev. B* **24**, 410 (1981).
- [38] R. J. Glauber, *J. Math. Phys.* **4**, 191 (1963).
- [39] A. J. Bray, *J. Phys. A* **22**, L67 (1989).
- [40] K. G. Wilson and J. Kogut, *Phys. Reports* **12**, 75 (1974).
- [41] see for example D. J. Amit, *Field Theory, the Renormalization Group, and Critical Phenomena*, (World Scientific, Singapore, 1984).



- [42] T. Nagai and K. Kawasaki, *Physica A* **134**, 483 (1986).
- [43] P. C. Hohenberg and B. I. Halperin, *Rev. Mod. Phys.* **49**, 435 (1977).
- [44] M. Doi, *J. Phys. A* **9**, 1465 (1976); M. Doi, *J. Phys. A* **9**, 1479 (1976).
- [45] L. S. Schulman, *Techniques and Applications of Path Integration*, (Wiley, New York, 1981) p. 242 ff.
- [46] M. Bramson and J. L. Lebowitz, *J. Stat. Phys.* **62**, 297 (1991).
- [47] M. Bramson and J. L. Lebowitz, *J. Stat. Phys.* **65**, 941 (1991).
- [48] K. Kang *et al.*, *J. Phys. A* **17**, L665 (1984).
- [49] K. Kang and S. Redner, *Phys. Rev. A* **32**, 435 (1985).
- [50] Z. Rácz, *Phys. Rev. Lett.* **55**, 1707 (1985).
- [51] F. Family and J. G. Amar, *J. Stat. Phys.* **65**, 1235 (1991).
- [52] V. Privman, *Phys. Rev. A* **46**, R6140 (1992).
- [53] V. Privman, (preprint).
- [54] L. Peliti, *J. Phys. A* **19**, L365 (1986).
- [55] T. Ohtsuki, *Phys. Rev. A* **43**, 6917 (1991).
- [56] M. Droz and L. Sasvári, *Phys. Rev. E* **48**, R2343 (1993).
- [57] B. Friedman, G. Levine, and B. O'Shaughnessy, *Phys. Rev. A* **46**, R7343 (1992).
- [58] A. S. Mikhailov, *Phys. Lett. A* **85**, 214 (1981); A. S. Mikhailov, *Phys. Lett. A* **85**, 427 (1981).
- [59] A. S. Mikhailov and V. V. Yashin, *J. Stat. Phys.* **38**, 347 (1985).
- [60] D. ben-Avraham, *Phys. Rev. Lett.* **71**, 3733 (1993).
- [61] A. A. Ovchinnikov and Ya. B. Zeldovich, *Chem. Phys.* **28**, 215 (1978).
- [62] K. Kang and S. Redner, *Phys. Rev. Lett.* **52**, 955 (1984).
- [63] H. Schnörrer, I. M. Sokolov, and A. Blumen, *Phys. Rev. A* **42**, 7075 (1990).
- [64] S. Cornell, M. Droz, and B. Chopard, *Physica A* **188**, 322 (1992).

- [65] H. W. Diehl, in *Phase Transitions and Critical Phenomena*, edited by C. Domb and J. L. Lebowitz (Academic, New York, 1986), Vol. 10.
- [66] G. N. Watson, *A Treatise on the Theory of Bessel Functions*, (Cambridge, Cambridge, 1952).
- [67] L. Gálfi and Z. Racz, Phys. Rev. A **38**, 3151 (1988).
- [68] M. Araujo, *et al.* Phys. Rev. Lett. **71**, 3592 (1993).
- [69] B. P. Lee and J. L. Cardy, unpublished.
- [70] G. Mazenko, Phys. Rev. Lett. **63**, 1605 (1990); G. Mazenko, Phys. Rev. B **42**, 4487 (1990).
- [71] C. Yeung, Y. Oono, and A. Shinozaki, Phys. Rev. E **49**, 2693 (1994).